Mathematical Modelling of Bone Remodelling in Mechanical, Electro-magnetic Fields at the Cellular Level

Yanan Wang

A Thesis Submitted for the Degree of Doctor of Philosophy

of

The Australian National University

July 2010

Declaration

This thesis is an account of work undertaken between March 2007 and July 2010 in School of Engineering, at The Australian National University, Canberra, Australia.

This thesis contains no material that has been previously accepted for the award of any other degree in any university, and contains no material previously published or written by another person, except where acknowledged in the customary manner.

Yanan Wang

July 2010

Publications

Yanan Wang, Qing-Hua Qin, Shankar Kalyanasundaram, A Theoretical Model for Simulating Effect of Parathyroid Hormone on Bone Metabolism at Cellular Level, Molecular & Cellular Biomechanics, vol 6, no 2, pp.101-112, 2009. (Journal Paper)

Yanan Wang, Qing-Hua Qin, Parametric Study of Control Mechanism of Cortical Bone Remodelling under Mechanical Stimulus, Acta Mechanica Sinica, volume 26, issue 1, page 37, 2010. (Journal Paper)

Yanan Wang, Qing-Hua Qin, A Mathematical Model of Cortical Bone Remodelling at Cellular Level under Mechanical Stimulus, Journal of Mechanics in Medicine and Biology, JMMB-D-10-00085, 2010 (Accepted for publication). (Journal Paper)

Yanan Wang, Qing-Hua Qin, The Effect of Mechanical Stimulus on Bone Remodeling, presented on the Third International Conference on Mechanics of Biomaterials and Tissues (ICMOBT2009), 13-17th, December, 2009, Clearwater Beach, Florida, USA. (Conference paper)

Yanan Wang, Qing-Hua Qin, Micromechanics for Determining Effective Material Properties of Dentine Composites, Chapter 9 of Advances in Engineering Mechanics, volume 1, ISBN: 978-1-60876-901-8, © 2010 Nova Science Publishers, Inc. (Book chapter)

Acknowledgements

I am heartily thankful to my supervisor, Prof. Qing-Hua Qin, whose encouragement, guidance and support from the initial to the final level enabled me to develop an understanding of the subject and finish it on time.

I would also like to thank my advisors Dr. Ling Yin and Dr. Shankar Kalyanasundaram for their helpful discussions. I am also grateful to Prof. Zbigniew Stachurski for his support and discussion. I would also like to show my gratitude to Helen Shelper who is the Administrator of School of Engineering for her help and general support on a daily basis.

I also offer my regards and blessings to all of those who supported me in any respect during the completion of the project, especially my office mates: Mark Euston, Sivakumar Dhar Malingam, Sudharshan Venkatesan, Cheuk Yu Lee, and our biomechanics research group members: Leilei Cao and Yuming Lin.

Lastly, I would like to thank my parents, my brother and his family especially my niece and nephew for all of their support during these three and half years. Most importantly, special thanks go to my partner Dan for her love, support and wisdom since the first day we were together.

Abstract

The skeleton is a metabolically active organ that undergoes continuous remodelling throughout life. At the cellular level, bone remodelling is an organised process whereby osteoclasts remove old bone and osteoblasts replace them with newly formed bone. The osteoclasts and osteoblasts work together in a coupled manner within a so-called 'basic multicellular unit' (BMU).

Bone remodelling helps to repair microdamages in bone matrix, preventing the accumulation of old bone. It also plays an important role in maintaining plasma calcium homeostasis. The regulation of bone remodelling is both systemic and local. The most important systemic regulator is parathyroid hormone (PTH), which has been used as a therapy to treat osteoporosis in clinics; however, the underlying mechanism by which PTH is regulated is still not clear.

As far as local regulation of bone remodelling is concerned, the discovery of the RANK/RANKL/OPG pathway is significant to the understanding of the interaction between osteoclastic cells and osteoblastic cells in BMU. A large number of therapeutic drugs and other stimuli have been found to apply their effects via RANK/RANKL/OPG.

Mechanical stimulus has significant influence on bone remodelling. Disuse or lack of loading causes bone remodelling with bone resorption dominating bone formation and thus a loss of bone mass or density. Conversely, overuse or increased loading causes bone mass or density to increase. Additionally, loadings with different characteristics such as frequency, number of loading cycles in a session and rest time between loading bouts affects bone remodelling differently. However, the underlying mechanisms are not fully understood despite a great deal of experimental work in this field.

Pulsed electro-magnetic fields (PEMF) devices have been widely used in clinics to treat bone fracture non-union and shorten the recovery period of fracture. Despite the clinical success, it is still not clear how PEMF stimulus interacts with cells, factors or molecules that are involved in bone remodelling.

This thesis will use a computational system biology approach to address the issues proposed above. Computational system biology is a systems biology approach that integrates experimental and computational research in order to understand complex biological systems such as bone remodelling. Based on the latest experimental results and mathematical advances, a

mathematical model of bone remodelling at the cellular level is developed with PTH included. Building on this platform model, mechanical stimulus and PEMF are taken into account. Thus, their effects on bone remodelling and the underlying control mechanisms at the cellular level are investigated.

The work in the thesis will further current understanding of bone remodelling at the cellular level. The quantitative analysis using our model will help pharmacological and non-pharmacological therapies developments, which eventually benefit patients who suffer from bone loss diseases such as osteoporosis.

Keywords: bone remodelling; osteoblast; osteoclast, mathematical model; PTH, mechanical; PEMF;

Contents

List of Tables

List of Figures

Chapter 1: Introduction

1.1 Basic Bone Biology

Bone is a highly specialised support tissue that is characterized by its rigidity and hardness. It is composed of support cells (osteoblasts and osteocytes), remodelling cells (osteoclasts), non-mineral matrix of collagen and non-collagenous proteins (osteoid) and inorganic mineral salts deposited within the matrix. The major functions of bone are: to provide structural support for the body and protection of vital organs; to provide an environment for marrow (both blood forming and fat storage); and to act as a mineral reservoir for calcium homeostasis in the body.

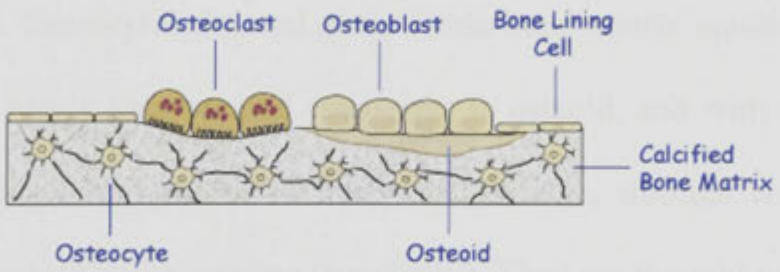

Figure 1.1: Schematic illustration of main bone cells in a remodelling site

Bone cells that are concerned with production, maintenance and remodelling of the osteoid are (see Figure 1.1):

- Osteoclasts: these cells are large, multinucleated cells, like macrophages, derived from the hematopoietic lineage. Osteoclasts

function in the resorption of mineralised tissue and are found attached to the bone surface at sites of active bone resorption. Their characteristic feature is a ruffled edge where active resorption takes place with the secretion of bone-resorbing enzymes, which digest bone matrix.

- Osteoblasts: these cells are derived from mesenchymal stem cells and are responsible for bone matrix synthesis and its subsequent mineralisation. In the adult skeleton, the majority of bone surfaces that are undergoing neither formation nor resorption (i.e. not being remodelled) are lined by bone lining cells (the inactive form of the osteoblast).
- Osteocytes: these cells are osteoblasts that become incorporated within the newly formed osteoid, which eventually becomes calcified bone. Osteocytes situated deep within bone matrix maintain contact with newly incorporated osteocytes in osteoid, and with osteoblasts and bone lining cells on the bone surfaces, through an extensive network of cell processes (canaliculi). They are thought to be ideally situated to respond to changes in physical forces upon bone and to transduce messages to the osteoblastic cells on the bone surface, directing them to initiate resorption or formation responses.

1.2 Research Background

Osteoporosis is a condition in which the bones become fragile and brittle, leading to a higher risk of fractures than in normal bone[1]. It occurs when bones lose minerals, such as calcium, more quickly than the body can replace them, leading to a loss of bone mass or density. As a result, bones become thinner and less dense (see Figure 1.2), so that even a minor bump or accident can cause serious fractures.

Osteoporosis is quite common in Australia, the data from the official government website of Osteoporosis Australia (www.osteoporosis.org.au) states that every five to six minutes, someone is admitted to an Australian hospital with an osteoporotic fracture. This is expected to rise to every three to four minutes by the year 2021, as the population ages and the number of osteoporotic fractures increases.

Bone is a dynamic, living tissue; its shape and structure continuously evolve throughout life. It has the ability to change its structure by removing old bone and replacing it with newly formed bone in a local process called bone remodelling. Osteoporosis is the result of dysfunction of bone remodelling, which means with osteoporosis, the rate of bone loss is greater

[1] Definition from Osteoporosis Australia (www.osteoporosis.org.au)

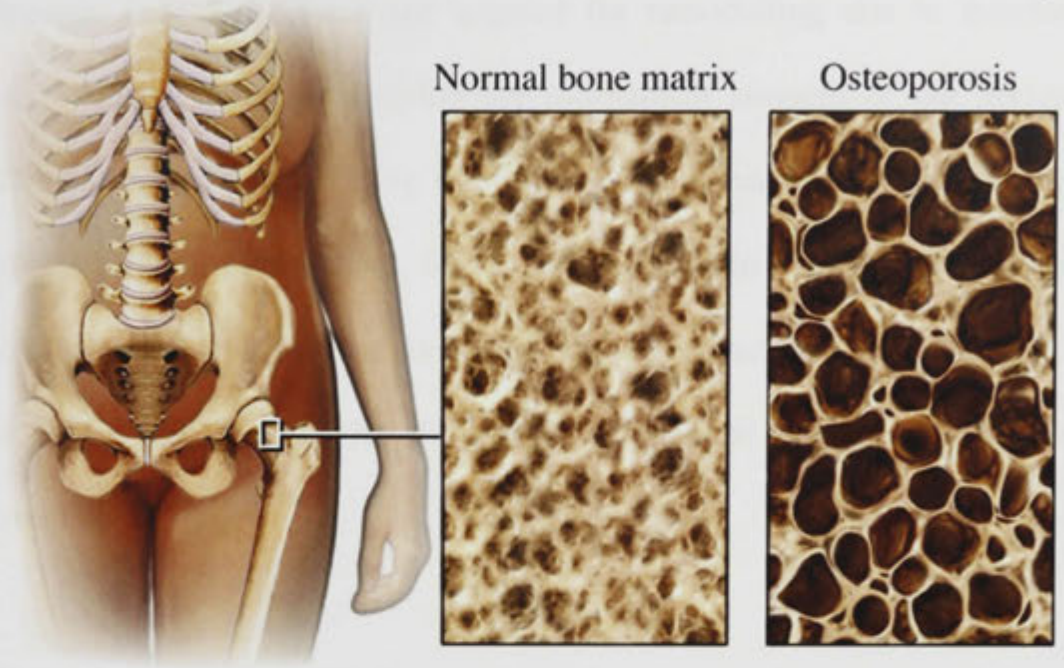

Figure 1.2: Comparison between normal bone matrix and osteoporosis in the human hip[2]

than that of bone gain, which causes porous bone that breaks easily.

Bone remodelling is a complex process performed by the coordinated activities of osteoblasts and osteoclasts. Together, these cells form temporary anatomical structures, called basic multicellular units (BMUs), which execute bone remodelling. The interactions between osteoblasts and osteoclasts, which guarantee a proper balance between bone gain and loss, is known as coupling [1].

---

[2] Picture from http://www.halanmediacorp.com/wp-content/uploads/2009/11/osteoporosis.jpg

Specific regions of bone are targeted for remodelling due to structural microdamage, thus maintaining the mechanical strength of the skeleton (targeted remodelling) [2, 3]. In addition, bone remodelling plays a major role in mineral homeostasis, by providing access to stores of calcium and phosphate [4]. In this case, bone remodelling occurs at random locations, so that every part of the skeleton is remodelled periodically (random remodelling) [2, 3].

The net amount of old bone removed and new bone restored in the remodelling cycle is a quantity called the bone balance. While coupling rarely is affected, bone balance can vary quite widely in many disease states; for example, in osteoporotic patients, resorption and formation are coupled but there is a negative bone balance, i.e. more bone is resorbed than is replaced by the typical BMUs.

BMUs are constantly remodelling bone tissue in the growing, adult, and senescent skeleton. Most metabolic bone diseases appear when a biochemical or cellular link of this finely organised network is chronically disrupted, such as osteoporosis, hyperparathyroidism, osteomalacia and corticosteroid-induced osteopenia. Remodelling also permits the restoration of microdamage caused by fatigue and shock. This constant care of the

bone matrix prevents its premature deterioration and maintains its overall strength.

Bone, being a major reservoir of body calcium, is under the hormonal control of Parathyroid Hormone (PTH) [5]. PTH is the most important hormone regulating calcium homeostasis and bone remodelling. Moreover, PTH is currently involved in numerous clinical trials as an anabolic agent for the treatment of low bone mass in osteoporosis [6]. Interestingly, the overall effect of PTH on bone mass depends primarily on its mode of administration; whereas a continuous increase in PTH levels decreases bone mass, intermittent PTH administration increases bone mass [7-11]. Despite many attempts to identify the source of these differential dosing effects on bone turnover, the precise mechanism remains elusive. Prevention and reversal of bone loss require a thorough understanding of the remodelling process in bone, and the mechanism of bone formation and resorption, including the actions of hormones such as PTH.

Long-term physical activity on a regular basis plays a particularly important role in maintaining healthy bones. Exercise can maintain and increase bone strength by increasing bone mass or by changing bone structure at micro- and macro-levels. Two main types of exercises are

beneficial to bone health: weight-bearing exercise and resistance exercise (lifting weights with arms or legs).

Weight-bearing exercise involves any exercise that is performed while a person is standing so that gravity is exerting a force. Examples of weight-bearing activities are jogging, walking, tennis, dancing, golf and netball. Activities that are high-impact, such as aerobics, running and jumping, have a greater effect on bone strength than 'low-impact' activities, such as walking and cycling.

Resistance exercises, also called strength training, can also have a positive effect on the health of bones. The strong muscle contractions that are required to move a heavy weight place stress or strain on the bone to which the muscles are attached. When a bone is repeatedly strained (as also happens in regular exercise training), it responds by increasing bone mass to become stronger.

Generally speaking, physical activities place mechanical loading on the skeleton and mechanical loading has profound influences on bone remodelling. Disused or reduced loading due to long-term bed rest, cast immobilisation or microgravity conditions (such as experienced by astronauts in a space station or shuttle) induces obvious bone loss and

mineral changes. Conversely, overuse or increased loading has the opposite effect; in tennis players, the bones of the racquet arm display significantly greater bone mineral density and cortical bone content than the non-playing arm. Although there exists a great deal of general knowledge about the role of mechanical loading on bone remodelling, further understanding of the underlying mechanism is needed.

Electro-magnetic field (EMF) devices have been widely used clinically for bone fracture healing (non-union or slow union), and some bone-related diseases such as osteoporosis and osteoarthritis for many years. The application of an EMF to stimulate osteogenesis is based on the idea of stimulating the natural endogenous streaming potentials in bone. In the beginning, current was applied directly via electrodes and was produced by forcing electric current through a wire coil placed over the fracture. Periodic changes of the current then produced the required EMF in bone through Faraday induction. The most effective medical devices used today are time-dependent EMF, especially pulsed EMF (PEMF), and the frequency range is 1–100 Hz. The physiological frequency range (8–30 Hz), which is caused by natural muscle contraction and the subsequently induced EMF in bone tissue is mostly used in clinical therapies. The osteogenesis effect caused by a PEMF device is of great significance to

patients, especially those who have already undergone failed surgical intervention [12].

Based on random and prospective clinical studies, the Food and Drug Administration (FDA) USA approved PEMF as a safe and effective way to treat non-union and osteoporosis diseases [13, 14], although the specific molecular mechanism is not fully understood.

In summary, the current understanding of bone remodelling is primarily based on experimental results *in vivo* and *in vitro*. A great deal of research has been conducted on the interactions of autocrine, paracrine and endocrine activities of receptors and ligands in bone remodelling, the role of bone cells involved in this process at the cellular and genetic level, and the influence of different stimuli and factors such as mechanical stimulus, PEMF and PTH on bone formation in bone remodelling. Based on these observations, many hypotheses have been proposed as to the role played by different signalling pathways and the communication between bone cells in bone remodelling. However, due to the complexity of the bone regulation system, which involves numerous factors and interactions, the understanding of the 'system behaviour' is still fragmentary.

Mathematical modelling is a powerful tool to reduce ambiguity as to causes and effects in complex systems. It allows one to test various experimental and theoretical hypotheses that may be difficult (such as time- or money-consuming) or impossible to test *in vivo* or *in vitro*. The development of a pharmaceutical treatment for bone diseases can also be enhanced by computational system biology that uses mathematical modelling to integrate experimental data into a system level model, enabling the various interactions to be efficiently and methodically investigated [15]. However, only a few mathematical models thus far have been proposed regarding bone remodelling [5, 6, 16-20].

In this thesis, in order to remove the limitations to generalisation with respect to causes and effects of bone remodelling under mechanical stimulus and PEMF at the cellular level, mathematical models are used to provide a dynamic, quantitative and systematic description of the relationships among interacting components of the biological system-bone remodelling at the cellular level.

1.3 Aims and Organisation of the Research

The major aim of this project is to develop a mathematical framework of the cell population dynamics model of bone remodelling under mechanical

stimulus and PEMFs at the cellular level, based on the latest experimental findings and mathematical advances. Four steps have been taken in order to achieve this goal. First, a foundation model of bone remodelling at the cellular level is proposed in Chapter 3. In particular, this model incorporates the most important systemic hormone in bone remodelling—PTH and is able to simulate the anabolic effect of PTH when applied intermittently, which has been used as a therapy to treat osteoporosis in clinics. Second, based on this foundation model, the effect of mechanical stimulus on bone remodelling is investigated in Chapter 4. Third, a parametric study of the control mechanism of bone remodelling under mechanical stimulus is conducted in Chapter 5, based on the work in Chapter 4. Fourth, based on the foundation model and Chapter 5, the theoretical study of bone remodelling under PEMF at the cellular level is performed together with the control mechanism investigation in Chapter 6. Conclusions and future work are presented in Chapter 7.

1.4 The Structure of the Thesis

Chapter 1 introduces the basic bone biology related to bone remodelling in order to provide the entry knowledge needed to understand the work. It includes the structure description of bone and the principal cells involved such as osteoclasts, osteoblasts and osteocytes.

The research background in Section 1.2 justified the need for this research, by introducing the common disease in Australia called osteoporosis, which is the result of the dysfunction of bone remodelling. The effects of mechanical stimuli and EMF on bone remodelling were then briefly introduced and will be discussed in detail in Chapter 2.

In Chapter 2, bone remodelling is explained in detail, including the origin, definition, bone remodelling cycle, BMU and receptor activator of nuclear factor (NF)-Kb (RANK)/RANK ligand (RANKL)/osteoprotegerin (OPG) pathway. In addition, a gap in the current literature is identified as a lack of mathematical modelling of bone remodelling. Bone remodelling under mechanical stimulus is followed, with details provided about the factors involved in this process such as frequency, number of cycles and their effects. Finally, the reason why mathematical modelling is needed is discussed. A similar method is also used in Section 2.3 of bone remodelling under PEMF.

In Chapter 3, a theoretical model for simulating the effects of PTH on bone metabolism at the cellular level is developed. PTH therapy is introduced in Section 3.1, which includes PTH's interaction with RANKL and OPG, the interaction within the RANK/RANKL/OPG pathway, as well as a

convergence hypothesis and the description of the model structure together with the lineage of the osteoblastic and osteoclastic cells involved.

In Section 3.2, the law of mass action is applied to model receptors and ligands interactions such as PTH with its receptor, RANKL with RANK and RANKL with OPG. Based on these receptors and ligands formulations and using balance equations, a series of ordinary differential equations (ODEs) are proposed to model the population of principal cells such as osteoblasts and osteoclasts included in the model. Finally, a series of results are provided in the form of figures then discussed in Section 3.4, including the coupling effect between osteoblasts and osteoclasts.

Chapter 4 provides the mathematical modelling of bone remodelling under mechanical stimulus—one of the most important stimuli. Background knowledge such as the RANK/RANKL/OPG pathway and mechanotransduction of bone remodelling under mechanical stimulus are explained at the beginning of the chapter. In the mathematical model section, the Hill equation is used to model the stimulatory and inhibitory effects of ligand-receptor reactions. The balance equations are then used to describe the evolution of the number of osteoblastic and osteoclastic cells in each maturation stage. Finally, in the numerical investigation, the mathematical model developed is used to simulate the experiments and a

comparison of results between simulation and experiment is made to test the validity of the model.

The parametric study of the control mechanism of bone remodelling under mechanical stimulus is conducted in Chapter 5. The mathematical model used is from Chapter 4, so its development is only briefly reviewed in Section 5.1. The justification of the existence of the control mechanism of bone remodelling is given in Section 5.2, followed by an explanation of the method of parametric study. Finally, the results of parametric study are presented by figures and tables, accompanied by discussions.

Bone remodelling under electro-magnetic fields is discussed in Chapter 6. The PEMF's effects on bone remodelling are reviewed, supported by the experimental results from the literature. The model structure of bone remodelling under PEMF is proposed then the mathematical models are proposed accordingly in Section 6.1. A numerical investigation of the model is conducted in Section 6.2, including the cell concentration dynamics of active osteoclasts (OCA), active osteoblasts (OBA) and osteoblastic precursors (OBP), as well as factors such as OPG and RANKL. Similar to Chapter 5, the parametric study of bone remodelling under PEMF is provided in Section 6.3.

Conclusions and future work are presented in Chapter 7. Supplementary information is given in Appendices A, B, C and D.

Chapter 2: Literature Review

The literature related to the research in this thesis is reviewed in this chapter, including the bone biology of remodelling, mathematical models of bone remodelling at the cellular level, experimental findings and mathematical models of bone remodelling under mechanical stimulus, and experimental results and mathematical models of bone remodelling under PEMF.

2.1 Bone Remodelling

Bone is a living organ that undergoes remodelling throughout life. Remodelling results from the action of osteoblasts and osteoclasts, which are two principal cell types found in bone, and defects such as microfractures are repaired by their coupling reaction [21]. The osteoblast produces the matrix, which becomes mineralised in a well-regulated manner. This mineralised matrix can be removed by the activity of the osteoclast when activated. In a homeostatic equilibrium, resorption and formation are balanced so that old bone is continuously replaced by new tissue, which is regulated by a variety of biochemical, mechanical and electro-magnetic factors. In 1963, Frost defined this phenomenon as bone remodelling [22].

For normal adults, there is a balance between the amount of bone resorbed by osteoclasts and the amount of bone formed by osteoblasts [23]. In this complex process, bone is remodelled by groups of cells derived from different sources, which are usually called BMUs [24], that follow an activation-resorption-formation sequence event. The BMU is a mediator mechanism bridging individual cellular activity to whole bone morphology [25].

There are four stages in the bone remodelling cycle (see Figure 2.1). This starts with resorption that activates multinucleated osteoclasts derived from bone marrow monocytes, which resorb a discrete area of mineralised bone matrix. After the completion of osteoclastic resorption, there is a reversal phase when subsequent osteoblast precursor cells, which can locally proliferate and differentiate into osteoblasts, migrate into the resorption lacuna and disclose the former osteoclastic activity. The formation phase follows with osteoblasts depositing new bone matrix, which is initially unmineralised and called osteoid, and in this way fills the resorption lacuna. After the completion of the formation stage, the quiescence stage starts whereby the osteoblasts embedded in osteoid mature into terminally differentiated osteocytes. The osteoblasts lying on the surface of the newly formed bone are lining cells.

The assumption that a coupling mechanism must exist between bone formation and resorption was first reported in 1964 [26]. However, the exact molecular mechanism that describes the interaction between cells of the osteoblastic and osteoclastic lineages was identified approximately 30 years later [27]. This breakthrough in the understanding of osteoclast differentiation and activation has come from the analysis of a family of biologically related tumour necrosis factor receptor (TNFR)/tumour necrosis factor (TNF)-like proteins: OPG, RANK and RANKL, which together regulate osteoclast function [23, 28, 29]. With the discovery of RANK, RANKL and OPG, a revolutionary understanding of osteoclastogenesis was born. The RANKL/OPG system is one of the major signalling systems that mediates bone remodelling.

Osteoblasts have RANKL on their surface and via contact-dependent signalling, they activate RANK on the surface of osteoclast progenitors, resulting in osteoclast maturation and bone resorption. Osteoblasts also produce OPG, which acts as a decoy receptor, binding RANKL, thereby preventing it from binding RANK. Additionally, osteoblasts secret soluble RANKL, which can bind excess OPG, reducing its inhibitory effects.

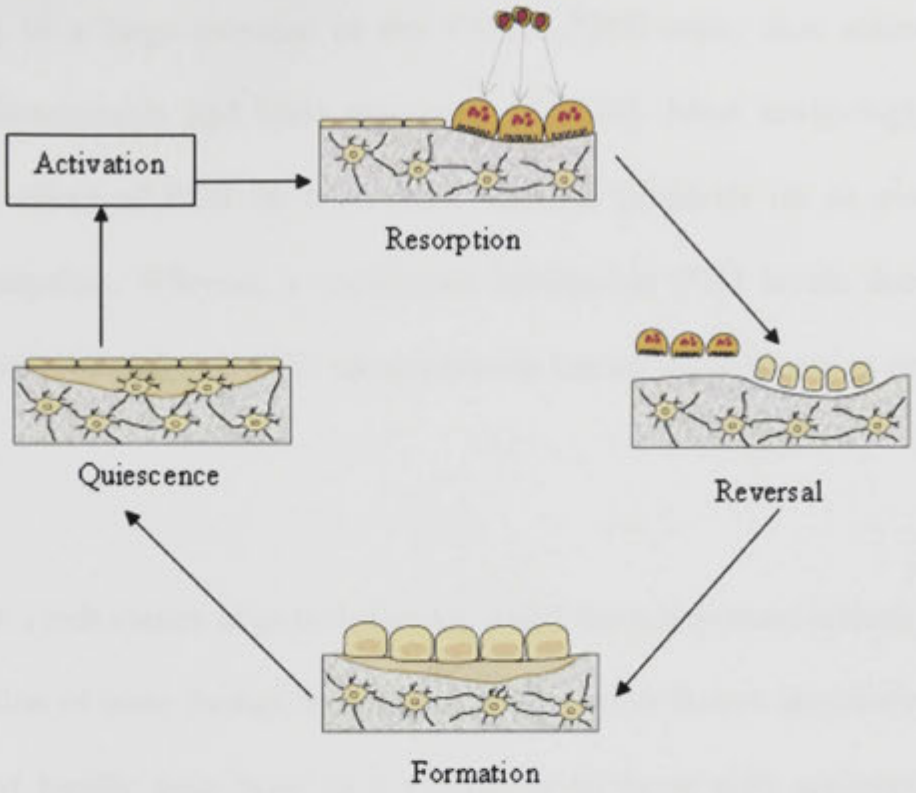

Figure 2.1: Schematic diagram of bone remodelling cycle

Bone remodelling is regulated by systemic hormones and local factors and it plays an important role in mineral homeostasis by providing access to stores of calcium and phosphate [4, 30]. PTH is the most important regulator of calcium homeostasis. It maintains serum calcium concentrations by stimulating bone resorption, increasing renal tubular calcium reabsorption and renal calcitriol production [21]. PTH is secreted in response to a drop in plasma Ca^{2+} levels. With the goal of maintaining plasma Ca^{2+}, PTH increases bone resorption to release Ca^{2+} stored in bone. Acting on osteoblasts, PTH alters the expression of RANKL and OPG,

leading to a large increase in the RANKL/OPG ratio, thus stimulating osteoclastogenesis and bone resorption [31, 32]. Most intriguingly, the overall effect of PTH on bone mass depends primarily on its mode of administration. Whereas a continuous increase in PTH levels decreases bone mass, intermittent PTH administration has an anabolic action on bone [7-11].

Bone is a rich source of growth factors, which have important actions in the regulation of bone formation and resorption. These factors are likely to be released locally from bone as it resorbs or by bone cells activated as a consequence of the resorption process. When it comes to the local regulation of bone remodelling at the cellular level, the RANK/RANKL/OPG pathway provides a clear picture of the control of osteoclastogenesis and coupling between osteoclastic and osteoblastic cells. It has been hypothesised that OPG and RANKL can be the mediators for the stimulatory or inhibitory effects of a variety of systemic hormones, growth factors, and cytokines on osteoclastogenesis. This is referred to as 'convergence hypothesis' in which the activity of the resorptive and antiresorptive agents 'converges' at the level of these two mediators, whose final ratio controls the degree of osteoclast differentiation, activation and apoptosis [33]. The TGF-β superfamily may be particularly important in the coupling that links bone formation to bone resorption. Bone resorption

leads to the release of active TGF-β from bone and exposure of osteoblast precursors to active TGF-β proliferation. The potential interactions between those factors are complex, but it will be essential to unveil them to understand the local control of bone remodelling.

After a thorough search through the literature, to the author's knowledge, only a few mathematical models thus far have been proposed regarding bone remodelling. Komarova et al. [17] presented a theoretical model of autocrine and paracrine interactions among osteoblasts and osteoclasts. Komarova et al. [18] also developed a mathematical model that describes the actions of PTH at a single site of bone remodelling, where osteoblasts and osteoclasts are regulated by local autocrine and paracrine factors. Potter et al. [19] proposed a mathematical model for PTH receptor (PTH1R) kinetics, focusing on the receptor's response to PTH dosing to discern bone formation responses from bone resorption. Lemaire et al. [6] incorporated detailed biological information and a RANK/RANKL/OPG pathway into the remodelling cycle; however, only the catabolic effect of PTH on bone is included in the model. Pivonka et al. developed an extended bone-cell population model based on the work of Lemaire et al. [6] to explore the model structure of cell-cell interactions theoretically [20], then investigated the role of the RANK/RANKL/OPG system in bone remodelling [15].

Incorporating the latest experimental findings and mathematical advances, a mathematical model of bone cell population dynamics at the cellular level [34] was developed and is discussed in Chapter 3. This model incorporates a different understanding of the RANK/RANKL/OPG pathway into the bone remodelling model, and is able to simulate PTH's anabolic effect observed in clinical trials. It is expected that the model concerning systemic and local regulation of bone remodelling will lead to new approaches in the diagnosis and treatment of skeletal disorders. In particular, this model will help to develop new therapeutic approaches at the molecular and cellular level based on the definition of abnormalities of the osteoblastic and osteoclastic lineage that lead to bone diseases such as osteoporosis.

2.2 Bone Remodelling under Mechanical Stimulus

Bone is a metabolically active tissue capable of adapting its structure and mass to the biological and mechanical environment and repairing damaged sections through remodelling. In particular, mechanical loading has significant influence on bone remodelling. Disuse or reduced loading due to long-term bed rest, cast immobilisation or microgravity conditions (such as experienced by astronauts in a space station or shuttle) induces obvious bone loss and mineral changes [35, 36], probably because of a lack of convective fluid flow in the canalicular network. Overuse or increased

loading such as that which is experienced with weight lifting exercises causes damage to bone tissue, which in turn stimulates bone remodelling and eventually achieves bone gain. One of the important roles of bone remodelling is to replace and repair damaged bone tissue continuously. Osteoclasts start resorbing bone in response to signals that are as yet unknown but may include direct damage to osteocytes via micro-cracks in the bone matrix.

The adaptive response of bone to mechanical loading is highly site-specific. This is clearly evident at the whole bone level, with only the bone that is actually loaded undergoing adaptation [37]. This concept is supported by much human research investigating skeleton health indices in athletes. This is especially noticeable in players of racquet sports such as tennis, as the bones of the racquet arm or dominant arm display significantly greater bone mineral density and cortical bone content than the non-playing arm [38, 39]. The site-specific depositing of new bone is functionally important. It puts newly formed bone where it is most required and increases bone strength in the resistible direction of loading, while not necessarily increasing the bone mass or density [38].

Experimental observations [39] show that in comparison with other organ systems, skeleton tissue is hypocellular and primarily composed of

extracellular matrix. Trabecular bone is a porous latticework of struts or plates of long bones, whereas cortical bone is a dense tissue of low porosity found in the diaphyses of long bones. The micro-structure of cortical bone is organised as a hierarchical arrangement of porosities, including a network of cellular spaces (lacunae), interconnections (canaliculi) and larger vascular (osteonal) canals. This spectrum of micro-architecture features implies the transformation of whole skeleton loading to localised changes in remodelling cycles.

The current understanding of bone remodelling under mechanical stimulus is primarily based on experimental results *in vivo* and *in vitro*. A recent report [40] suggested that osteocytes are the professional mechanosensory cells of bone and the lacuno-canalicular porosity is the structure that mediates mechanosensing. It was also shown that the dynamic mechanical load causes fluid flow in the lacuno-canalicular network [41]. The experiments *in vivo* indicated that the fluid flow serves as the physical mediator of mechanotransduction of osteocytes [42]. It is the fluid flow shear stress [43-46] that stimulates osteocytes to produce signalling molecules within minutes [47] such as prostaglandins (especially prostaglandin E2-PGE_2) [46-53] and nitric oxide (NO) [45, 49, 50, 54-56], which modulate the activities of osteoblasts and osteoclasts and furnish the transduction from mechanical stimuli to biochemical signalling [49]. NO is

a strong inhibitor of bone resorption and acts by inhibiting the RANKL expression in osteoblast precursors and increasing OPG production in OBA. Consequently, it can decrease the RANKL/OPG ratio, reduce recruitment of osteoclasts and elevate bone formation [57]. Alternatively, PGE_2 has strong osteogenic effects, which contribute to increases in osteoblasts differentiation from marrow stromal cells through the EP_4 receptor [48, 50, 58-60].

The literature demonstrates that Huiskes and his colleagues studied trabecular bone extensively, in aspects ranging from prediction of the development of trabecular architecture [61] to the effects of mechanical forces on the maintenance and adaptation of form in trabecular bone [62, 63]. Based on the trabecular bone remodelling theory developed by Weinans et al. [64], Li et al. [65] developed a new trabecular bone remodelling model that could simulate both the underload and overload resorption that often occur in dental implant treatments.

However, compared with trabecular bone, which represents 20% of the skeletal mass [21], even less theoretical work has been performed on cortical bone, which comprises 80% of the skeleton and has a high resistance to bending and torsion [21]. To the author's knowledge, only three papers that mathematically analysed cortical bone remodelling have

been published. Two of them [66, 67] presented a mathematical model at the cellular level, only introducing magnitude of force and number of osteocytes to consider production of NO and PGE_2. The third paper [68] proposed a macroscopic model to describe the time-dependent characteristics of the bone remodelling process, which is difficult to uncover in the microscopic mechanism.

In Chapter 4 of the thesis, inspired by current advances in bone biology experiments and based on [20], this study's cell population dynamics model is the first to incorporate several new features that can provide a deeper understanding of the mechanical bone remodelling mechanism at the cellular level, such as the osteocyte being the physical mediator of mechanotransduction and the extended Hill equation. Quantitative analysis using this model provides an insight into the effects of mechanical loading on cortical bone remodelling. From a control theory perspective, it is expected that there are several control mechanisms working in bone remodelling, which is a complex system. Based on the model developed in Chapter 4, an extensive parametric study of the control mechanism is performed in Chapter 5. The identified control mechanisms represented by parameter combinations are believed to be able to further the understanding of mechanical bone remodelling, and eventually help researchers to

develop combined pharmacological-mechanical therapies to cure bone loss diseases.

2.3 Bone Remodelling under PEMF

The use of electrical stimulation in bone dates back hundreds of years to when a patient with tibia non-union was successfully cured in 1812 [69]. In 1957, Fukuda and Yasuda discovered the piezoelectricity of bone. When bone is under compression, an electronegative potential is induced, while an electropositive potential is produced by bone under tension [70]. In 1982, Fukuda hypothesised that the growth of bone was regulated to best resist external force, and the controlling signal seemed to be the electric potential generated by shear piezoelectricity in collagen fibres and/or streaming potential in canaliculae [71]. Those two discoveries raised the possibility that the behaviour of bone cells could be affected by an externally applied electrical stimulus [72]. In 1982, Bassett was the first to use a pair of Helmholtz coils to produce a magnetic field across a fracture site and enhance oeteogenesis [73]. Since then, several major forms of electrical stimulation have been reported to produce osteogenesis, including capacitively and inductively coupled electro-magnetic and direct current fields [74, 75]. In addition, intense research into electrically induced osteogenesis on bone has been conducted using these methods both *in vivo*

and *in vitro* [34, 74, 76, 77]. The osteogenesis effect on bone could not only be used on long bone fractures [73], but could also be used in osteoarthritic joints [78] and osteoporotic bone [79], as well as in reversing femoral head necrosis and augmenting spinal fusions [80].

The biological process involved in the osteogenesis of bone caused by PEMF devices is bone remodelling. At the cellular level, bone remodelling is an organised process whereby osteoclasts remove old bone and osteoblasts replace it with newly formed bone. The osteoclasts and osteoblasts work in a coupled manner as a BMU, which is a mediator mechanism bridging individual cellular activity to whole bone morphology [81] and follows an activation-resorption-formation sequence [23]. After the discovery of the RANK/RANKL/OPG pathway [82], there is a clearer picture regarding the control of osteoclastogenesis and bone remodelling in general.

Bone cell differentiation and proliferation are important factors during bone remodelling and clinical PEMF devices have been shown to affect differentiation and proliferation of bone cells *in vitro* [83, 84]. Although it has been proposed that gap junctions, which are specialised intercellular junctions, are mediators of the PEMF-related cellular responses [83, 85-87], the underlying mechanism at the cellular level that regulates bone

remodelling under PEMF remains poorly understood due to the inconsistent or even contradictory results from experiments. For example, cell proliferation, as assayed by cell number and H-thymidine incorporation, has been reported to increase, decrease, and remain unaffected by PEMF exposure. Similarly, the production of alkaline phosphatise has been reported to either increase or decrease following PEMF exposure.

Although many *in vitro* and *in vivo* studies have been performed, the cellular mechanism by which PEMF affects bone remodelling is still elusive. To the author's knowledge, no study has been published about this research using a mathematical model. To clarify the underlying mechanism at the cellular level regulating PEMF's effect on bone remodelling, based on the cell population dynamics model [20] and the author's previous work [34, 88], the computational system biology method is used (see Chapter 6) with the purpose of better understanding bone remodelling under PEMF. The validated model generated using computational system biology can be used as a tool to reduce ambiguity as to the causes and effects in complex systems such as bone remodelling. In addition, it allows for the testing of various experimental and theoretical hypotheses 'in silico' [89], and more important pharmaceutical and clinical interventions on metabolic bone diseases.

2.4 Summary

In this chapter, bone remodelling was reviewed including the history of the term, the definition and the roles that PTH plays in the system. Bone remodelling under mechanical stimulus, one of the most profound stimuli, was reviewed in Section 2.2. Finally, bone remodelling under PEMF was reviewed in Section 2.3 along with the findings from experimental studies.

Chapter 3: A Theoretical Model for Simulating the Effect of Parathyroid Hormone on Bone Metabolism at the Cellular Level

PTH has been used clinically to treat bone loss diseases. Interestingly, when PTH is administered continuously, it causes bone loss; however, when PTH is applied intermittently, it causes bone gain in patients. The underlying mechanism of this phenomenon remains unclear although PTH has been approved by FDA as a therapy to treat osteoporosis. In this chapter, mathematical modelling of bone remodelling is developed then used to address this issue.

3.1 Model Development

The overall integrity of bone appears to be controlled by hormones and many other proteins secreted by both hemopoietic bone marrow cells and bone cells. There is both systemic and local regulation of bone cell function. PTH is the most important regulator of calcium homeostasis, which can stimulate bone formation when it is given intermittently and bone resorption when it is secreted continuously [90]. Moreover, PTH is currently involved in numerous clinical trials as an anabolic agent for the treatment of low bone mass in osteoporosis. Forteo (PTH 1-34) was

approved as an anabolic therapy by the FDA [91, 92]. The insulin-like growth factor (IGF) system is also important for skeleton growth, it is among the major determinants of adult bone mass through its effect on the regulation of both bone formation and resorption [93]. IGF-1 promotes chondrocyte and osteoblast differentiation and growth. It is also a pivotal factor in the coupling of bone turnover because it is stored in the skeletal matrix and released during bone resorption [94] and stimulates bone formation directly.

PTH receptors are largely expressed on the osteoblastic surface [95, 96]. Quasi-steady state levels of plasma PTH, by binding these receptors, stimulates the production of RANKL and inhibits the production of OPG by osteoblasts [96-98], which causes an increase in activated osteoclasts (AOC) numbers. A direct effect of PTH on osteoblasts that are anti-apoptosis has also been experimentally observed [95, 99].

As far as the local regulation of bone cell function is concerned, after the recent discovery of the RANK/RANKL/OPG system, there is a clearer picture regarding the control of osteoclastogenesis and bone remodelling in general. The main switch for osteoclastic bone resorption is the RANKL [100], a cytokine that is released by activated osteoblasts. Its action on the RANK receptor is regulated by OPG, a decoy receptor, which is also

derived from osteoblastic lineage-preosteoblasts. Osteoclast-to-osteoblast cross-talk occurs mostly through growth factors, such as transforming growth factor-β (TGF-β), which are released from the bone matrix during resorption.

The opposite phenotypes of OPG overexpression or with RANKL deletion mice (osteopetrosis) and OPG-deficient or with RANKL overexpression (osteoporosis) have led to the hypothesis that OPG and RANKL can be the mediators for the stimulatory or inhibitory effects of a variety of systemic hormones, growth factors and cytokines on osteoclastogenesis [21]. This is recently referred to as 'the convergence hypothesis' in that the activity of the resorptive and antiresorptive agents 'converges' at the level of these two mediators, whose final ratio controls the degree of osteoclast differentiation, activation and apoptosis [33].

The logical structure of the model is presented in Figure 3.1, which shows the simplified lineages of osteoblasts, osteoclasts and their interactions.

The previously described BMU comprises a collection of different cell types with different origins. The osteoclast teams that line the cutting cone are derived from hematopoetic stem cells residing mainly in the marrow and spleen. Osteoclastogenesis begins when a hematopoetic stem cell is

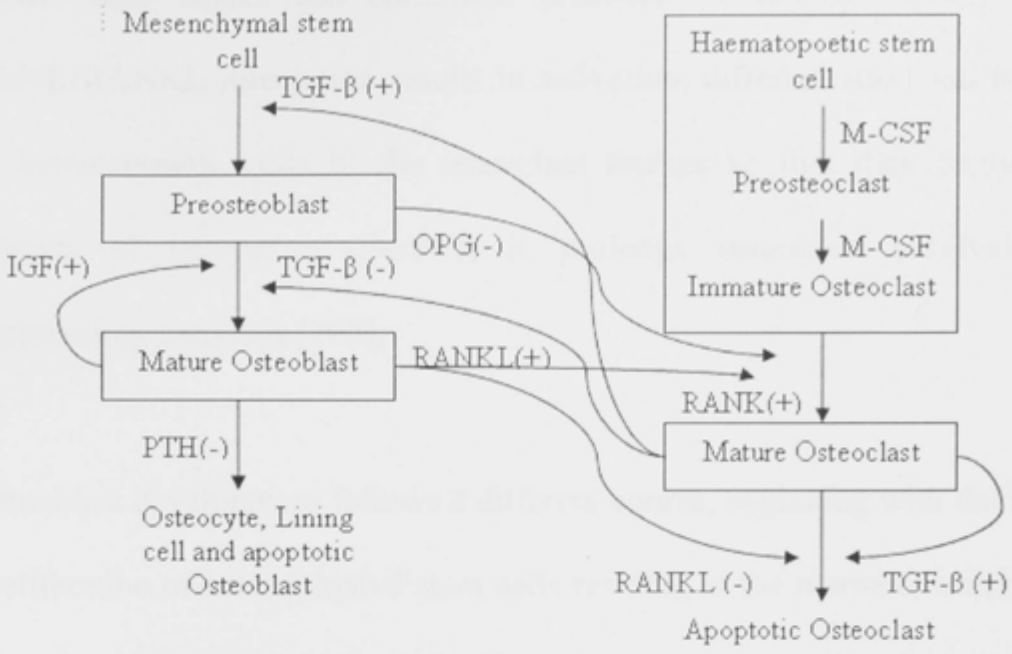

Figure 3.1: Schematic representation of the structure of the model [34]. The solid arrows with a (+) or (-) next to them represent a stimulatory or inhibitory action by the factor. The thin frame squares indicate types of cells that are included in this model

stimulated to generate mononuclear cells, which then become committed preosteoclasts and are introduced into the blood stream. This step requires expression of the Ets family transcription factor PU.1 and macrophage colony stimulating factor (M-CSF) [101, 102]. The circulating precursors exit the peripheral circulation at or near the site to be resorbed, and fuse with one another to form a multinucleated immature osteoclast. Fusion of the mononuclear cells into an immature osteoclast requires the presence of M-CSF and RANKL, a tumour-necrosis factor family member [103]. RANKL interacts with a receptor on osteoclast precursor called RANK. Further differentiation of the immature osteoclast into mature and AOC

occurs only under the continued presence of RANKL [104]. The RANK/RANKL interaction results in activation, differentiation and fusion of hematopoietic cells of the osteoclast lineage so that they begin the process of resorption. Further, it prolongs osteoclast survival by suppressing apoptosis [105].

Osteoblast development follows a different course, beginning with the local proliferation of mesenchymal stem cells residing in the marrow, which can also give rise to other types of cells such as myocytes, chondrocytes and adipocytes [106]. Proliferating precursors are pushed toward the preosteoblasts—responding osteoblasts (ROB) under the complex effects of specific factors such as PTH and TGF-β [106]. After further differentiation, ROB mature to AOB, which are responsible for bone formation. Eventually, osteoblasts die or transform to either lining cells or osteocytes [107].

Bone matrix is the largest source of TGF-β in the body [108]. TGF-β, as well as growth factors and specific components embedded in the bone matrix, are released by osteoclasts during bone resorption [109]. TGF-β's effect on osteoblasts is bi-directional, depending upon the state of maturation of the osteoblasts [6]. On one hand, TGF-β has the potential to stimulate osteoblast recruitment, migration and proliferation of osteoblast

precursors (meaning ROBs in this study's model) [110]. On the other, TGF-β inhibits terminal osteoblastic differentiation into AOBs [111]. TGF-β is also known to induce osteoclast apoptosis [108, 112].

3.2 Mathematical Formulation

In the model shown in Figure 3.1, cellular interactions are performed via the activation of cell receptors. The receptors bind with molecules secreted by other cell types called paracrine, with molecules secreted by the same cell called autocrine or with other transmembrance molecules via direct cell-to-cell contacts. The different cell types represented in the model respond to the activation of their receptors by producing new molecules, differentiating or dying [6]. The mathematical formulation of the model is primarily influenced by physiological events involving receptor binding and intracellular signalling modelling [113, 114]. Applying the law of mass action [6] that is used to describe the reactions of receptors and corresponding ligands including PTH (P) with its receptor (P_r), RANKL (L) with OPG (O), RANKL (L) with RANK (K) and IGF (I) with its receptor (IR).

$$\frac{dP}{dt} = S_P + I_P + \left(k_6 \cdot P_r \bullet P - k_5\left(R_T^P - P_r \bullet P\right)\cdot P\right)\cdot\left(B + R\right) - k_P \cdot P \tag{3.1}$$

$$\frac{dP_r \bullet P}{dt} = k_5\left(R_T^P - P_r \bullet P\right) - k_6 \cdot P_r \cdot P \tag{3.2}$$

$$\frac{dO}{dt} = p_O - k_1 \cdot O \cdot L + k_2 \cdot O \bullet L - d_O \tag{3.3}$$

$$\frac{dO \bullet L}{dt} = k_1 \cdot O \cdot L - k_2 \cdot O \bullet L \tag{3.4}$$

$$\frac{dL}{dt} = p_L - k_1 \cdot O \cdot L + k_2 \cdot O \bullet L - k_3 \cdot K \cdot L + k_4 \cdot K \bullet L - d_L \tag{3.5}$$

$$\frac{dK \bullet L}{dt} = k_3 \cdot K \cdot L - k_4 \cdot K \bullet L \tag{3.6}$$

The large dot above represents a receptor-ligand complex, while the small dot stands for the multiplication. The details of the meaning and values of the parameters and coefficients can be found in Appendix A.

This model proposes that the cell proliferation rate is proportional to the receptor occupancy [6]; this rule is applied to other types of cell responses besides cell proliferation. Moreover, the anti-proliferative cell responses are inversely proportional to the receptor occupancy. Consequently, the production rate of OPG (P_O) is down-regulated by PTH and up-regulated by TGF-β, the expression of P_O is:

$$p_O = K_O^P \cdot \left(\frac{1}{\pi_P} + \pi_C \right) R + I_O \tag{3.7}$$

where the proportion of occupied PTH receptor is:

$$\pi_P = \sqrt{\frac{P_r \bullet P}{R_T^P}} = \sqrt{\frac{\overline{P} + P^0}{\overline{\overline{P}} + P^s}} = \sqrt{\frac{I_P/k_P + S_P/k_P}{I_P/k_P + k_6/k_5}} \tag{3.8}$$

Applying the same rule as obtaining P_O, the following can deduced [6]:

$$p_L - d_L = r_L \cdot \left(1 - \frac{L + O \bullet L + K \bullet L}{K_L^P \cdot \pi_P \cdot B}\right) + I_L \tag{3.9}$$

$$L = \frac{K_L^P \cdot \pi_P \cdot B}{1 + k_3 K/k_4 + k_1 O/k_2} \cdot \left(1 + \frac{I_L}{r_L}\right) \tag{3.10}$$

$$O = \frac{K_O^P}{k_O \pi_P} R + \frac{I_O}{k_O} \tag{3.11}$$

The entering flow into the ROB compartment depends on the mesenchymal stem cells response to c binding. This response is represented by a proportionality relationship with the TGF-β receptor occupancy π_C:

$$D_R \cdot \pi_C = D_R \cdot \sqrt{\frac{C + C^0}{C + C^S}} \tag{3.12}$$

The outgoing flow of the ROB compartment is also the feeding flow to the AOB compartment. Under the influence of TGF-β and IGF, which inhibit and stimulate AOB production respectively:

$$D_B \cdot R \cdot \left(\frac{1}{\pi_C} + \pi_I \right) \tag{3.13}$$

RANK-RANKL binding promotes the differentiation of mesenchymal stem cells into AOC [6], the differentiation rate is proportional to the RANK occupancy ratio π_L:

$$D_C \cdot \pi_L = D_C \cdot \frac{K \bullet L}{K} \tag{3.14}$$

TGF-β induces osteoclast apoptosis via binding to specific receptors and under the influence of RANKL, this phenomenon is then represented as:

$$D_A \cdot (\pi_C - \pi_L) \cdot C = D_A \cdot \frac{C + C^0}{C + C^S} \cdot C \tag{3.15}$$

The equations governing the evolution of the number of cells in each compartment are simply balance equations [6], which means each cell compartment is fed by an entering flow and is emptied by the outgoing flow of differentiated or apoptotic cells:

$$\frac{dR}{dt} = D_R \cdot \pi_C - D_B \cdot R \cdot \left(\frac{1}{\pi_C} + \pi_I \right) \tag{3.16}$$

$$\frac{dB}{dt} = D_B \cdot R \cdot \left(\frac{1}{\pi_C} + \pi_I \right) - \left(k_B - \pi_P \right) \cdot B \tag{3.17}$$

$$\frac{dC}{dt} = D_C \cdot \pi_L - D_A \cdot \left(\pi_C - \pi_L \right) \cdot C \tag{3.18}$$

The rate of bone resorption and formation is assumed proportional to the numbers of osteoclasts and osteoblasts respectively:

$$\frac{dZ}{dt} = -m_1 \cdot C + m_2 \cdot B \tag{3.19}$$

where Z is total bone mass. Noting that at equilibrium, where the simulation starts, the numbers of AOB, AOC and ROB do not change with time; solving the following three equations can determine the initial values of B, C and R:

$$0 = D_R \cdot \pi_C - D_B \cdot R \cdot \left(\frac{1}{\pi_C} + \pi_I \right) \tag{3.20}$$

$$0 = D_B \cdot R \cdot \left(\frac{1}{\pi_C} + \pi_I \right) - \left(k_B - \pi_P \right) \cdot B \tag{3.21}$$

$$0 = D_C \cdot \pi_L - D_A \cdot \left(\pi_C - \pi_L \right) \cdot C \tag{3.22}$$

Values of model parameters and initial conditions of variables are listed in Appendix A. Model equations (3.16) to (3.19) are then solved using

numerical integration by a fourth Runge-Kutta algorithm implemented in Matlab. This is performed in the next section.

3.3 Results and Discussion

To demonstrate the tight coupling between osteoblast and osteoclast, this system was computationally perturbed by adding or removing specific cells such as AOB and AOC. The results are displayed in Figures 3.2–3.7.

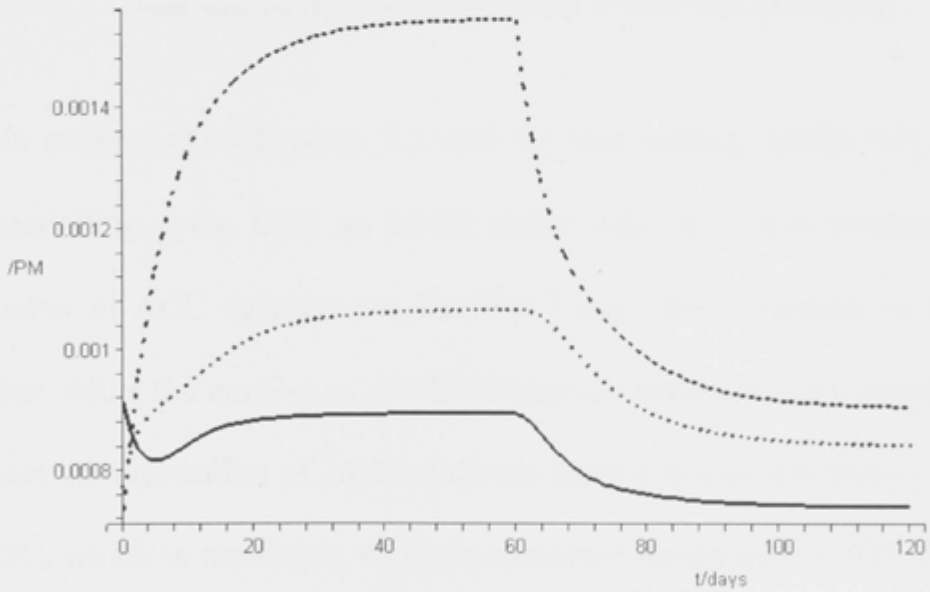

Figure 3.2: The AOBs are added at a constant (0.0001pM/day) rate for 60 days from start. From top to bottom, dash curves, dot curves and solid curves represent AOB, ROB and AOC respectively

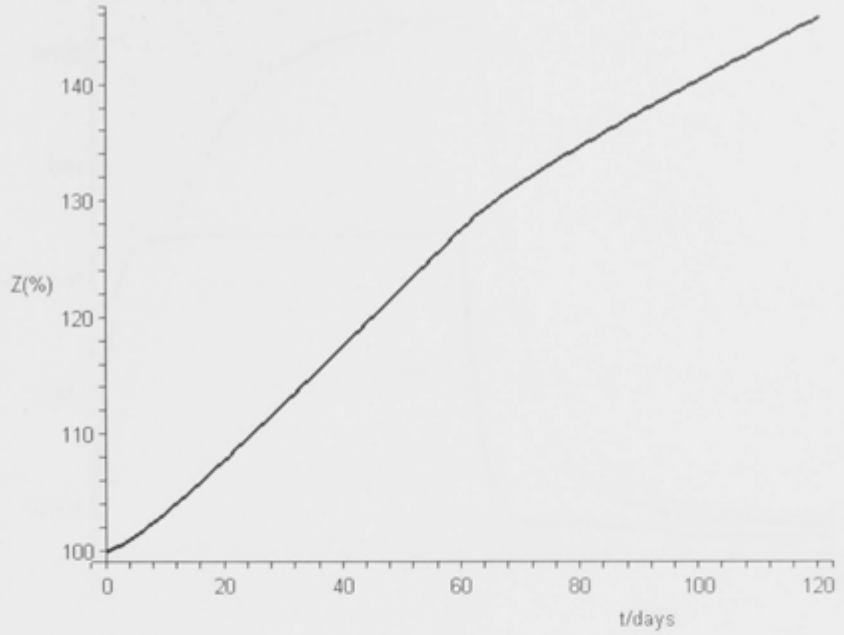

Figure 3.3: The effect of adding AOBs at a constant rate (0.0001pM/day) on bone mass. Changes in bone mass are expressed as a percentage of initial bone mass (100%)

It is evident from Figures 3.2 and 3.3 that adding AOBs can initiate a remodelling cycle from an initial stable state. It is also evident that the number of AOC decreases in the first 7 days, then increases to the initial value, while the number of AOB increases as expected. This means that the direct administration of AOBs does not have a strong stimulatory effect on AOC, which is consistent with experimental observation [103]. Figure 3.3 clearly displays that bone mass increases with the administration of AOBs and rises a little more slowly after AOB injection ceases.

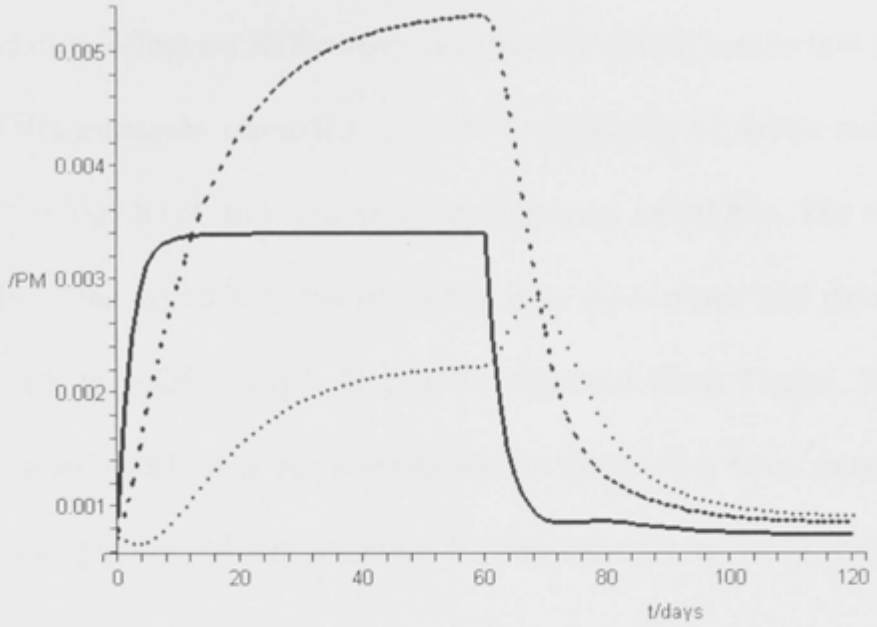

Figure 3.4: The AOCs are added at a constant rate (0.001pM/day) for 60 days from start

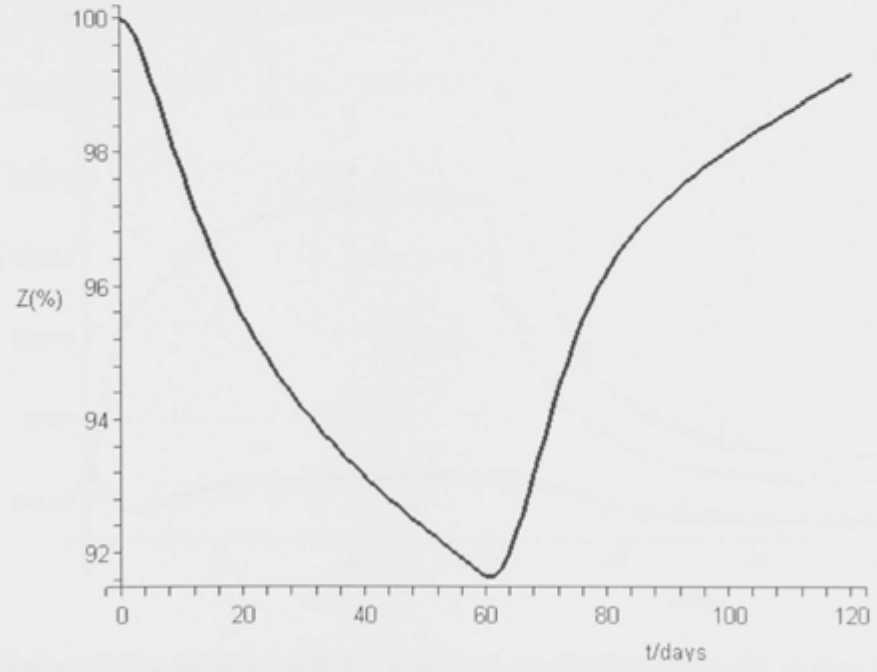

Figure 3.5: The effect of adding AOCs at a constant rate (0.001pM/day) on bone mass

Figure 3.4 shows that the administration of AOCs initiates a remodelling cycle and its number remains almost unchanged from approximately the

seventh day to the 60th day. It also exhibits a strong and immediate stimulatory effect on ROBs (top dash curve), which means that the number of ROBs increases immediately with the injection of AOCs and decreases to the initial level after stopping the injection of AOCs. The response of AOBs to the administration of AOCs is to slow down and delay until the injection of AOCs stops. It can be observed from Figure 3.5 that the amount of AOBs that are responsible for producing bone mass begins to increase quickly, which accounts for the increase of bone mass after the 60th day.

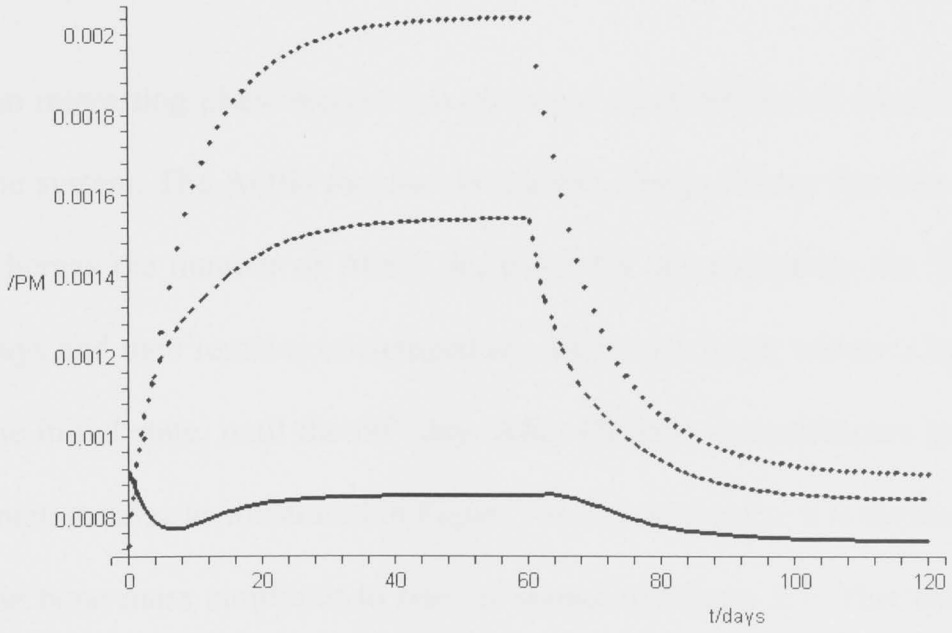

Figure 3.6: The ROBs are added at a constant rate (0.0001pM/day) for 60 days from start

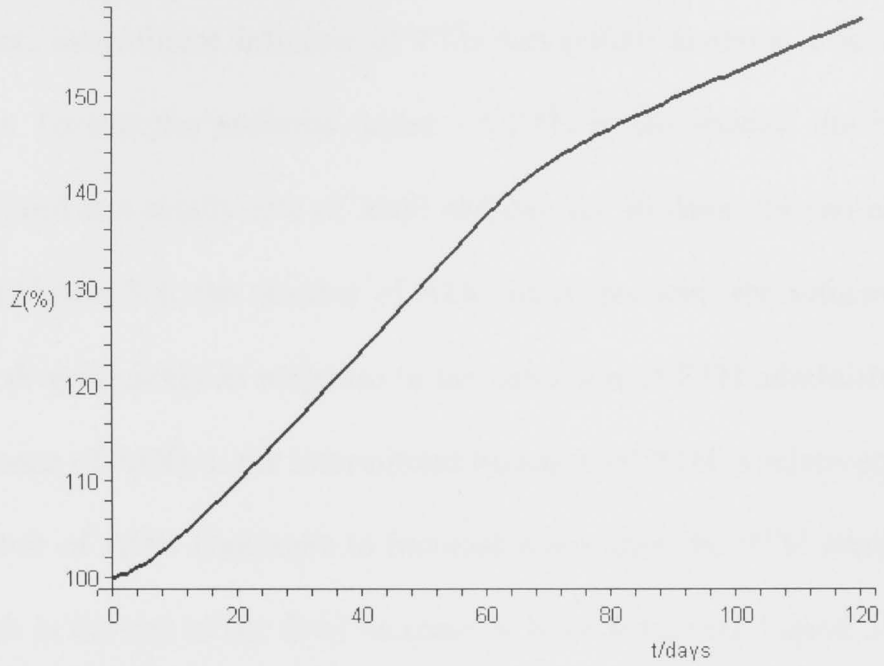

Figure 3.7: The effect of adding ROBs at a constant rate (0.0001pM/day) on bone mass

An interesting phenomenon was observed when ROBs are administered to the system. The AOBs increase in number along with an increase in ROB, whereas the number of AOCs decreases for approximately the first seven days and then remains unchanged at a particular level, which is lower than the initial state, until the 60^{th} day. After 60 days, it equilibrates to an even smaller value as illustrated in Figure 3.6. Consequently, it is reasonable that the bone mass continues to rise, as shown in Figure 3.7. This observation may have the potential to be exploited as a therapeutic target for metabolic diseases.

The only systemic hormone considered in the model is PTH. As mentioned earlier, intermittent infusion of PTH has potent anabolic effects on bone mass. To test the anabolic action of PTH in the model, the hormone is delivered at a steady rate of 3000 pM/day for 60 days. As can be observed from Figure 3.8, the number of AOC increases with the infusion of PTH, then drops quickly in response to the cessation of PTH administration. The response of AOB to the intermittent injection of PTH is relatively slow; the number of AOB continues to increase even after the PTH administration, which is the key to the final increase in bone mass (see Figure 3.9). This is in agreement with the experimental observation [91].

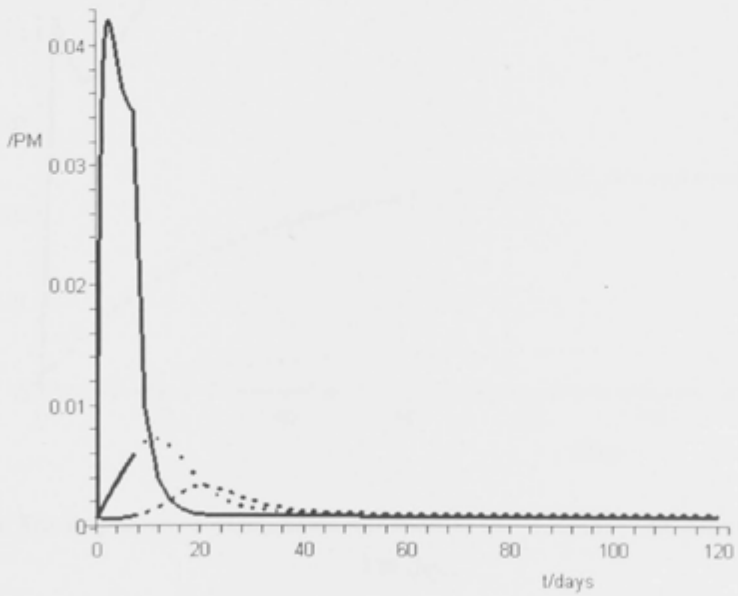

Figure 3.8: The responses of AOC, AOB and ROB to the intermittent administration of PTH for the first seven days

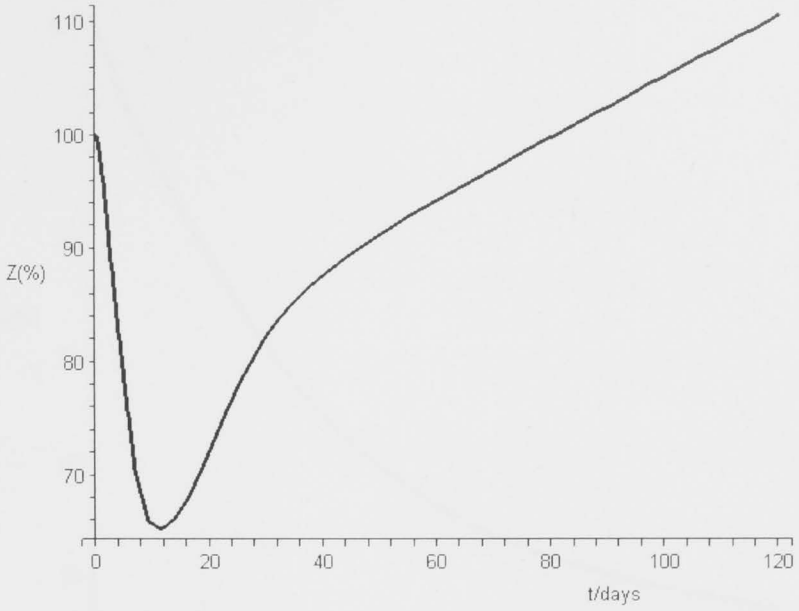

Figure 3.9: The effect of intermittent administration of PTH for the first seven days on bone mass

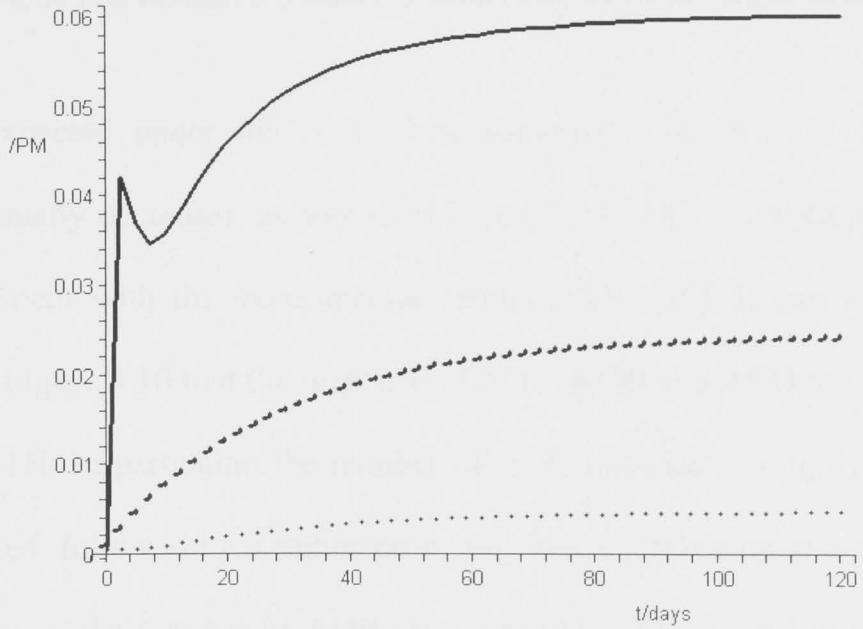

Figure 3.10: The responses of AOC, AOB and ROB to the continuous administration of PTH for 120 days

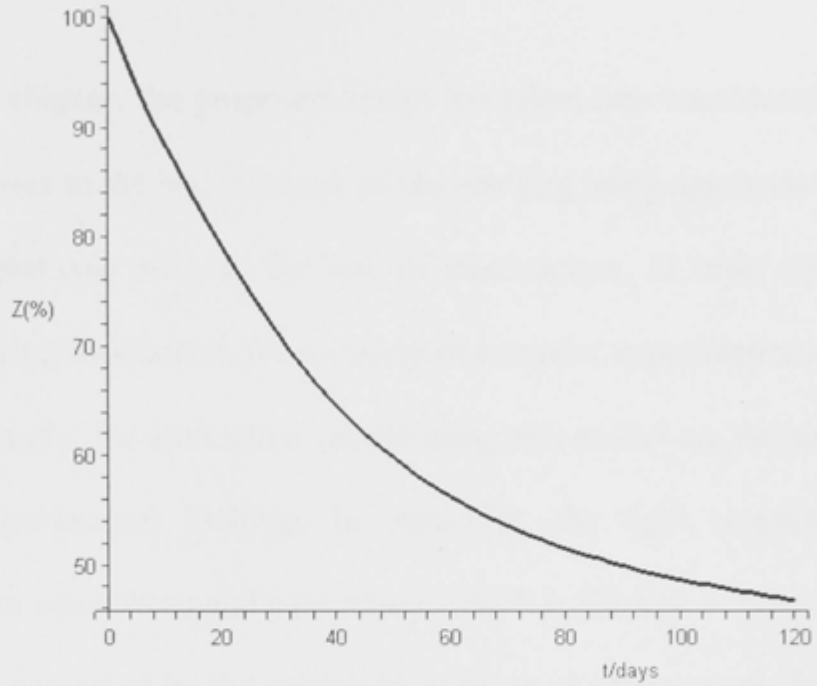

Figure 3.11: The effect of continuous administration of PTH for 120 days on bone mass

As expected under the continuous administration of PTH, bone mass continually decreases, as shown in Figure 3.11. This simulation is in good agreement with the experimental results [115, 116]. It can be observed from Figure 3.10 that the response of AOC, ROB and AOB are affected by the PTH. In particular, the number of AOC increases promptly as PTH is injected, followed by a minor drop, and then keeps rising at a slower rate. However, the number of AOB increases only slightly and at a very slow rate over the first 120 days. Through the direct stimulatory effect of TGF-β released by AOC, the number of ROB increases at a higher rate than the AOB.

3.4 Summary

In this chapter, the proposed model has taken into consideration the latest progresses in the bone biology of remodelling using appropriate parameters and equations, such as the law of mass action, in order to provide the underlying mechanism for a variety of complex experimental observations. Importantly, the simulation results using this model are consistent with all the experimental findings. In particular, the tight coupling behaviour between osteoblasts and osteoclasts, which is the key in bone remodelling, is well explained by the model. In addition, the theoretical simulation is in good agreement with the widely used PTH therapy for osteoporosis approved by the FDA.

Chapter 4: Bone Remodelling under Mechanical Stimulus

Mechanical loadings have profound influences on bone remodelling. Disuse or reduced loading due to long-term bed rest for example, experienced by fracture patients, induces obvious bone loss and mineral changes. Conversely, overuse or increased loading has the opposite effect; in tennis players, the bones of the racquet arm display significantly greater bone mineral density and cortical bone content than the non-playing arm. Although a large amount of general knowledge regarding the role of mechanical loading in bone remodelling has been gained from experiments, further quantitative understanding of the underlying mechanism is still needed.

4.1 Model Development

4.1.1 RANK/RANKL/OPG Signalling Pathway

The assumption that a coupling mechanism must exist between bone formation and resorption was first articulated in 1964 [22]. The exact molecular mechanism that describes the interaction between cells of the osteoblastic and osteoclastic lineages was identified over thirty years later [82]. Recent breakthroughs in the understanding of osteoclast

differentiation and activation have come from the analysis of a family of biologically related TNFR/TNF-like proteins: OPG, RANK and RANKL, which together regulate osteoclast function [23, 28]. With the discovery of RANK/RANKL/OPG, a revolutionary understanding of osteoclastogenesis was born.

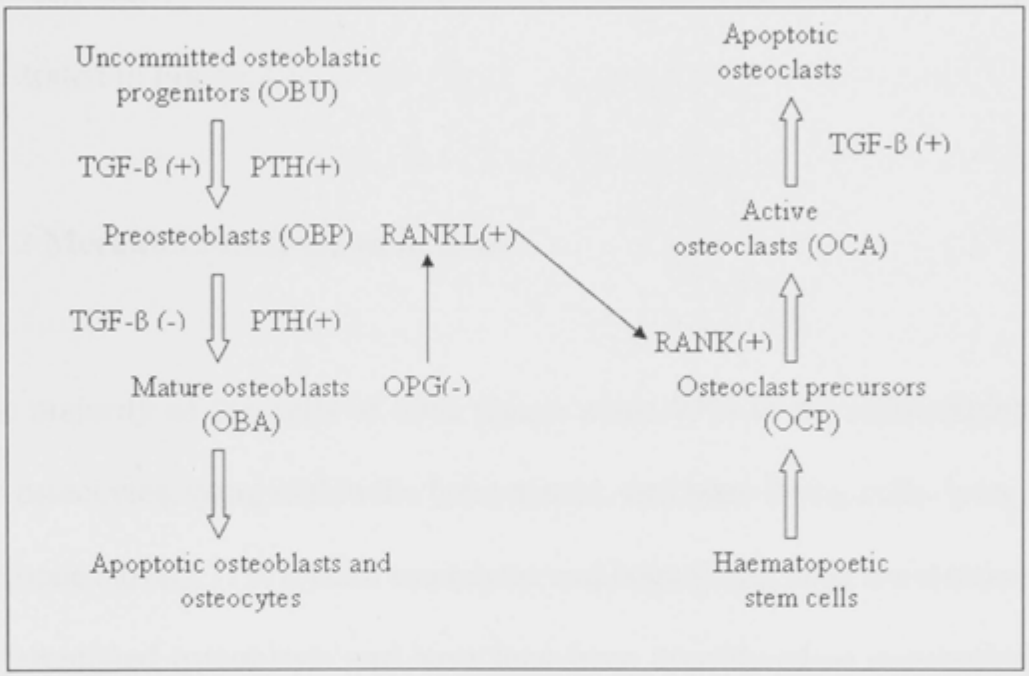

Figure 4.1: Illustration of the bone cell model with RANK/RANKL/OPG signalling pathway, PTH and dual action of TGF-β. A (+) or (-) symbol beside a factor represents a stimulatory or inhibitory action by the factor

As far as the local regulation of bone cell function is concerned, after the recent discovery of the RANK/RANKL/OPG system, there is a clearer overall picture regarding the control of osteoclastogenesis and bone remodelling. The main switch for osteoclastic bone resorption is the RANKL [100], a cytokine that is released by preosteoblasts [20]. Its action

on the RANK receptor is regulated by OPG, a decoy receptor, which is also derived from osteoblastic lineage-active osteoblasts [20]. Osteoclast-to-osteoblast cross-talk occurs mostly through growth factors, such as transforming growth factor-β (TGF-β), which are released from the bone matrix during resorption. The RANK/RANKL/OPG signalling pathway between osteoblasts and osteoclasts, PTH and the dual action of TGF-β is illustrated in Figure 4.1.

4.1.2 Mechanotransduction in Bone

The majority of the cells of bone tissue, some 95% in the adult skeleton, are osteocytes, lying within the bone matrix, and bone lining cells, lying on the bone surface [117]. Both osteocytes and bone lining cells are terminally differentiated osteoblasts and have long been considered as metabolically inactive, with limited roles in bone biology. However, osteocytes remain in contact with the bone surface cells and with neighbouring osteocytes via long slender cell processes that connect by means of gap junctions [118, 119]. Consequently, their abundance and connectivity make them a three-dimensional network for sensing mechanical strains. Recent work [40] demonstrates that osteocytes are the professional mechanosensory cells of bone and lacuno-canalicular porosity is the structure that mediates mechanosensing.

It has also become clear that dynamic mechanical load causes fluid flow in the lacuno-canalicular network [41]. Experiments *in vivo* [42] have indicated that this fluid flow serves as the physical mediator of the mechanotransduction of osteocytes and it is the fluid flow shear stress [43] that stimulates osteocytes within minutes to produce signalling molecules [47] such as prostaglandins (especially PGE_2) [46] and NO [45]. These modulate the activities of osteoblasts and osteoclasts, thus completing the transduction from mechanical stimuli to biochemical signals [49]. NO is a strong inhibitor of bone resorption and acts by inhibiting RANKL expression in osteoblast precursors, while increasing OPG production in OBA, thereby decreasing the RANKL/OPG equilibrium and leading to the reduced recruitment of osteoclasts and positive bone formation [57]. Alternatively, PGE_2 has strong osteogenic effects, which contribute to increases in osteoblast differentiation from marrow stromal cells through the EP_4 receptor [58].

4.2 Mathematical Model

The schematic diagram of the mathematical model structure of mechanical loading-caused bone remodelling is shown in Figure 4.2.

In biochemistry, the Hill equation is used to describe the fraction of the macromolecule saturated by a ligand as a function of the ligand concentration; it is used in determining the degree of cooperativity of the ligand binding to the enzyme or receptor. It was originally formulated by Hill in 1910 [120] to describe the sigmoidal O_2 binding curve of haemoglobin:

$$\theta = \frac{L^n}{K_d + L^n} = \frac{L^n}{K_A{}^n + L^n} \tag{4.1}$$

where θ is the fraction of ligand binding sites filled, L is the ligand concentration, K_d is the apparent dissociation constant derived from the law of mass action, K_A is the ligand concentration producing half occupation and n is the Hill coefficient.

In cell biology, cell responses such as differentiation, proliferation and apoptosis are all related to various ligand-receptor reactions of which some are stimulatory and others are inhibitory [20]. In modelling cell responses, the Hill equation is often used to describe the molecular input function. The activation (act) and repression (rep) forms of the Hill equation [121] for the production rate of a new cell or molecule are [20]:

$$f\left(x^*\right)=\beta\cdot\Pi_{act}=\frac{\beta x^*}{K_1+x^*} \tag{4.2}$$

$$f\left(x^*\right)=\beta\cdot\Pi_{rep}=\frac{\beta}{1+\frac{x^*}{K_2}} \tag{4.3}$$

where x^* is the active form of concentration x, which is a ligand that governs the production of a cell or molecule z through binding to its receptor on cell; β is the maximal production rate of z, and K_1 and K_2 are activation and repression coefficients. It has been assumed that the Hill coefficient equals one. In this model, the Hill equation is extended to the case in which two ligands (x and y) both affect the production of z through binding to their respective receptors on the same cell. Then the production rate of z can be expressed as:

$$f(x^*,y^*)=\beta\left(k_x\cdot\Pi^{x^*}_{act/rep}+k_y\cdot\Pi^{y^*}_{act/rep}\right) \tag{4.4}$$

where k_x and k_y are the relative influence of ligands x and y respectively, as a percentage in the cellular process, and $k_x+k_y=1$.

For convenience, in the following related formulation, the abbreviated forms are used for the factors involved. As in Figure 4.1, OBU was used

for uncommitted osteoblastic progenitors, OBP for preosteoblast, OBA for mature osteoblast, OCP for osteoclast precursor, OST for osteocyte and OCA for active osteoclast. RL is used for RANKL, RK for RANK, Tβ for TGF-β and P2 for PGE_2, while OPG, NO and PTH remain unchanged.

The equations governing the evolution of the number of osteoblastic and osteoclastic cells in each maturation stage are simply balance equations [6], which means that each cell stage is fed by an entering flow and is emptied by the outgoing flow of differentiated or apoptotic cells (see Figure 4.1). As a result, utilising Figure 4.1 and Figure 4.2, and based on the formulation in [20], the bone cell population dynamics can be formulated as follows:

$$\frac{dOBP}{dt} = D_{OBU} \cdot \left(k_{T\beta} \cdot \Pi^{T\beta}_{act,OBU} + k_{P2} \cdot \Pi^{P2}_{act,OBU} \right) - D_{OBP} \cdot OBP \cdot \Pi^{T\beta}_{rep,OBP} \quad (4.5)$$

$$\frac{dOBA}{dt} = D_{OBP} \cdot OBP \cdot \Pi^{T\beta}_{rep,OBP} - A_{OBA} \cdot OBA \quad (4.6)$$

$$\frac{dOST}{dt} = T_{OBA} \cdot OBA - A_{OST} \cdot OST \quad (4.7)$$

$$\frac{dOCA}{dt} = D_{OCP} \cdot \Pi^{RL}_{act,OCP} - A_{OCA} \cdot OCA \cdot \Pi^{T\beta}_{act,OCA} \quad (4.8)$$

where the subscript 'cell' in the input functions $\Pi^{molecule}_{act/rep,cell}$ means the cell type that a specific molecule binds to and 'molecule' denotes the ligand involved in a particular cell response. D_{OBU} is the differentiation rate of

uncommitted OB progenitors, D_{OBP} is the differentiation rate of preosteoblasts, D_{OCP} is the differentiation rate of preosteoclasts, A_{OBA} is the

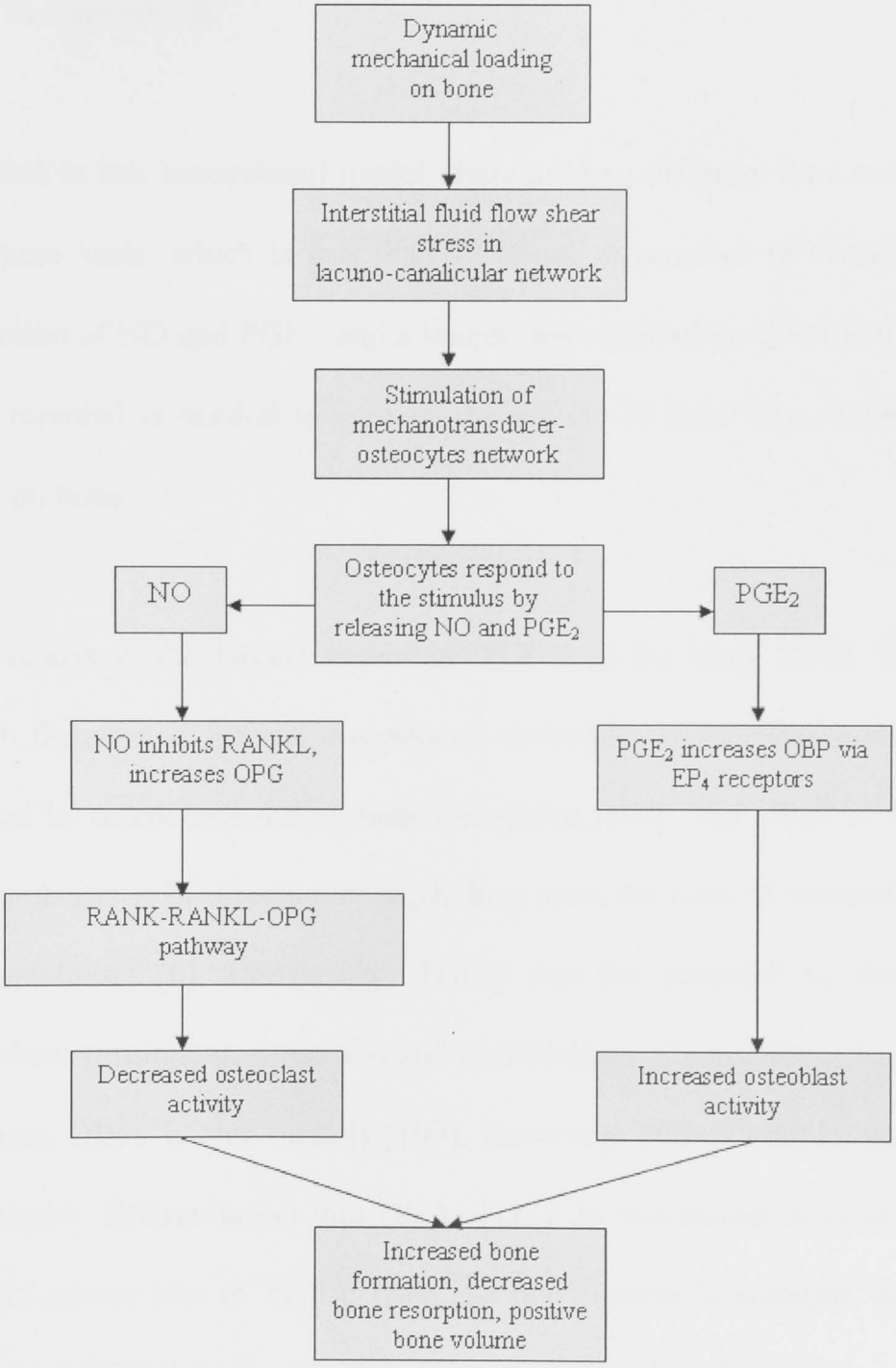

Figure 4.2: Schematic diagram of the mathematical model structure of mechanical loading causing bone remodelling at the cellular level

rate of elimination of OBA, A_{OCA} is the rate of elimination of OCA and A_{OST} is the rate of elimination of OST. All the constants and their values can be found in Appendix B.

Note that in this hierarchical model, there are two different time scales. A short time scale, which is less than 12 hours, is required to describe the production of NO and PGE_2, and a longer time scale of several months (up to 12 months) is needed to capture the effects of these two factors and others on bone.

Bone matrix is the largest source of TGF-β in the body [108]. TGF-β, growth factors and specific components embedded in the bone matrix are released by osteoclasts during bone resorption [109]. The effect of TGF-β on osteoblasts is bi-directional, depending upon the state of maturation of the osteoblasts [6]. Conversely, TGF-β has the potential to stimulate osteoblast recruitment, migration and proliferation of osteoblast precursors (meaning OBPs in this model) [109]. However, TGF-β inhibits terminal osteoblastic differentiation into OBAs [111]. In this model, it is assumed that the release rate of TGF-β from the bone matrix is constant, and the binding of TGF-β to its receptors is much faster than the changes in the number of OCA. Using the short time scale and a quasi-steady state assumption, the expression of TGF-β is [20]:

$$T\beta = \frac{\alpha \cdot K_{res} OCA + S_{T\beta}}{\tilde{D}_{T\beta}} \tag{4.9}$$

$S_{T\beta}$ is a source/sink term for TGF-β, α is the TGF-β content stored in bone matrix, K_{res} is the relative rate of bone resorption and $\tilde{D}_{T\beta}$ is the rate of degradation of TGF-β. Consequently, the activation and repression forms of TGF-β can be obtained by substituting Equation (4.9) into Equations (4.2) and (4.3):

$$\Pi^{T\beta}_{act,OBU} = \frac{T\beta}{K_{D1,T\beta} + T\beta} \tag{4.10}$$

$$\Pi^{T\beta}_{rep,OBP} = \frac{1}{1 + T\beta / K_{D2,T\beta}} \tag{4.11}$$

$$\Pi^{T\beta}_{act,OCA} = \frac{T\beta}{K_{D3,T\beta} + T\beta} \tag{4.12}$$

$K_{D1,T\beta}$ is the activation coefficient related to TGF-β binding on OBU, $K_{D2,T\beta}$ is the repression coefficient related to TGF-β binding on OBP and $K_{D3,T\beta}$ is the activation coefficient of TGF-β binding on OCA. Applying the law of mass action [6] used to describe the reactions of receptors and corresponding ligands, the formulations including PTH with its receptor,

RANKL with OPG and RANKL with RANK, can be found in the author's previous work [34].

In the model, PTH is used as a regulator of RANKL and OPG production. The assumption is that PTH endogenous production is constant, and $PTH_{\max} \gg PTH$ and PTH binding to its receptors on OBP and OBA is the same, to obtain PTH concentration and its according activation and repression functions as [20]:

$$PTH = \frac{\beta_{PTH} + P_{PTH,d}(t)}{\tilde{D}_{PTH}} \tag{4.13}$$

$$\Pi^{PTH}_{act,OBP} = \frac{PTH}{K_{D4,PTH} + PTH} \tag{4.14}$$

$$\Pi^{PTH}_{rep,OBA} = \frac{1}{1 + PTH/K_{D5,PTH}} \tag{4.15}$$

where β_{PTH} is the synthesis rate of systemic PTH, $P_{PTH,d}(t)$ represents an external PTH dosing term, $\tilde{D}_{PTH}$ is the rate of degradation of PTH, $K_{D4,PTH}$ is the activation coefficient for $RANKL_{eff}$ on OBP related to PTH binding and $K_{D5,PTH}$ is the repression coefficient for OPG production related to PTH binding on OBA. This thesis has already argued that NO stimulates the production of OPG expressed in OBA (see Section 4.1.2) while PTH down-

regulates OPG production of OBA [34]. Therefore, based on the work of [20] and using Equation (4.4), the OPG concentration can be expressed as:

$$OPG = \frac{\beta_{OPG} \cdot OBA \cdot \left(k_{PTH} \cdot \Pi_{rep,OBA}^{PTH} + k_{NO} \cdot \Pi_{act,OBA}^{NO}\right) + P_{OPG,d}(t)}{\frac{\beta_{OPG} \cdot OBA \cdot \left(k_{PTH} \cdot \Pi_{rep,OBA}^{PTH} + k_{NO} \cdot \Pi_{act,OBA}^{NO}\right)}{OPG_{\max}} + \tilde{D}_{OPG}} \tag{4.16}$$

where β_{OPG} is the production rate of OPG per OBA, k_{PTH} is the relative influence of PTH binding in production of OPG in OBA, k_{NO} is the relative influence of NO in production of OPG in OBA, $P_{OPG,d}(t)$ is an external OPG administration term, $\tilde{D}_{OPG}$ is the rate of degradation of OPG and $OPG_{\max}$ is the maximum possible OPG concentration. In addition, NO inhibits RANKL expression in OBP and PTH up-regulates the RANKL 'effective carrying capacity' of OBP [34]. Building on [20], the concentration of RANKL can be obtained:

$$RL = \left(\frac{R_{RL} \cdot OBP \cdot \Pi_{act,OBP}^{PTH}}{1 + K_{A1,RL} \cdot OPG + K_{A2,RL} \cdot RK}\right) \cdot \left(\frac{\beta_{RL} \cdot OBP \cdot \Pi_{rep,OBP}^{NO} + P_{RL,d}(t)}{\beta_{RL} \cdot OBP \cdot \Pi_{rep,OBP}^{NO} + \tilde{D}_{RL} \cdot R_{RL} \cdot OBP \cdot \Pi_{act,OBP}^{PTH}}\right) \tag{4.17}$$

R_{RL} is the maximum RANKL on OBP, $K_{A1,RL}$ is the association binding constant RANKL-OPG, $K_{A2,RL}$ is the association binding constant RANKL-

RANK, β_{RL} is the production rate of RANKL per OBP, $P_{RL,d}(t)$ is an external RANKL administration term and $\tilde{D}_{RL}$ is the rate of degradation of RANKL. Then the activation function of RANKL on differentiation of osteoclast precursor cells OCP can be obtained using Equations (4.2) and (4.17):

$$\Pi_{act,OCP}^{RL} = \frac{RL}{K_{D6,RL} + RL} \tag{4.18}$$

$K_{D6,RL}$ is the activation coefficient related to RANKL binding on OCP.

Now the unknown parameters are $\Pi_{act,OBA}^{NO}$, $\Pi_{rep,OBP}^{NO}$ and $\Pi_{act,OBU}^{P2}$:

$$\Pi_{act,OBA}^{NO} = \frac{NO}{K_{D7,NO} + NO} \tag{4.19}$$

$$\Pi_{rep,OBP}^{NO} = \frac{1}{1 + NO/K_{D8,NO}} \tag{4.20}$$

$$\Pi_{act,OBU}^{P2} = \frac{P2}{K_{D9,P2} + P2} \tag{4.21}$$

which directly relate to the concentrations of NO and PGE_2 caused by mechanical loading. Here, $K_{D7,NO}$ is the activation coefficient for OPG production on OBA related to NO, $K_{D8,NO}$ is the repression coefficient for

RANKL production on OBP related to NO and $K_{D9,P2}$ is the activation coefficient for OBU differentiation related to PGE_2.

Here, a loading regime is defined, which is also widely used in animal tests [38, 122]. The number of loading cycles during a training day is N, T_{rest} (h) is the rest time between loading bouts and n is the number of loading bouts per day. The amplitude (A [Pa]) and frequency (f [Hz]) of the interstitial fluid shear stress ($IFSS$) caused by the loading can be measured using the method in [123]. Therefore, the peak fluid shear stress rate R_{IFSS} (Pa-Hz) can be defined as [45]:

$$R_{IFSS} = 2\pi \cdot A \cdot f \tag{4.22}$$

The interstitial fluid flow is only formulated in terms of load, as can be observed in Equation (4.22), which means that being an intermediate variable it is not actually modelled. However, it is still worth stating the interstitial flow being the physical mediator of mechanotransduction by osteocytes. This completes the crucial transduction from mechanical stimuli to biochemical signals, which is concluded for the first time in the field after an extended literature review. This conclusion will help other researchers in the field understand the mechanism of mechanotransduction

of bone remodelling under mechanical stimulus and propose other possible models in the future.

To study the sensitivity of bone remodelling to mechanical loading, the mechanosensitivity of osteocytes (MS_{OST}) is defined with the frequency (f), number of loads per day (N), the rest time between bouts (T_{rest}) and the length of loading period (t). The experimental results indicate that loading will not have an effect on bone formation if its frequency is less than 0.5 Hz [124], and the sensitivity of bone changes little when the loading frequency becomes greater than 10 Hz [125]. However, [126] demonstrated that loading at frequencies up to 90Hz can still have an effect on bone formation. A logarithmic function is used to describe the relationship between frequency (f) and osteocyte mechanosensitivity (MS_{OST}):

$$MS_{OST} \propto \ln(f + 0.5),\ MS_{OST} \geq 0 \tag{4.23}$$

Data from [2] show that osteocyte sensitivity to mechanical loading is proportional to $1/(N+1)$:

$$MS_{OST} \propto \frac{1}{N+1} \tag{4.24}$$

which means that bone loses more than 95% of its mechanosensitivity after only 20 loading cycles. It can be imagined that osteocytes will regain their sensitivity after a period of rest between loading bouts. Data from [127] demonstrated the following relationship:

$$MS_{OST} \propto \left(2 - e^{-T_{rest}/\tau}\right) \tag{4.25}$$

where τ is a time constant approximately equal to 6h [127]. It is noted that 98% of bone mechanosensitivity is regained after 24h of rest.

Bone cells accommodate to routine loading, which means that bone mechanosensitivity drops as the loading period extends. Here, it is hypothesised that bone mechanosensitivity follows the relationship with loading period t (days):

$$MS_{OST} \propto e^{-t/T_{acc}} \tag{4.26}$$

where T_{acc} is the time constant describing the rate at which accommodation takes place, here assumed to be 24 days [128]. Making use of Equations (4.23) to (4.26), the osteocyte mechanosensitivity can be written as:

$$MS_{OST} = K_{MS} \cdot \frac{\ln(f+0.5)}{N+1} \cdot \left(2 - e^{-T_{rest}/\tau}\right) \cdot e^{-t/T_{acc}} \tag{4.27}$$

where K_{MS} is a proportionality constant.

In most animal experiments, the mechanical stimulation is applied no more than one hour per day and lasts for several months [38, 122]. The conclusions from animal studies are that limited benefit is derived from additional loading cycles above approximately 40 cycles per day [23], and it has been clear that NO and PGE_2 production appears within minutes [47] when the mechanical loading starts and finishes several hours after the loading stops [129]. In this chapter, the short time scale is used to describe NO and PGE_2 production caused by mechanical stimulus, which is assumed to be much faster than changes in the number of osteocytes (long time scale) in remodelling BMUs. Using Equations (4.22) and (4.27), and based on the experimental results [44, 45], the concentration changes of NO and PGE_2 during bone remodelling process are defined as:

$$\frac{dNO}{dt} = K_{NO} \cdot R_{IFSS} \cdot OST \cdot n \int_0^N MS_{OST}\, dN - \tilde{D}_{NO} \cdot NO \tag{4.28}$$

$$\frac{dP2}{dt} = K_{P2} \cdot R_{IFSS} \cdot OST \cdot n \int_0^N MS_{OST}\, dN - \tilde{D}_{P2} \cdot P2 \tag{4.29}$$

K_{NO} is the secretion rate of NO by osteocytes, n is the number of loading bouts per day, K_{P2} is the secretion rate of PGE_2 by osteocytes, $\tilde{D}_{NO}$ is the rate of degradation of NO and $\tilde{D}_{P2}$ is the rate of degradation of T PGE_2.

There are now six unknown variables, OBP, OBA, OST, OCA, NO and $P2$, and six independent equations (4.5), (4.6), (4.7), (4.8), (4.28) and (4.29). Using Matlab, this ODE system can be solved and the numerical results for each variable can be obtained.

Then, following the method used in the author's previous work [34], it is assumed that bone formation and resorption rates are proportional to the number of active bone cells, that is:

$$\frac{dBMC}{dt} = K_{for} \cdot \left[OBA(t) - OBA(0) \right] - K_{res} \cdot \left[OCA(t) - OCA(0) \right] \qquad (4.30)$$

Note that BMC is the bone mineral content (BMC) in percentage (%) and K_{for} and K_{res} are the relative bone formation and resorption rates. The simulation starts from a so-called 'steady-state' in which the values of model variables keep constants as initial values such as $BMC(t) = 100\%$, $OBA(t) = OBA(0)$ and $OCA(t) = OCA(0)$. Therefore, model Equations (4.5) to (4.8) become (4.31) to (4.34) respectively:

$$0 = D_{OBU} \cdot \Pi^{T\beta}_{act,OBU} - D_{OBP} \cdot OBP(0) \cdot \Pi^{T\beta}_{rep,OBP} \tag{4.31}$$

$$0 = D_{OBP} \cdot OBP(0) \cdot \Pi^{T\beta}_{rep,OBP} - A_{OBA} \cdot OBA(0) \tag{4.32}$$

$$0 = T_{OBA} \cdot OBA(0) - A_{OST} \cdot OST(0) \tag{4.33}$$

$$0 = D_{OCP} \cdot \Pi^{RL}_{act,OCP} - A_{OCA} \cdot OCA(0) \cdot \Pi^{T\beta}_{act,OCA} \tag{4.34}$$

By solving Equations (4.31) to (4.34) the initial values of the model variables in Table 4.1 can be obtained.

Table 4.1: Initial values of the model variables

Symbol	Unit	Value
OBA(0)	pM	0.2126991130e-3
OBP(0)	pM	0.8986869185e-5
OCA(0)	pM	0.2769166993e-3
OST(0)	pM	0.1029189256e-2

The mechanical stimulus is able not only to increase bone mass but also to improve bone strength by influencing collagen alignment as new bone is being formed by osteoblasts during bone turnover. Cortical bone tissue located in regions subject to predominantly tensile stresses has a higher percentage of collagen fibres aligned along the bone long axis [23]. In

regions of predominantly compressive stresses, collagen fibres are more likely to be aligned transverse to the long axis [130]. Evidently, this arrangement functionally improves bone tensile properties with more collagen fibres oriented in the longitudinal direction [131], whereas bone compressive properties are improved by transversely oriented collagens [132].

In an experiment by Robling et al. [38], cyclic mechanical loads were applied axially along the ulna of adult rats for 16 weeks. The results indicated that the pattern of bone formation caused by loading resembled the stress distribution, with more bone formation where the stresses were highest. Robling et al. tested the mechanical properties and BMC of the sample before and immediately after the experiment stopped. They compared and analysed the data (before and after the experiment) and found that the bone structure had improved, with a 69% increase in the second moment of area. Bone strength increased by 64% and the energy absorbed before fracture (BFE), which is of more practical interest to clinical practice, increased by 94%, while the BMC improved by only 7%. The results demonstrate that BMC is only one of the factors that contributes to bone strength and it is the BFE that is able to evaluate the effect of mechanical bone remodelling comprehensively. Consequently, using BMC to characterise bone remodelling, which has been used in the

existing mathematical models [6, 20], is not suitable to measure the effect of bone remodelling under mechanical stimulus and is therefore replaced by BFE in this model.

In this chapter, the BFE that the energy absorbed before fracture is used as a more appropriate standard to assess the significance of bone remodelling under mechanical stimulus. The BFE can be measured through experimentation; here, using the cell population dynamics model, it is proposed that the formulation of calculating BFE is:

$$\frac{dBFE}{dt} = K_{for} \cdot \left[OBA(t) - OBA(t_0) \right] - K_{res} \cdot \left[OCA(t) - OCA(t_0) \right] + K_{to} \cdot \sqrt{OBA(t) + OCA(t)} \tag{4.35}$$

where K_{to} is the relative rate of bone turnover. By substituting Equation (4.30) into Equation (4.35), it can be observed that BMC contributes to BFE:

$$\frac{dBFE}{dt} = \frac{dBMC}{dt} + K_{to} \cdot \sqrt{OBA(t) + OCA(t)} \tag{4.36}$$

It is proposed in the paper that BMC linearly contributes to BFE, which is the first term in Equation (4.36). The second term in Equation (4.36)

represents the contribution of bone turnover $(OBA(t)+OCA(t))$ to BFE in order to consider the structural effects of optimised collagen alignment to bone strength in newly formed bone. It is observed in the experiment [23, 130-132] that the contribution of bone turnover to the increment of bone strength diminishes as bone turnover increases. This thesis postulates that the square root of bone turnover contributes to the derivative of BFE to time. By applying the superposition principle, the relationship of BFE with BMC and bone turnover can be obtained in the form of Equation (4.36). The validity of the proposed equations will be tested in the following section. This equation might not be completely accurate but it fits the model well, which at least provides an alternative understanding as to the relationship between BFE, BMC and bone turnover.

In this chapter, all the parameter values used in the model are from experiments, and are not varied or modified to fit the experimental data. A cursory examination of the parameters indicates two classes. The first class corresponds to the physico-chemical parameters: $K_{D1,T\beta}$, $K_{D2,T\beta}$, $K_{D3,T\beta}$, $K_{D4,PTH}$, $K_{D5,PTH}$, $K_{D6,RL}$, $K_{D7,NO}$, $K_{D8,NO}$, $K_{D9,P2}$, T_{acc}, $K_{A1,RL}$, $K_{A2,RL}$, k_{NO}, k_{PTH}, k_{P2}, $k_{T\beta}$, β_{PTH}, β_{RL}, β_{OPG}, $\tilde{D}_{PTH}$, $\tilde{D}_{RL}$, $\tilde{D}_{OPG}$, $\tilde{D}_{T\beta}$, $\tilde{D}_{NO}$, $\tilde{D}_{P2}$ and τ. These parameters generally remain fixed under different physiological conditions, are easily measured through experiments and have values reported in the

literature. The second class of parameter value may fluctuate slightly if the larger physiological environment changes, these are: A_{OBA}, D_{OBU}, D_{OBP}, T_{OBA}, A_{OST}, D_{OCP}, A_{OCA}, K_{NO}, K_{P2}, K_{for}, K_{res}, K_{to}, RK, α, $OPG_{\max}$ and R_{RL}. The values for these parameters are averaged from a range of acceptable values for each parameter by checking the literature. In this paper, most parameter values are referred from previous models in the field [6, 20], the new parameter values are from [66, 67, 127, 128] (see details in Appendix B).

4.3 Numerical Investigation

Mathematical models of biology are a form of complex hypothesis. To test the validity of the hypothesis, external data is utilised, which has never been used in the creation of the model, to see if the model matches the experiments. Ideally, the model should be tested by as many experiments as possible to see if it is valid in a statistical sense. However, the reality is that due to the complexity of such experiments and suitability of the specific model, there are not many experiments available for comparison. This paper simulates five experiments of two different types in [122] and [38]. The future work will be to test the model using more experiments when available.

First, this study simulates the three experiments conducted in [122], in which 57 female Sprague-Dawley rats were randomised to three groups: group I, loading was applied for five weeks followed by ten weeks of time off (1×5); group II, loading was applied for five weeks followed by five weeks of time off and loading again for five weeks (2×5); and group III, loading was applied continuously for 15 weeks (3×5). An axial load was applied to the right ulna for 360 cycles per day, at 2 Hz, three days per week at 15 N. This study simulates the effects of three different loading schemes on BMC and compares them with the experimental results, which are shown in Figure 4.3.

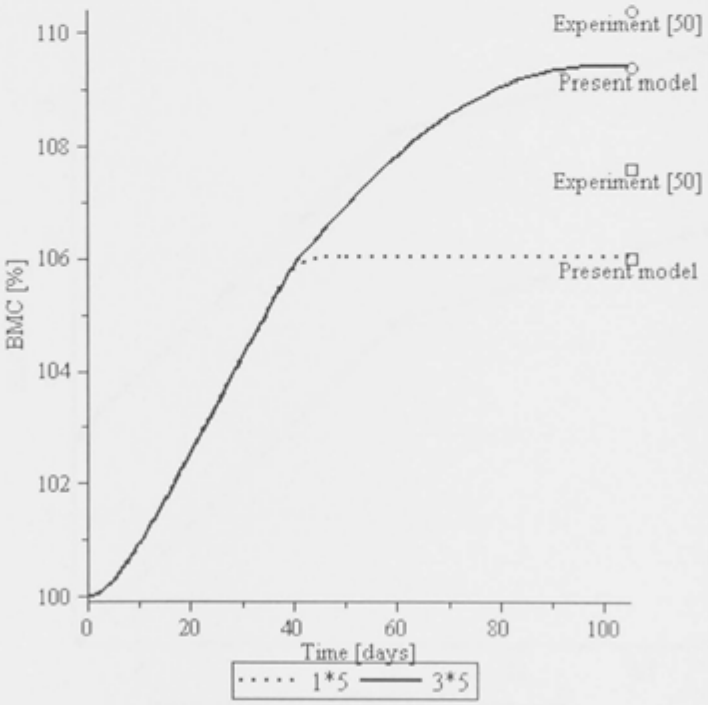

a

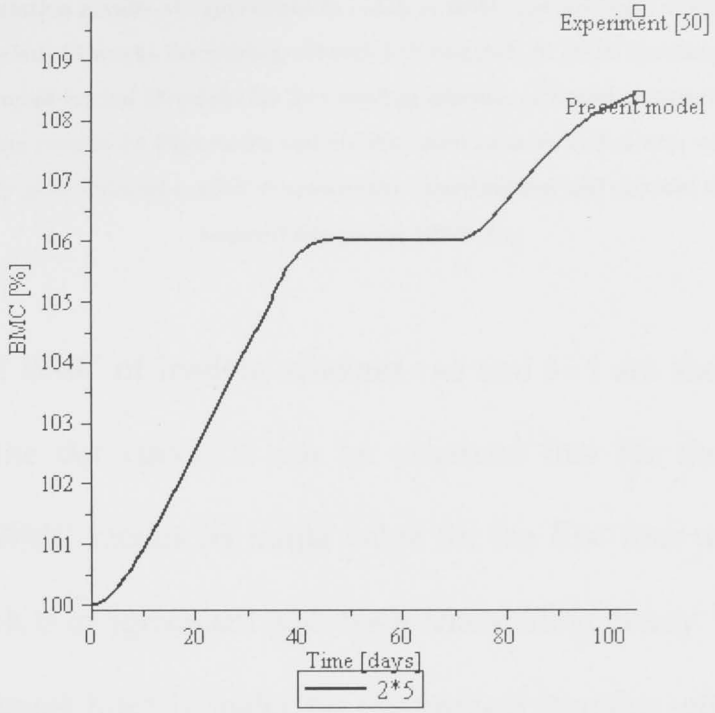
Experiment [50]
Present model
BMC [%]
109
108
107
106
105
104
103
102
101
100
0
20
40
60
80
100
Time [days]
2*5

b

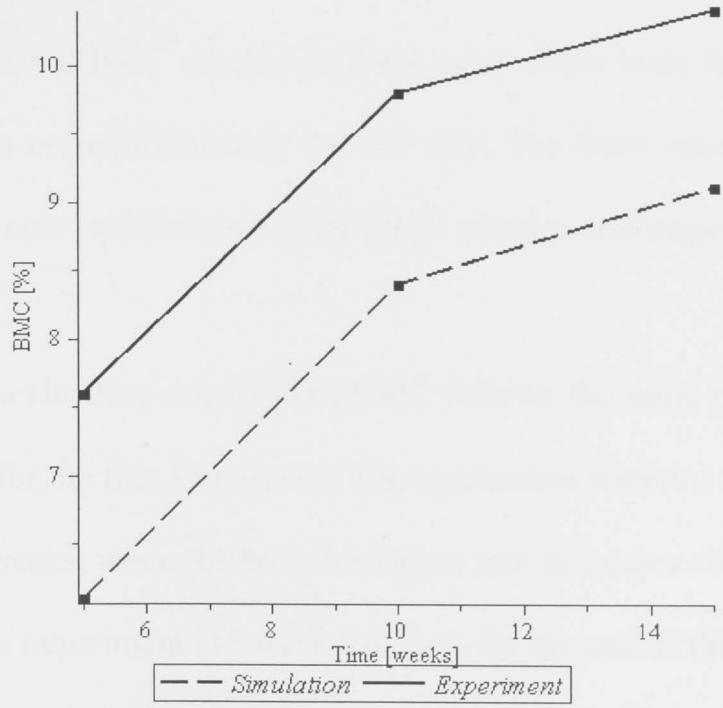
BMC [%]
10
9
8
7
6
8
10
12
14
Time [weeks]
Simulation
Experiment

c

Figure 4.3 Simulation results of experiment in [122]. a: BMC (percentage) dynamics during the experiment period, 15 weeks for loading scheme 1×5 and 3×5. b: BMC (percentage) dynamics during the experiment period 15 weeks for 2×5 loading scheme. c: Trend comparison of experiment and simulation results. In Figures 3a and 3b, the small squares and circles with the words 'Experiment [50]' and 'Present model' represent the experimental and current simulation results respectively on the 105th day

The trends of BMC of loading schemes 1×5 and 3×5 are shown in Figure 4.3a. From the dot curve, it can be observed that for the 1×5 loading scheme, the BMC retains its initial value for the first four to five days of loading, which is in agreement with bone remodelling theory. It then begins to increase almost linearly under the mechanical stimulus until the loading stops on the 35th day. Next, due to the accumulated NO and PGE_2, the BMC continues to increase but the bone formation rate (the gradient of curve) drops until BMC reaches its peak value when bone formation rate becomes zero on approximately the 50^{th} day. The bone remodelling then maintains its new equilibrium and the BMC remains unchanged.

During the 3×5 loading scheme, the BMC follows the same pattern as the 1×5 scheme for the first five weeks. The mechanical stimulus continues for another ten weeks, when the bone formation rate decreases slowly towards the end of the experiment (15 week loading). By the end of the experiment, each rat's BMC was measured and compared with its BMC before the experiment. The measured BMC increases (in percentage) are shown in the graph by the small circles and squares with the word 'Experiment [122]'.

They are 7.6% and 10.4% for the 1×5 and 3×5 schemes respectively. The simulation results are shown by the small circles and squares with the word 'Present model', predicting 6.1% and 9.1% increases for the 1×5 and 3×5 schemes respectively.

The pattern of BMC with respect to time (days) for the 2×5 loading scheme is plotted in Figure 4.3b. From day 0 to day 70 (five-week loading plus five-week rest), the BMC demonstrates exactly the same pattern as that in the 1×5 scheme, as expected. After a five-weeks break, the bone cells regain some mechanosensitivity and start to respond to the mechanical loading from day 71 as predicted. However, the graph shows clearly that the bone formation rate is less than that in the first five weeks, which implies that the bone mechanosensitivity has not fully recovered after five weeks of rest. Eventually, the experiment shows a 9.8% increase and the simulation predicts an 8.4% increase (see the small squares with the words 'Experiment [122]' and 'Present model', representing experimental and current simulation results).

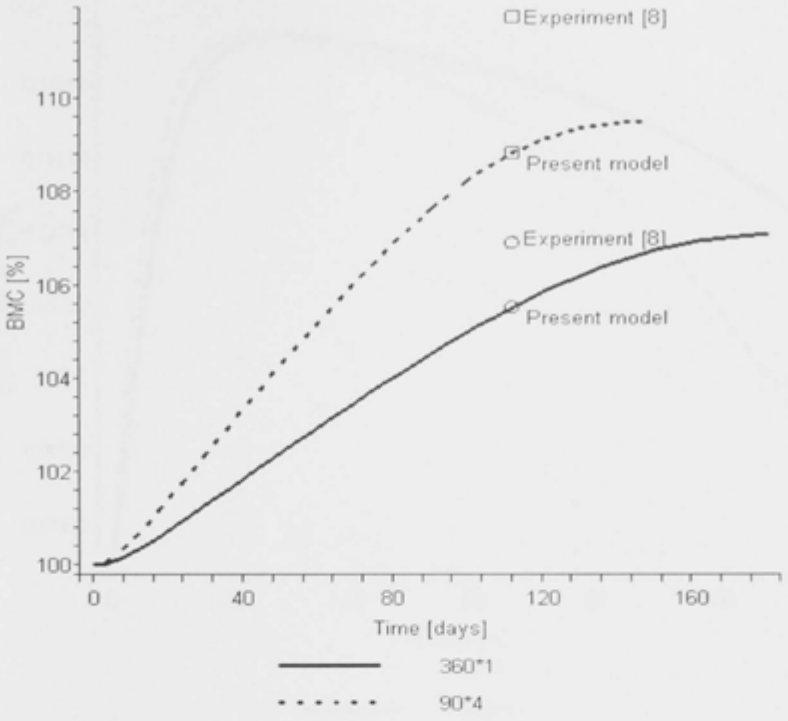
Experiment [8]
Present model
Experiment [8]
Present model
BMC [%]
110
108
106
104
102
100
0
40
80
120
160
Time [days]
360*1
90*4

a

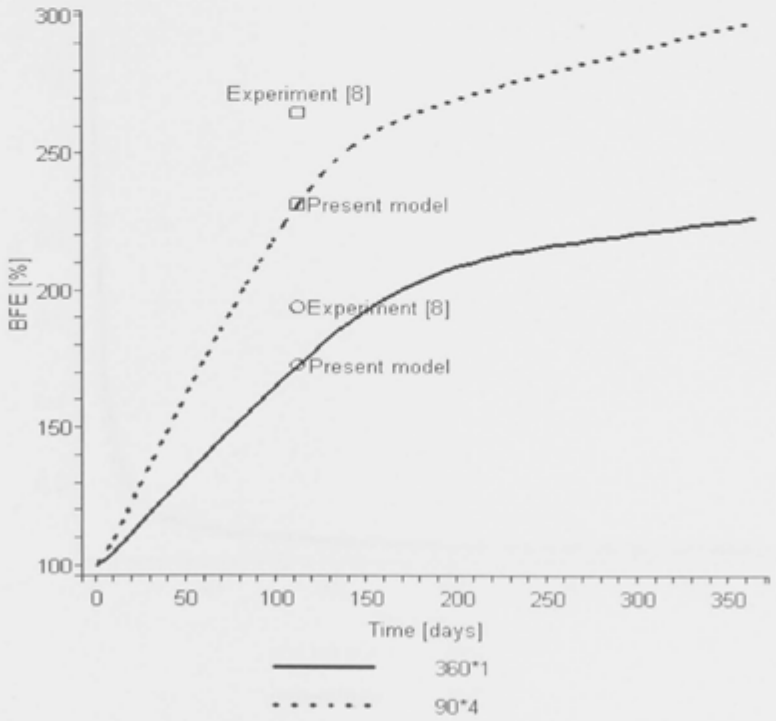
Experiment [8]
Present model
Experiment [8]
Present model
BFE [%]
300
250
200
150
100
0
50
100
150
200
250
300
350
Time [days]
360*1
90*4

b

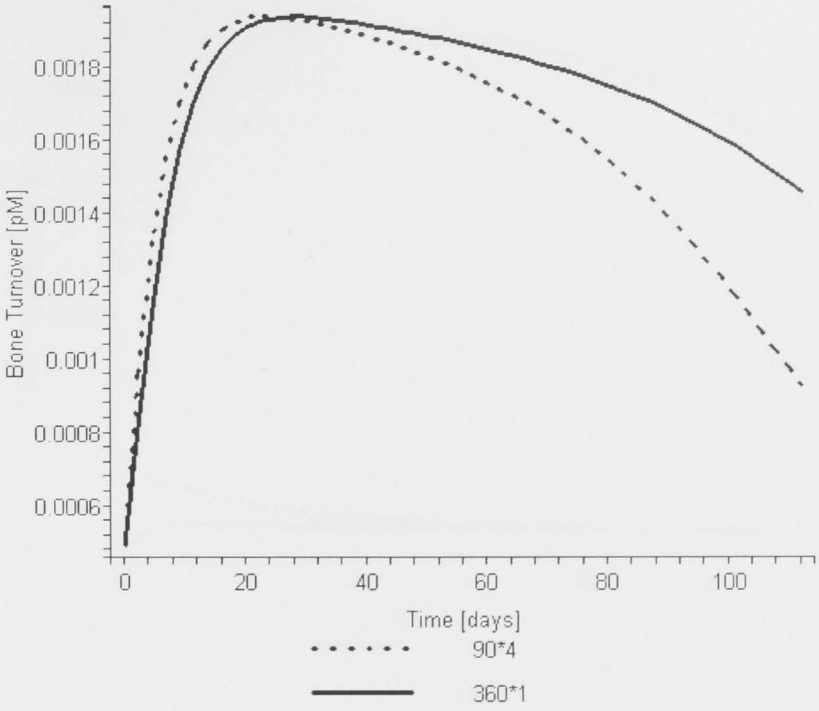
Bone Turnover [pM]
0.0018
0.0016
0.0014
0.0012
0.001
0.0008
0.0006
0
20
40
60
80
100
Time [days]
90*4
360*1

c

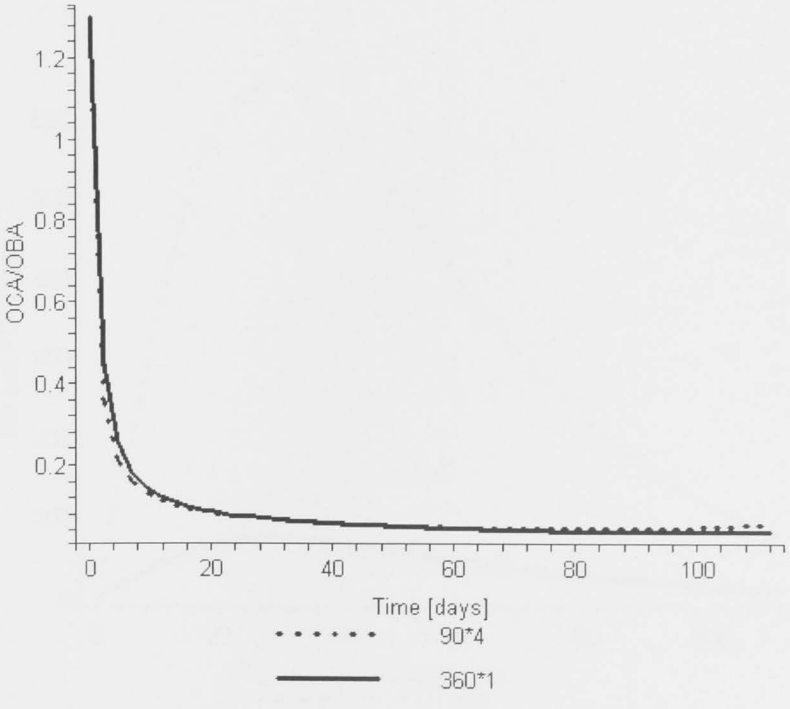
OCA/OBA
1.2
1
0.8
0.6
0.4
0.2
0
20
40
60
80
100
Time [days]
90*4
360*1

d

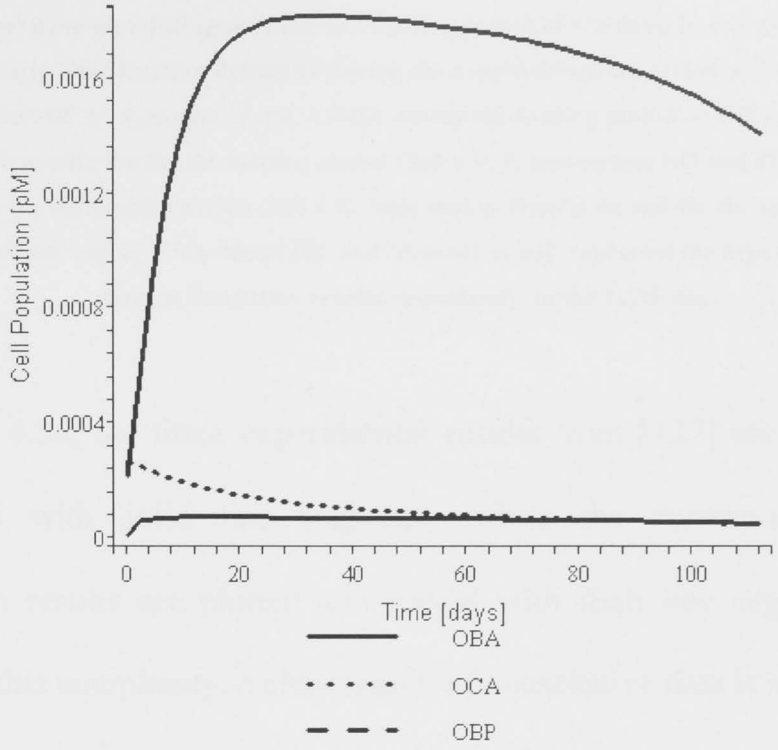
Cell Population [pM]
0.0016
0.0012
0.0008
0.0004
0
0
20
40
60
80
100
Time [days]
OBA
OCA
OBP

e

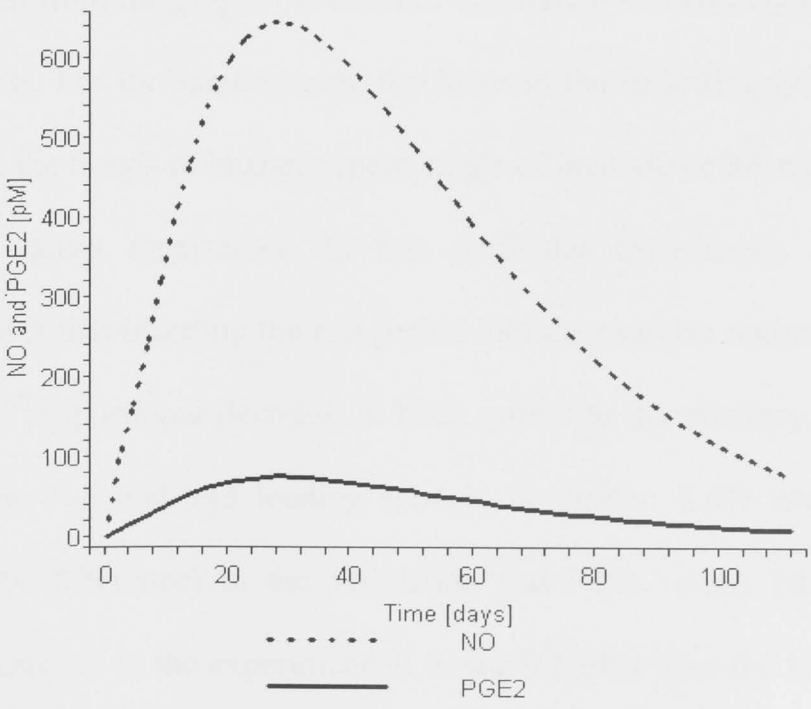
NO and PGE2 [pM]
600
500
400
300
200
100
0
0
20
40
60
80
100
Time [days]
NO
PGE2

f

Figure 4.4: Simulation results and comparison with those from the experiment in [38]. a: BMC (percentage) dynamics during the extended loading period of 170 days. b: energy (percentage) absorbed before bone fracture dynamics during the extended loading period of 365 days. c: bone turnover (OBA+OCA) dynamics. d: OCA/OBA during the loading period. e: OBA, OCA, OBP cell population dynamics during the loading period (360 x 1). f: messengers NO and PGE2 population dynamics during the loading period (360 x 1). Note that in Figures 4a and 4b, the small squares and circles with the words 'Experiment [8]' and 'Present model' represent the experimental and current simulation results respectively on the 112th day.

In Figure 4.3c, the three experimental results from [122] are plotted and connected with solid line segments, while the corresponding three simulation results are plotted and linked with dash line segments. In a model of this complexity, a close match of quantitative data is mostly based on the careful choice of parameters. However, what is more important is the ability of the model to predict the qualitative pattern of the response. As can be seen from the graph, the trend of simulation is inconsistent with the experiments. For the same reason, the focus in the following comparisons will be on the trends of changes (percentage of increase or decrease) rather than the values themselves. In this particular experiment, one clear conclusion is that inserting the rest period into the exercise regime does not result in a proportional decrease in bone gain. On the contrary, the bone gain in the 2×5 and 3×5 loading scheme is similar: 8.4% *versus* 9.1% (only 8.3% difference) in the simulation and 9.8% *versus* 10.4% (only 6.1% difference) in the experiment. It is much higher than the 1×5 loading scheme, which is 6.1% in the simulation and 7.6% in the experiment.

In another two experiments from [38], the right ulnas of 26 adult female rats were subjected to 360 load cycles/day, delivered in a haversine waveform at 17 N peak force, 2 Hz, three days per week for 16 weeks. Half of the rats (13) were administered all 360 daily cycles in a single uninterrupted bout (360×1); the other half were administered 90 cycles four times per day (90×4), with 3h rest time between bouts. At the end of intervention, the BMC and BFE were measured for each rat, and statistically analysed and compared with the non-loaded baseline control group. The simulation and experimental results are demonstrated in Figure 4.4.

Figure 4.4a shows the BMC dynamics during an extended loading period (more than 16 weeks) for the 360×1 and 90×4 loading schemes. BMC remains almost its initial value in the first week, which agrees with the bone remodelling cycle theory. The bone formation rate and BMC value for loading scheme 90×4 then become greater than the 360×1 loading scheme, which agrees with the experimental observation [38]. The bone formation rate in both cases diminishes as time elapses as can be observed from the graph. The study continues to draw the graph (which means the loading continues in the experiment) and it is interesting to note that it takes less time for BMC to achieve peak value in the 90×4 loading scheme

(150 days) than the 360×1 loading scheme (180 days). Unfortunately, there is no such experiment to verify this finding.

By the end of the experiment (16 weeks loading), the simulation shows a 5.5% and 8.8% increase of BMC for the 360×1 and 90×4 loading schemes respectively (see the small circles and squares with the words 'Present model' on the solid and dot curves), while the measured changes in experiments are 6.9% and 11.7% respectively [38] (see the small circles and squares with words 'Experiment [38]'). Again, the significance of the model is the ability to predict the trend of the increase percentage of BMC, which is 60% in simulation (from 5.5% to 8.8%) and compares well with the 69.6% (from 6.9% to 11.7%) in the experiment. The conclusion is significant to mechanical stimulus therapies because separating loading into short bouts such as 90×4 in this experiment not only achieves greater BMC but also uses less time compared with one long loading bout such as 360×1 in this case.

Using the newly proposed standard, the dynamics of the BFE in the extended loading period (365 days) are calculated in Figure 4.4b. The results show that the BFE increases in an almost linear way with respect to time (days) until approximately the 150th day in the 90×4 loading scheme and the 180th day in 360×1 loading scheme, which matches the timing when

BMC peaks in Figure 4.4a. The BFE then continues to grow linearly at a smaller rate, probably because the BMC stops increasing in both cases. The distinguishing difference between Figure 4.4a and Figure 4.4b is that the BFE continues to grow even after BMC stops increasing, which means that bone strength continues to benefit from mechanical stimulus although bone mass hardly gains. The simulation results indicate a 72.8% and 131.6% increase of BFE for 360×1 and 90×4 loading schemes respectively after a 16 week loading period (see the small circles and squares with words 'Present model' on the solid and dot curves). The measured changes in the experiment are 94% and 165% respectively [38] (see the small circles and squares with words 'Experiment [38]'). Once again the quantitative value itself of each increase in the loading schemes 360×1 and 90×4 is not the focus, what is more important is the trend of increase percentage, which is 80.8% (from 72.8% to 131.6%) in simulation. This compares well with 75.5% (from 94% to 165%) in experiments.

Comparing the increase of BMC in Figure 4.4a and BFE in Figure 4.4b, the present study shows that these small gains in BMC (from 5.5% to 8.8%) impart very large increases in BFE (from 72% to 131%) because the new bone formation is localised to the most mechanically needed sites. Consequently, it is possible to enhance fracture resistance significantly through mechanical loading such as exercises. Most exercise intervention

studies yield increases in BMC of only a few per cent at most. This might be a significant difference between pharmacologically-induced bone formation and loading-induced bone formation. For example, intermittent administration of PTH adds new bone mainly to the endocortical and trabecular surfaces, which makes relatively little contribution to resist bending [133]. Therefore, mechanical loading appears to be able to not only increase bone mass but also more importantly, spatially optimise the new bone formation to obtain maximal bone strength.

The dynamics of bone turnover (OBA+OCA) during the loading period for 360×1 and 90×4 loading schemes can be observed in Figure 4.4c. From the beginning to approximately the 30th day, both loading schemes cause bone turnover to increase quickly at a similar rate (with the value of 90×4 slightly greater than that of 360×1). Next, it is surprising that the bone turnover of 90×4 drops faster than the 360×1 loading scheme, which implies less bone cell activity in samples from the 90×4 loading scheme after bone cells become desensitised from the 30th day.

Figure 4.4d presents the ratio OCA/OBA dynamics in the loading period for 360×1 and 90×4 loading schemes, starting from $OCA/OBA\approx1.25$ in healthy adults, which is consistent with [6]. Both ratios show almost the same pattern and value: they drop quickly since the mechanical loading

applies, from 1.25 to about 0.1 on the 20th day, and then remain almost unchanged until the end of experiment, which predicts an osteogenic outcome after loading.

Using the model from this study, besides BMC, which can be measured easily through experimentation, insight can also be gained into the cellular dynamics of OBA, OCA and OBP during the loading period, which is difficult or perhaps impossible to measure during the experiment. Figure 4.4e shows the population dynamics of OBA, OCA and OBP during the 360×1 loading period. It can be observed that OBA reacts quickly to the mechanical loading with a large increase rate because of the positive effect of PGE_2 in the first 30 days. It then continues to drop slowly to the end of experiment, which is consistent with the decrease of PGE_2 in Figure 4.4f. Due to the inhibitory effect of NO on OCA through the RANK/RANKL/OPG pathway, the number of OCA drops slightly because of limited production and degradation. Under the stimulatory effect of TGF-β (limited because of the limited activity of OCA) and PGE_2, the OBP number increases slightly compared with the initial value and reaches almost the same value as OCA from day 60.

Figure 4.4f depicts the population dynamics of NO and PGE_2 in the 360×1 loading period. NO responds to the mechanical stimulus quickly, with a

rapid increase in number at a high rate. PGE_2 is also found to increase, which is consistent with the experimental results (see Section 4.2.1). Both numbers of NO and PGE_2 start to decrease from the 30^{th} day, probably because the bone cells accommodate the routine loading and become desensitised.

4.4 Summary

The proposed model is developed based on the following assumptions and limitations:

- The bone remodelling initiated by mechanical loading starts by programmed cell death in osteocytes [134]. It is still not known what factors cause osteocyte death. In the model, the osteocyte death at the beginning of bone remodelling is not taken into account.
- The amounts of uncommitted osteoblastic progenitors (OBU) and OCP are assumed very large, for which reason the numbers of OBU and OCP do not appear in the model.
- In the numerical simulations, the RANK concentration is fixed and this assumption could be relaxed in a future study.
- PTH endogenous production is considered as constant and not further regulated.

- The model is based on the so-called 'convergence hypothesis' that all the activities of resorptive or anti-resorptive agents converge at the level of RANKL and OPG through which the final effects are achieved.
- The change in bone shape, namely the macroscopic bone surface remodelling, is not included here, which explains why there is no spatial distribution in the current model.

In this chapter, a bone cell population dynamics model was proposed for cortical bone remodelling under mechanical stimulus. A few features of this model are proposed for the first time in this field:

- The osteocyte is proposed as the physical mediator of mechanotransduction in bone remodelling under mechanical stimulus and its population is introduced into the mathematical model;
- Three new rate equations describing changes of osteocytes, nitric oxide (NO) and prostaglandin E2 (PGE_2) are incorporated into this model;
- The effect of loading frequency on bone mechanosensitivity is investigated;

- The influence of the number of loading cycles during a loading day and the recovery of bone mechanosensitivity between two loading bouts as well as during the whole loading period are explored;
- The Hill equation is extended to two ligands binding to the same cell; and
- The good agreement between the simulations and the experimental results is very encouraging, and indicates the correct understanding of the mechanical bone remodelling at the cellular level.

Chapter 5: Parametric Study of Control Mechanism of Bone Remodelling under Mechanical Stimulus

From a perspective of control mechanism, it is believed that there are several control mechanisms working simultaneously in bone remodelling, which is a complex process. In this chapter, an extensive parametric study is conducted to investigate model parameter space related to cell differentiation and apoptosis, which can describe the fundamental cell lineage behaviours. After analysing all the combinations of 728 permutations in six model parameters, a small number of parameter combinations have been identified that can lead to physiologically realistic responses, which are similar to theoretically idealised physiological responses.

5.1 Mathematical Model Development

Following the same method used in the author's previous work, this study uses the abbreviated forms for the concentration (unit: pM) of factors involved, including: OBU for uncommitted osteoblastic progenitors; OBP for preosteoblast; OBA for mature osteoblast; OCP for osteoclast precursor; OCA for active osteoclasts; OST for osteocytes; RL for RANKL; RK for RANK; Tβ for TGF-β; and P2 for PGE_2. OPG, NO and PTH remain

unchanged. In the following section, the model developed in Chapter 4 is briefly recalled.

In modelling cell responses, the Hill equation is often used to describe the molecular input function. The activation (act) and repression (rep) forms of the Hill equation [121] for the production rate of a new cell or molecule are [20]:

$$f\left(x^*\right)=\beta\cdot\Pi_{act}=\frac{\beta x^*}{K_1+x^*} \tag{5.1}$$

$$f\left(x^*\right)=\beta\cdot\Pi_{rep}=\frac{\beta}{1+\frac{x^*}{K_2}} \tag{5.2}$$

where x^* is the active form of concentration, x is a ligand that governs the production of a cell or molecule (z) through binding to its receptor on cell, β is the maximal production rate of z, and K_1 and K_2 are activation and repression coefficients. It has already been assumed that the Hill coefficient equals one.

The equations governing the evolution of the number of osteoblastic and osteoclastic cells in each maturation stage are simply balance equations, which means each cell stage is fed by an entering flow and is emptied by

the outgoing flow of differentiated or apoptotic cells. As a result, the mechanical bone cell population dynamics can be formulated as follows:

$$\frac{dOBP}{dt} = D_{OBU} \cdot \left(k_{T\beta} \cdot \Pi^{T\beta}_{act,OBU} + k_{P2} \cdot \Pi^{P2}_{act,OBU} \right) - D_{OBP} \cdot OBP \cdot \Pi^{T\beta}_{rep,OBP} \quad (5.3)$$

$$\frac{dOBA}{dt} = D_{OBP} \cdot OBP \cdot \Pi^{T\beta}_{rep,OBP} - A_{OBA} \cdot OBA \quad (5.4)$$

$$\frac{dOST}{dt} = T_{OBA} \cdot OBA - A_{OST} \cdot OST \quad (5.5)$$

$$\frac{dOCA}{dt} = D_{OCP} \cdot \Pi^{RL}_{act,OCP} - A_{OCA} \cdot OCA \cdot \Pi^{T\beta}_{act,OCA} \quad (5.6)$$

the input functions $\Pi^{molecule}_{act/rep,cell}$ are derived using the Hill equations, whereby 'cell' means the cell type a specific molecule binds to, 'molecule' denotes the ligand involved in a particular cell response and 'rep/act' means repressor or activator function. For example, $\Pi^{T\beta}_{act,OBU}$, $\Pi^{T\beta}_{rep,OBP}$ and $\Pi^{T\beta}_{act,OCA}$ are the activator/repressor functions related to TGF-β binding to its receptors on osteoclasts and osteoblasts. D_{OBU} is the differentiation rate of uncommitted OB progenitors, D_{OBP} is the differentiation rate of preosteoblasts, D_{OCP} is the differentiation rate of preosteoclasts, A_{OBA} is the rate of elimination of OBA, A_{OCA} is the rate of elimination of OCA and A_{OST} is the rate of elimination of OST. All the model parameters and their values can be found in Appendix B.

Here, a loading regime is defined, which is also widely used in animal tests [3, 4]. The number of loading cycles during a training day is N, T_{rest} (h) is the rest time between loading bouts and n is the number of loading bouts per day. The amplitude (A [Pa]) and frequency (f [Hz]) of the interstitial fluid shear stress ($IFSS$) caused by the loading can be measured using the method in [123]. Therefore, the peak fluid shear stress rate R_{IFSS} (Pa-Hz) can be defined as [45]:

$$R_{IFSS} = 2\pi Af \tag{5.7}$$

To study the sensitivity of bone remodelling to mechanical loading, the mechanosensitivity of osteocytes (MS_{OST}) is defined with the frequency (f), number of loads per day (N), the rest time between bouts (T_{rest}), the length of loading period (t) and the time constant describing the rate at which accommodation takes place (T_{acc}). The osteocyte mechanosensitivity can be written as:

$$MS_{OST} = K_{MS} \cdot \frac{\ln(f+0.5)}{N+1} \cdot \left(2 - e^{-T_{rest}/\tau}\right) \cdot e^{-t/T_{acc}} \tag{5.8}$$

where K_{MS} is a proportionality constant.

Using Equations (5.7) and (5.8), and based on the experimental results [44, 45], the concentration changes of NO and PGE_2 during the bone remodelling process can be defined as:

$$\frac{dNO}{dt} = K_{NO} \cdot R_{IFSS} \cdot OST \cdot n \int_0^N MS_{OST} dN - \tilde{D}_{NO} \cdot NO \tag{5.9}$$

$$\frac{dP2}{dt} = K_{P2} \cdot R_{IFSS} \cdot OST \cdot n \int_0^N MS_{OST} dN - \tilde{D}_{P2} \cdot P2 \tag{5.10}$$

K_{NO} is the secretion rate of NO by osteocytes, n is the number of loading bouts per day, K_{P2} is the secretion rate of PGE_2 by osteocytes, $\tilde{D}_{NO}$ is the rate of degradation of NO and $\tilde{D}_{P2}$ is the rate of degradation of T PGE_2. In the end, this study defines the system output as the BMC and BFE:

$$\frac{dBMC}{dt} = K_{for} \cdot \left[OBA(t) - OBA(0)\right] - K_{res} \cdot \left[OCA(t) - OCA(0)\right] \tag{5.11}$$

$$\frac{dBFE}{dt} = K_{for} \cdot \left[OBA(t) - OBA(0)\right] - K_{res} \cdot \left[OCA(t) - OCA(0)\right] + K_{to} \cdot \sqrt{OBA(t) + OCA(t)} \tag{5.12}$$

Note that BMC and BFE are in percentage (%), K_{for}, K_{res} and K_{to} are the relative bone formation rate, bone resorption rate and the relative rate of bone turnover respectively. This study starts the simulation from a so-

called 'steady-state' in which BMC and BFE are 100%, $dBMC/dt = 0$, $dBFE/dt = 0$, correspondingly $OBA(t)$ is $OBA(0)$ and $OCA(t)$ is $OCA(0)$.

5.2 Parametric Study of the Control Mechanism

In normal adults, there is a balance between the amount of bone resorbed by osteoclasts and the amount of bone formed by osteoblasts [23]. In this complex process, bone is remodelled by groups of cells derived from different sources, usually called the BMUs [24], that follow an activation-resorption-formation sequence event. The BMU is a mediator mechanism, bridging individual cellular activity to whole bone morphology [81], which is sensitive to any changes in the bone cell microenvironment. As a result, it is expected that any modification to the component of BMU will have a significant effect on its output behaviour.

In this paper, perturbations will be applied to the mechanical bone remodelling system that is in a steady state, by down- and up-regulating its six differentiation and apoptosis rate parameters DF_{obu}, DF_{ocp}, DF_{obp}, A_{oba}, A_{oca} and A_{ost}. In this case, there are six different parameters and each parameter could be either up- or down-regulated. Using a simple combination theory, the number of permutation is calculated

as $728 = \sum_{i=1}^{6} C_6^i \cdot 2^i$. Next, in order to investigate the system behaviour for a wide range of changes, the exponentially changed factor is now applied (1.5^{ex}) to each of the six differentiation and apoptosis rate parameters, whereby the exponent *ex* ranges from -10 to 10 in step increases of 0.5. The assessment of each of the parameter combinations to the system behaviour is chosen as the responses of BMC and BFE, which are sampled on 100th day to stand for the maximum change. Using Matlab (see the Matlab code in Appendix D.1), all of the 728 graphs can be plotted. Then, by summarising all of the plots of BMC and BFE *versus* variation of exponent *ex*, it is found that there are three subsets of curves, which are plotted in Figure 5.1.

Figure 5.1a and Figure 5.1b show an exponential increase and decrease of BMC and BFE respectively, for increasing the model parameter exponentially (exponent *ex* from -10 to 10). This type of behaviour is considered as physiologically unrealistic from a biological perspective and is obtained for quite a large range of model parameter combinations. Conversely, Figure 5.1c represents the other extreme, whereby only minor changes of BMC and BFE occur during the entire range of parameter variation. These three types of response curves are excluded from further

analysis because they do not provide an effective control mechanism for BMC and BFE.

In [20], the 'idealised' regulatory response by functionally active BMUs is discussed. As was stated earlier, the bone remodelling system starts from a steady state in which it can be identified that $\Delta BMC = 0$, $\Delta BFE = 0$, and concentrations of various hormones, growth factors that cause initial values of differentiation and apoptosis rates in BMUs. In order to respond to minor changes in concentrations, it is expected that BMUs should be rather insensitive to these fluctuations. Therefore, from Figure 5.2, it can be recognised that point A is the threshold concentration, which means any change of model parameter underneath A causes no change in BMC (/BFE). In addition, a region around the usual operation status of BMUs should be found with relatively small gradients of changes in BMC (/BFE) in response to changes in differentiation rates (regions C–D and D–E in Figure 5.2), with larger gradients for larger changes in differentiation rates (region E–F in Figure 5.2). It is expected that this response in BMC (/BFE) change will remain limited if the differentiation rates increase significantly (region further after point F in Figure 5.2) because the unlimited rise of BMC (/BFE) is not physiologically realistic. Conversely, it is expected that the rate of BMC (/BFE) change would also decrease in a limited manner if the differentiation rates decrease significantly. In fact, physiologically, it is

reasonable for the BMC (/BFE) change to be zero for extremely small differentiation rates. Additionally, it can be observed from Figure 5.2 that point F marks the maximum change in BMC (/BFE) (ΔB max). Since there is no point A, which is the maximum concentration that does not lead to further modifications of BMC (/BFE), there must be a transition region from point C to A that is characterised by point B, the lowest value of BMC (/BFE).

Having found a potential 'ideal response curve', a search for response curves that may meet these requirements can begin. Encouragingly, this research has been able to identify a small number of curves that possess similarity to the idealised response curve. Table 5.1 summarises all the parameter combinations that produce idealised response curves. Figure 5.3, illustrates the physiologically realistic response curve, which corresponds to the parameter permutation involving three parameters ($A_{OBA}, A_{OCA}, A_{OST}$=-/+/+) and is similar to the idealised response curve shown in Figure 5.2.

It is noticed that in a bone remodelling system without consideration of mechanical stimulus, the response involving three parameters ($D_{OBU} / D_{OBP} / A_{OCA}$=+/-/+) coincides with the known physiological action of TGF-β on bone cells. TGF-β promotes differentiation of osteoblast progenitors and inhibits differentiation of osteoblast precursor cells, while

promoting osteoclast apoptosis [20]. However, in the case of mechanical bone remodelling, this combination causes exponential increases for both BMC and BFE, which is similar to that which is illustrated in Figure 5.1a. In other words, with the introduction of mechanical stimuli, the bone remodelling system changes and this deserves attention from biologists and other researchers.

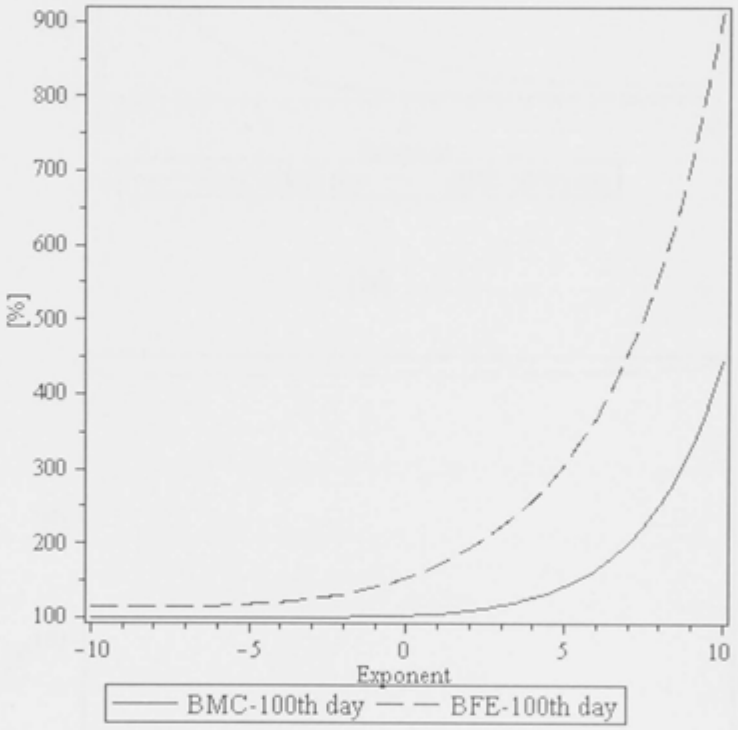

(a)

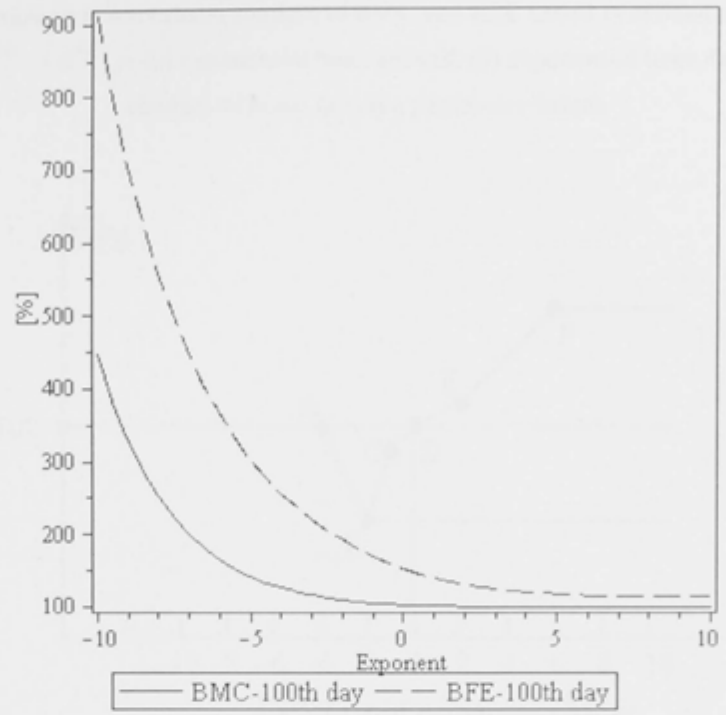
900
800
700
600
[%] 500
400
300
200
100
-10
-5
0
5
10
Exponent
BMC-100th day
BFE-100th day

(b)

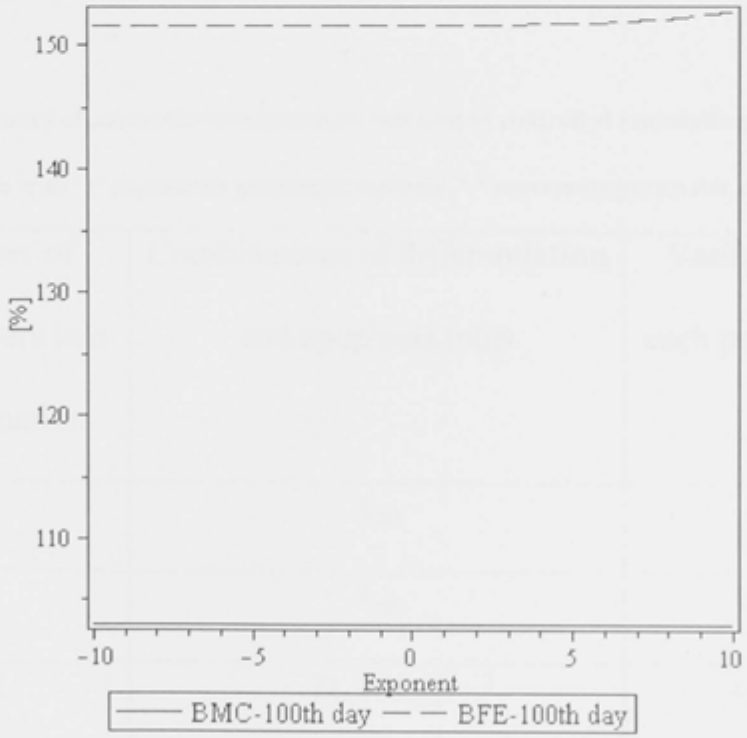
150
140
[%] 130
120
110
-10
-5
0
5
10
Exponent
BMC-100th day
BFE-100th day

(c)

Figure 5.1: Physiological unrealistic changes of BMC and BFE *versus* combined changes of model parameter $[1.5^{-10} - 1.5^{+10}]$ p: (a) exponential bone growth, (b) exponential bone decrease, (c) slight changes of bone. (p is the parameter value).

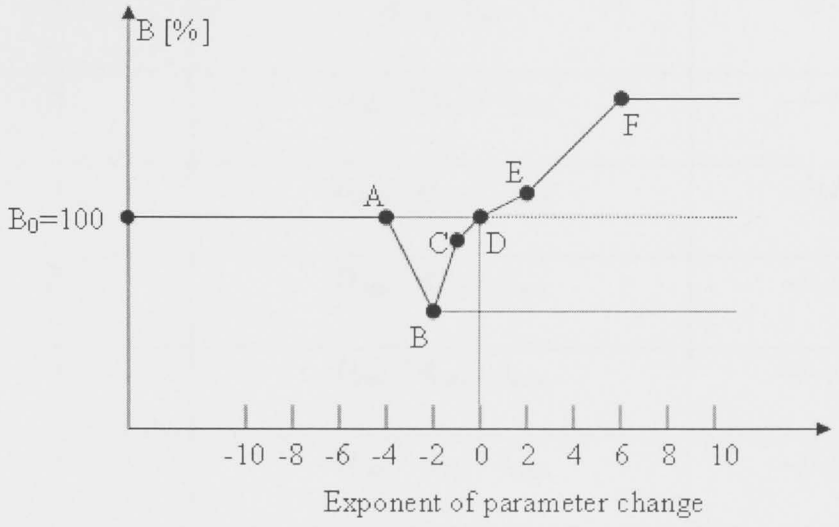

Figure 5.2: Schematic illustration of ideal response curve for combined changes of model parameters (Modified from Pivonka et al. [20])

Table 5.1: Summary of parameter combinations that lead to controlled remodelling processes. The variation with '+' represents parameter increase, '-' represents parameter decrease

Number of parameters in a combination	Combinations of differentiation and apoptosis rates	Variation of each parameter
1	A_{OBA}	–
1	A_{OST}	–
2	D_{OBP} / A_{OBA}	+/–
2	D_{OBP} / A_{OST}	–/–
2	D_{OCP} / A_{OBA}	–/–

2	D_{OCP} / A_{OST}	–/–
2	A_{OBA} / A_{OCA}	–/+
2	A_{OCA} / A_{OST}	+/–
3	D_{OBP} / D_{OCP} / A_{OBA}	–/–/–
3	D_{OBP} / D_{OCP} / A_{OBA}	–/+/–
3	D_{OBP} / A_{OBA} / A_{OCA}	–/–/–
3	D_{OBP} / A_{OBA} / A_{OCA}	–/–/+
3	D_{OBP} / A_{OBA} / A_{OST}	–/–/–
3	D_{OBP} / A_{OBA} / A_{OST}	+/–/+
3	A_{OBA} / A_{OCA} / A_{OST}	–/+/+
4	D_{OBU} / D_{OBP} / A_{OBA} / A_{OST}	+/+/+/–
4	D_{OBP} / D_{OCP} / A_{OBA} / A_{OCA}	–/–/–/–
4	D_{OBP} / D_{OCP} / A_{OBA} / A_{OCA}	–/–/–/+
4	D_{OBU} / D_{OCP} / A_{OBA} / A_{OST}	–/+/–/–
4	D_{OBP} / A_{OBA} / A_{OCA} / A_{OST}	–/–/+/–
4	D_{OBP} / A_{OBA} / A_{OCA} / A_{OST}	+/–/–/+
5	D_{OBU} / D_{OBP} / D_{OCP} / A_{OBA} / A_{OST}	–/–/+/–/–
5	D_{OBU} / D_{OBP} / D_{OCP} / A_{OBA} / A_{OST}	+/–/–/+/–
5	D_{OBU} / D_{OBP} / A_{OBA} / A_{OCA} / A_{OST}	–/+/–/–/–
5	D_{OBU} / D_{OBP} / A_{OBA} / A_{OCA} / A_{OST}	+/–/+/+/–

5	D_{OBP} / D_{OCP} / A_{OBA} / A_{OCA} / A_{OST}	−/+/−/−/−
5	D_{OBP} / D_{OCP} / A_{OBA} / A_{OCA} / A_{OST}	−/−/−/+/−
5	D_{OBP} / D_{OCP} / A_{OBA} / A_{OCA} / A_{OST}	−/−/−/−/+
6	D_{OBU} / D_{OBP} / D_{OCP} / A_{OBA} / A_{OCA} / A_{OST}	+/−/−/+/−/−
6	D_{OBU} / D_{OBP} / D_{OCP} / A_{OBA} / A_{OCA} / A_{OST}	+/−/−/+/+/−

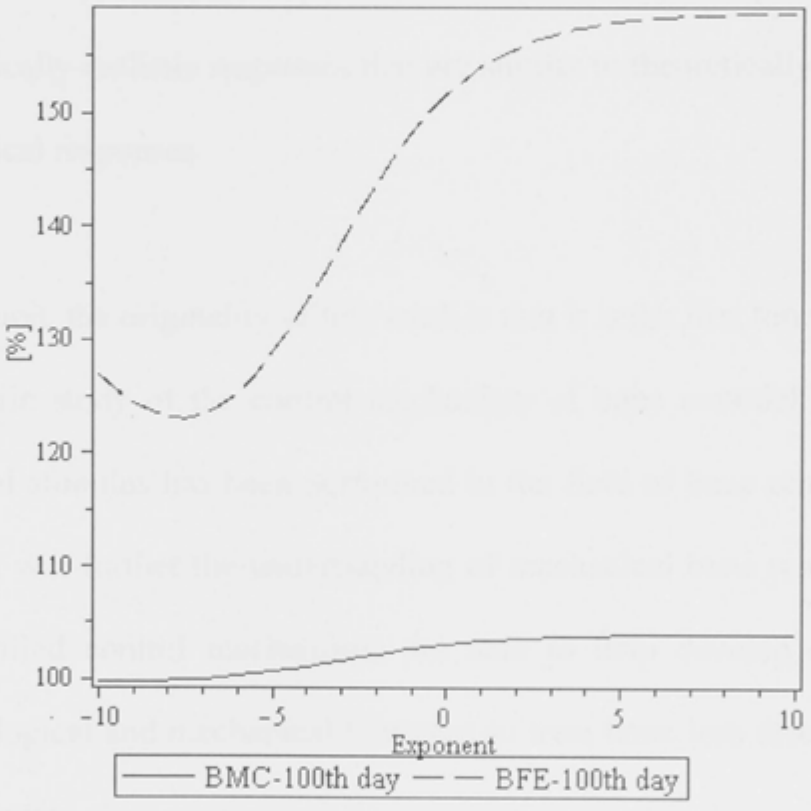

Figure 5.3 Typical physiologically-realistic fluctuations of BMC and BFE with combinations of parameter change

5.3 Summary

In this chapter, based on the work in Chapter 4, the parametric study of mechanical bone remodelling model was conducted in order to understand

the control mechanism of mechanical bone remodelling at the cellular level. Consequently, this study can perform an extensive parametric study investigating model parameter space related to cell differentiation and apoptosis, which describes the fundamental cell lineage behaviours, to investigate such a scenario. After analysing all the combinations (728 permutations) of six model parameters, this study successfully identified a small number of parameter combinations that are able to cause physiologically-realistic responses that are similar to theoretically-idealised physiological responses.

In conclusion, the originality of this work is that it is the first time in which a parametric study of the control mechanism of bone remodelling under mechanical stimulus has been performed in the field of bone remodelling. This work will further the understanding of mechanical bone remodelling. The identified control mechanisms are able to help develop combined pharmacological and mechanical therapies to treat bone loss diseases such as osteoporosis.

Chapter 6: Bone Remodelling under Pulsed Electro-magnetic Fields

PEMF devices have been widely used in clinics to treat non-union fracture or accelerate bone fracture recovery. From a control mechanism perspective, it is quite likely that there are several control mechanisms working simultaneously in bone remodelling under PEMF; however, the precise underlying mechanisms are still elusive. In this chapter, the computational system biology method is used to model bone remodelling under PEMF at the cellular level, mathematically based on experimental findings and mathematical advances. An extensive parametric study of the control mechanism based on this model is then conducted.

6.1 Model Development

6.1.1 PEMF's Effects on Bone Remodelling

The RANK/RANKL/OPG signalling pathway between osteoblasts and osteoclasts, PTH and the dual action of TGF-β is diagrammed in Figure 4.1. The 'convergence hypothesis' states that the activities of the resorptive and anti-resorptive agents 'converge' at the level of these two mediators, whose

final ratio controls the degree of osteoclast differentiation, activation, and apoptosis [33].

PEMF applies its effects on bone cells partly through this pathway, and this concept is supported by a number of studies. In an *in vitro* study [77], a PEMF with a frequency of 15 Hz (1 G [0.1 mT]; electric field strength 2 mV/cm) was applied to neonatal mouse calvarial bone cell cultures for 14 days. The results demonstrated that PEMF stimulation significantly increased the osteoblasts' proliferation. The OPG expression was up-regulated and the RANKL concentration was down-regulated, compared to the control group. In another study [135], researchers investigated the effect of PEMF with parameters modified from clinical bone stimulator devices and concluded that OPG might be a potential intermediary involved in the interplay between PEMF stimulation and osteoclastogenesis. Where appropriate, PEMF intensities could either promote or suppress OPG expressions in the osteoblastic lineage. In addition, the osteogenesis effect of PEMF was accompanied by the decrease of RANKL. The latest research also demonstrated that PEMF induces cells in the osteoblast lineage to express OPG [136].

Additionally, several studies have demonstrated that PEMF causes osteoblasts to produce other paracrine factors, including transforming

growth factor beta-1 (TGF-β1), prostaglandin E2 (PGE2) and bone morphogenetic protein-2 [137-139]. Moreover, macrophage colony-stimulating factor (M-CSF) has been shown to decrease after PEMF exposure [135] and bone morphogenetic protein-2, -4, -5 was found to increase in osteoblasts after PEMF application [140, 141]. However, these observations were not consistent in the literature; as a result, these factors are not included in the effects of PEMF on bone remodelling in this study's model.

PEMF stimulation, in comparison with drug administration, is able to produce a local concentration of growth factors synthesis, without any systemic side effects. However, it is important to keep in mind that, as with a drug, the dosage of physical stimulus is fundamental if positive effects on osteogenesis are to be produced. The biological effects of PEMF stimulation depend not only on the length of treatment time, but also on the signal characteristics such as intensity, waveform, frequency and length of the signal [142]. Research [143] found that PEMF is the most responsive, compared with other waveforms such as rectangular electro-magnetic fields (REMF), triangular electro-magnetic fields (TEMF) and sinusoidal electro-magnetic fields (SEMF) in terms of their effects on the proliferation and differentiation effects on osteoblastic cells.

With regard to the different types of PEMF, Bassett et al. [144] propose that single pulse is better than burst pulsed PEMF stimulation on osteoporosis prevention and non-union fracture healing, whereas burst pulsed PEMF stimulation had better effects on bone fracture healing acceleration. The study [145] examined the response of osteoblast-like cells to a PEMF stimulus, mimicking that of a clinically available device, using four protocols of the timing of the stimulus, each conducted over three days. Protocol one stimulated the cells for eight hours each day, protocol two stimulated the cells for 24 hours on the first day, protocol three stimulated the cells for 24 hours on the second day and protocol four stimulated the cells 24 hours on the third day. In terms of proliferation and differentiation of the cells compared with the control group, no clear trend was observed between the four protocols.

Intensity of the PEMF is also an important factor, as data from [135] demonstrated that PEMF with different intensities could regulate osteoclastogenesis, bone resorption, OPG, RANKL and M-CSF concentrations in marrow culture system. Specifically, in this experiment, the author used three different electric field intensities of PEMF fields (4.8μV/cm, 8.7 μV/cm, 12.2 μV/cm) and observed that the recruitment of osteoclast-like cells was inhibited by approximately 33% and increased by approximately 10% when electric field intensities of PEMF were 4.8

μV/cm and 12.2 μV/cm respectively. No significant differences at all time points were observed compared with the control group.

6.1.2 Mathematical Model

The schematic diagram of the mathematical model structure of bone remodelling under PEMF is illustrated in Figure 6.1.

In the cell population dynamics model, this study included three cell populations (see osteoblastic and osteoclastic lineages in Figure 4.1) into model equations including OBP, OBA and OCA. Uncommitted osteoblastic progenitors (OBU) and osteoclastic precursors (OCP) work as reservoirs whereby the cells will differentiate into functional cells such as osteoblasts and osteoclasts respectively. Their numbers are much larger than the functional cells OBP, OBA or OCA. As a result, OBU and OCP are assigned a very large constant compared with other cell numbers in the model (i.e. OBU=OCP=1×10^{-2} pM).

Similar to [20] and the author's previous work [34, 88], the Hill equation is used to describe the activation and repression of the receptor-ligand interactions. In biochemistry, the Hill equation is used to describe the fraction of the macromolecule saturated by a ligand as a function of the

ligand concentration; it is used in determining the degree of cooperativity of the ligand binding to the enzyme or receptor.

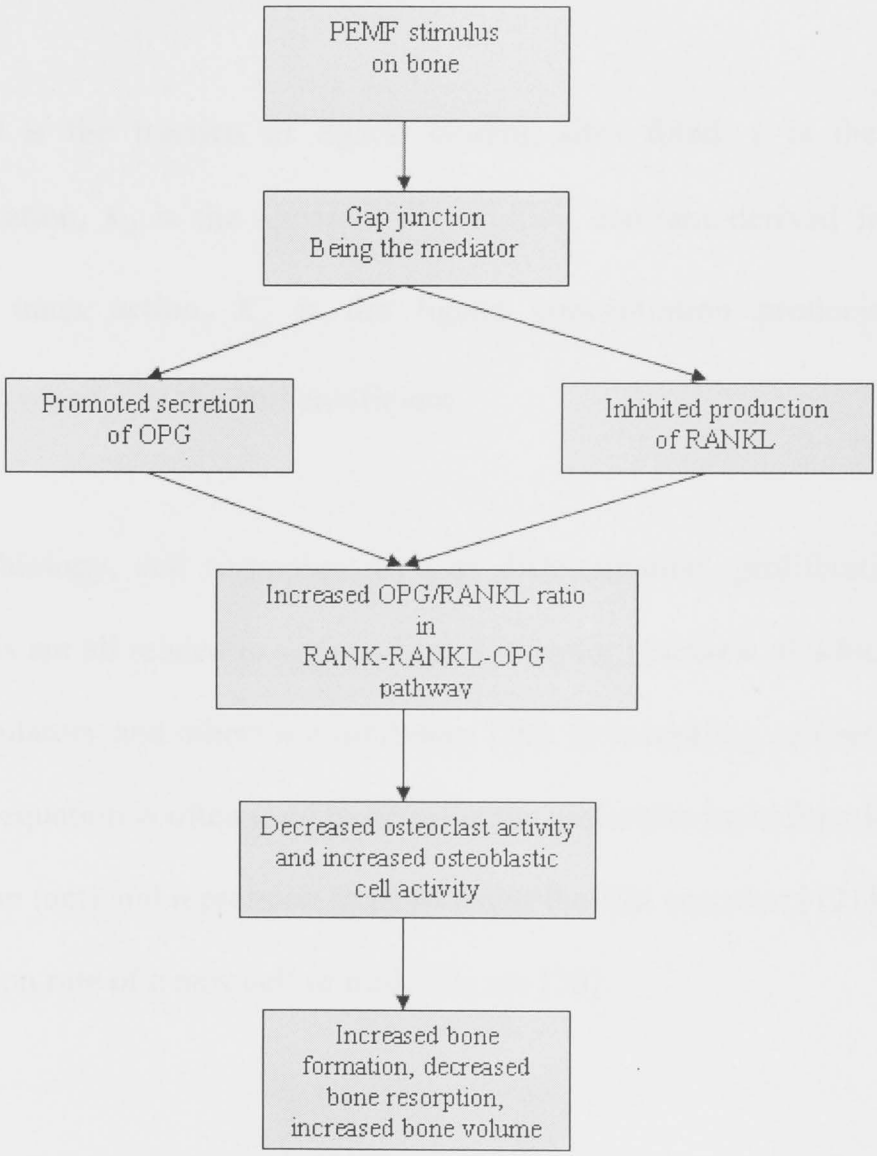

Figure 6.1: Schematic diagram of the mathematical model structure of PEMF stimulated bone remodelling at the cellular level

It was originally formulated by Hill in 1910 [120] to describe the sigmoidal O_2 binding curve of haemoglobin:

$$\theta = \frac{L^n}{K_d + L^n} = \frac{L^n}{K_A{}^n + L^n} \tag{6.1}$$

where θ is the fraction of ligand binding sites filled, L is the ligand concentration, K_d is the apparent dissociation constant derived from the law of mass action, K_A is the ligand concentration producing half occupation and n is the Hill coefficient.

In cell biology, cell responses such as differentiation, proliferation and apoptosis are all related to various ligand-receptor reactions of which some are stimulatory and others are inhibitory [20]. In modelling cell responses, the Hill equation is often used to describe the molecular input function. The activation (act) and repression (rep) forms of the Hill equation [121] for the production rate of a new cell or molecule are [20]:

$$f\left(x^*\right) = \beta \cdot \Pi_{act} = \frac{\beta x^*}{K_1 + x^*} \tag{6.2}$$

$$f\left(x^*\right) = \beta \cdot \Pi_{rep} = \frac{\beta}{1 + \frac{x^*}{K_2}} \tag{6.3}$$

where x^* is the active form of concentration, x is a ligand that governs the production of a cell or molecule (z) through binding to its receptor on cell, β is the maximal production rate of z, and K_1 and K_2 are activation and repression coefficients. This thesis has already assumed that the Hill coefficient equals one.

For convenience, here and later in the chapter, the abbreviated forms for the factors involved in the corresponding formulation have been used. As in Figure 1, this study used OBU for uncommitted osteoblastic progenitors, OBP for osteoblastic precursors, OBA for mature osteoblast, OCP for osteoclast precursor and OCA for active osteoclasts, RL for RANKL, RK for RANK and Tβ for TGF-β. OPG and PTH remain unchanged.

The equations governing the evolution of the number of osteoblastic and osteoclastic cells in each maturation stage are simply balance equations [6], which means that each cell stage is fed by an entering flow and is emptied by the outgoing flow of differentiated or apoptotic cells (see Figure 1). As a result, utilising Figure 6.1 and based on the formulation in [20], the bone cell population dynamics can be formulated as follows:

$$\frac{dOBP}{dt} = D_{OBU} \cdot OBU \cdot \Pi^{T\beta}_{act,OBU} - D_{OBP} \cdot OBP \cdot \Pi^{T\beta}_{rep,OBP} \tag{6.4}$$

$$\frac{dOBA}{dt} = D_{OBP} \cdot OBP \cdot \Pi^{T\beta}_{rep,OBP} - A_{OBA} \cdot OBA \tag{6.5}$$

$$\frac{dOCA}{dt} = D_{OCP} \cdot OCP \cdot \Pi^{RL}_{act,OCP} - A_{OCA} \cdot OCA \cdot \Pi^{T\beta}_{act,OCA} \tag{6.6}$$

$$\frac{dBV}{dt} = k_{for} \cdot \left[OBA(t) - OBA(0) \right] - k_{res} \cdot \left[OCA(t) - OCA(0) \right] \tag{6.7}$$

where subscript 'cell' in the input functions $\Pi^{molecule}_{act/rep,cell}$ represents the cell type that a specific molecule binds to, and 'molecule' denotes the ligand involved in a particular cell response. D_{OBU} is the differentiation rate of uncommitted OB progenitors, D_{OBP} is the differentiation rate of osteoblastic precursors, D_{OCP} is the differentiation rate of preosteoclasts, A_{OBA} is the rate of elimination of OBA and A_{OCA} is the rate of elimination of OCA. BV represents bone volume in percentage (%), and k_{for} and k_{res} are the relative bone formation and bone resorption rates respectively. The simulation starts from a so-called 'steady-state' whereby BV is 100%, $dBV/dt = 0$ correspondingly, $OBA(t)$ is $OBA(0)$ and $OCA(t)$ is $OCA(0)$. Equations (6.4) to (6.6) transform into Equations (6.8) to (6.10):

$$0 = D_{OBU} \cdot \Pi^{T\beta}_{act,OBU} - D_{OBP} \cdot OBP(0) \cdot \Pi^{T\beta}_{rep,OBP} \tag{6.8}$$

$$0 = D_{OBP} \cdot OBP(0) \cdot \Pi^{T\beta}_{rep,OBP} - A_{OBA} \cdot OBA(0) \tag{6.9}$$

$$0 = D_{OCP} \cdot \Pi^{RL}_{act,OCP} - A_{OCA} \cdot OCA(0) \cdot \Pi^{T\beta}_{act,OCA} \tag{6.10}$$

By solving equations (6.8) to (6.10), the initial values of the model variables in Table 6.1 can be obtained.

Table 6.1: Initial values of the model variables.

Symbol	Unit	Value
OBA(0)	pM	0.2126991130e-3
OBP(0)	pM	0.8986869185e-5
OCA(0)	pM	0.2769166993e-3

In the model, there are two different time scales: a short time scale is used to describe the receptor-ligand reactions such as RANK-RANKL, OPG-RANKL and TGF-β with its receptor; and a long time scale is required to capture the cell number changes such as OBP, OBA and OCA. Note that the receptor-ligand reaction is much faster than the changes in cell numbers; therefore, a quasi-steady state assumption is used in the model to describe the receptor-ligand reactions.

Bone matrix is the largest source of TGF-β in the body [108]. TGF-β, growth factors and specific components embedded in the bone matrix are released by osteoclasts during bone resorption [109]. The effect of TGF-β on osteoblasts is bi-directional, depending upon the state of maturation of the osteoblasts [6]. On one hand, TGF-β has the potential to stimulate osteoblast recruitment, migration and proliferation of osteoblast precursors (meaning OBPs in this model) [109]. On the other hand, TGF-β inhibits terminal osteoblastic differentiation into OBAs [31]. In this model, it is assumed that the release rate of TGF-β from the bone matrix is constant. Using the short time scale and a quasi-steady state assumption the expression of TGF-β is [20]:

$$T\beta = \frac{\alpha \cdot K_{res} OCA + S_{T\beta}}{\tilde{D}_{T\beta}} \tag{6.11}$$

$S_{T\beta}$ is a source/sink term for TGF-β, α is the TGF-β content stored in bone matrix, K_{res} is the relative rate of bone resorption and $\tilde{D}_{T\beta}$ is the rate of degradation of TGF-β. Consequently, the activation and repression forms of TGF-β can be obtained by substituting Equation (6.11) into Equations (6.2) and (6.3):

$$\Pi_{act,OBU}^{T\beta} = \frac{T\beta}{K_{D1,T\beta} + T\beta} \tag{6.12}$$

$$\Pi_{rep,OBP}^{T\beta} = \frac{1}{1 + T\beta / K_{D2,T\beta}} \tag{6.13}$$

$$\Pi_{act,OCA}^{T\beta} = \frac{T\beta}{K_{D3,T\beta} + T\beta} \tag{6.14}$$

$K_{D1,T\beta}$ is the activation coefficient related to TGF-β binding on OBU, $K_{D2,T\beta}$ is the repression coefficient related to TGF-β binding on OBP and $K_{D3,T\beta}$ is the activation coefficient of TGF-β binding on OCA. Applying the law of mass action [6] used to describe the reactions of receptors and corresponding ligands, the formulations, including PTH with its receptor, RANKL with OPG and RANKL with RANK, can be found in the author's previous work [34].

In this model, PTH is a regulator of RANKL and OPG production. The assumption is that PTH endogenous production is constant and $PTH_{\max} \gg PTH$ and PTH binding to its receptors on OBP and OBA is the same, to obtain PTH concentration and its according activation and repression functions as [20]:

$$PTH = \frac{\beta_{PTH} + P_{PTH,d}(t)}{\tilde{D}_{PTH}} \tag{6.15}$$

$$\Pi_{act,OBP}^{PTH} = \frac{PTH}{K_{D4,PTH} + PTH} \tag{6.16}$$

$$\Pi_{rep,OBA}^{PTH} = \frac{1}{1 + PTH / K_{D5,PTH}} \tag{6.17}$$

where β_{PTH} is the synthesis rate of systemic PTH, $P_{PTH,d}(t)$ represents an external PTH dosing term, $\tilde{D}_{PTH}$ is the rate of degradation of PTH, $K_{D4,PTH}$ is the activation coefficient for $RANKL_{eff}$ on OBP related to PTH binding and $K_{D5,PTH}$ is the repression coefficient for OPG production related to PTH binding on OBA.

As stated previously, it has already been concluded that PEMF stimulates the production of OPG expressed in OBA and inhibits the expression of RANKL in OBP, based on experimental observations (see Section 6.1.1). OPG and RANKL are the only two factors that are considered to be regulated by PEMF stimulation and modelled in the model. The systemic hormone PTH down-regulates OPG production in OBA [34]. Therefore, based on [20], the OPG concentration can be expressed as:

$$OPG = \frac{\beta_{OPG} \cdot OBA \cdot \left(\Pi_{rep,OBA}^{PTH} + F_{OPG}(I, f, t, w)\right) + P_{OPG,d}(t)}{\frac{\beta_{OPG} \cdot OBA \cdot \left(\Pi_{rep,OBA}^{PTH} + F_{OPG}(I, f, t, w)\right)}{OPG_{\max}} + \tilde{D}_{OPG}} \tag{6.18}$$

where β_{OPG} is the production rate of OPG per OBA, $F_{OPG}(I,f,t,w)$ is the influence of PEMF on OPG secretion characterised by its intensity, frequency, time and waveform, $P_{OPG,d}(t)$ is an external OPG administration term, $\tilde{D}_{OPG}$ is the rate of degradation of OPG and $OPG_{\max}$ is the maximum possible OPG concentration. In addition, PEMF inhibits RANKL expression in OBP and PTH up-regulates the RANKL 'effective carrying capacity' of OBP [34]. Building on [20] the concentration of RANKL can be obtained:

$$RL = \left(\frac{R_{RL} \cdot OBP \cdot \Pi_{act,OBP}^{PTH}}{1 + K_{A1,RL} \cdot OPG + K_{A2,RL} \cdot RK} \right) \cdot \left(\frac{\beta_{RL} \cdot OBP \cdot F_{RL}(I,f,t,w) + P_{RL,d}(t)}{\beta_{RL} \cdot OBP \cdot F_{RL}(I,f,t,w) + \tilde{D}_{RL} \cdot R_{RL} \cdot OBP \cdot \Pi_{act,OBP}^{PTH}} \right) \tag{6.19}$$

R_{RL} is the maximum RANKL on OBP, $K_{A1,RL}$ is the association binding constant RANKL-OPG, $K_{A2,RL}$ is the association binding constant RANKL-RANK, β_{RL} is the production rate of RANKL per OBP, $F_{RL}(I,f,t,w)$ is the effect of PEMF on RANKL production characterised by its intensity, frequency, time and waveform, $P_{RL,d}(t)$ is an external RANKL administration term and $\tilde{D}_{RL}$ is the rate of degradation of RANKL. Then, the activation function of RANKL on differentiation of osteoclast precursor cells OCP can be obtained using Equations (6.2) and (6.19):

$$\Pi_{act,OCP}^{RL} = \frac{RL}{K_{D6,RL} + RL} \tag{6.20}$$

$K_{D6,RL}$ is the activation coefficient related to RANKL binding on OCP. All the model parameters and their values can be found in Appendix C.

6.2 Numerical Investigation of the Model

Bone remodelling is an important biological system when it comes to bone fracture healing, non-union fracture and bone diseases such as osteoporosis. It is executed by coordinated activities of osteoclastic cells and osteoblastic cells in BMUs. The coupling between osteoclastic cells and osteoblastic cells is facilitated by the RANK/RANKL/OPG pathway, together with the systemic hormone PTH and transforming growth factor TGF-β. PEMF devices are used clinically to promote bone healing especially non-union fracture but relatively little is known about the mechanisms involved. This chapter proposes a mathematical model to simulate the PEMF's effect on bone remodelling at the cellular level, which would help to better understand the underlying mechanisms. Here, this study solved the ODEs (6.4) to (6.7) numerically, using Matlab and plotted a series of graphs about the concentration dynamics of OPG, RANKL, cell populations of OBA,

OCA and OBP, and bone volume, as can be observed in Figures 6.2–6.5, respectively. Note that the parameter values have been obtained from the models that this model is based on [20] and the author's previous work [34, 88].

The effects of PEMF on bone remodelling are characterised by its intensity, frequency, waveform and application time. According to the study [145], the timing of the PEMF stimulation does not affect the bone cell development, which is different from the bone remodelling under mechanical stimulus. In this numerical investigation, the specific parameter values of PEMF were chosen from the widely used PEMF devices in clinics [146] and this set of parameter values is the only one used in this study's model. Consequently, it is assumed that the PEMF effects on bone remodelling, specifically OPG or RANKL, in this model do not change (represented by two different constants F_{OPG} and F_{RL} in the model) throughout the simulation (three months).

The concentration dynamics of OPG during the three-month PEMF application is simulated in Figure 6.2. Consistent with experimental observations, the OPG concentration increases during the first ten days simulation. Surprisingly, the concentration of OPG keeps dropping from the 10^{th} day in simulation. For the reason that most *in vitro* experiments

were performed within two weeks, there is no available experimental data to compare with. The pattern of the OPG concentration might be explained by the fact that because of the PEMF's stimulus effect, OPG concentration increases in the short period after the PEMF's application, and then the binding of OPG with RANKL catches up as the bone remodelling occurs. More OPG are consumed than produced by osteoblast cells; as a result, OPG concentration drops until the end of the simulation.

Figure 6.3 shows the RANKL concentration dynamics during the three-month PEMF application. As can be observed from the graph, within two weeks (which is the time scale of most *in vitro* experiments), the RANKL concentration drops, compared with the initial value. However, it was not expected that the RANKL concentration would significantly increase immediately after the simulation began, followed by a dramatic decrease and the maintenance of a similar level throughout the rest of the simulation. A possible reason for this development pattern is that the number of preosteoblast cells that produce RANKL is increased by the PEMF's stimulus effect on the proliferation of bone marrow mesenchymal stem cells [34] immediately after the application of PEMF. Then, the inhibitory effect of PEMF on the OBP takes over and this overall trend is maintained until the end of the simulation.

The cell population dynamics of OBA, OCA and OBP can be observed in Figure 6.4. As expected, the OBA and OBP populations rise and OCA decreases in the first two weeks of the simulation, which is consistent with experimental observations. Due to the coupling effect between OCA and OBA, the OBA population starts to decrease after it peaks and continues to decrease until the end of simulation while maintaining a higher concentration than OCA, which accounts for the continuing growth of bone volume in Figure 6.5.

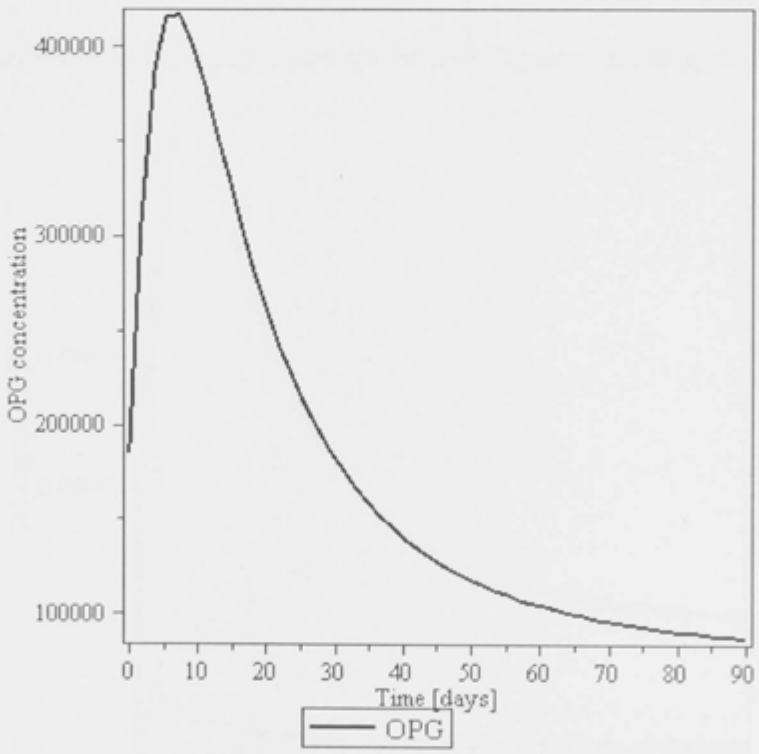

Figure 6.2: OPG concentration dynamics during three-month PEMF application

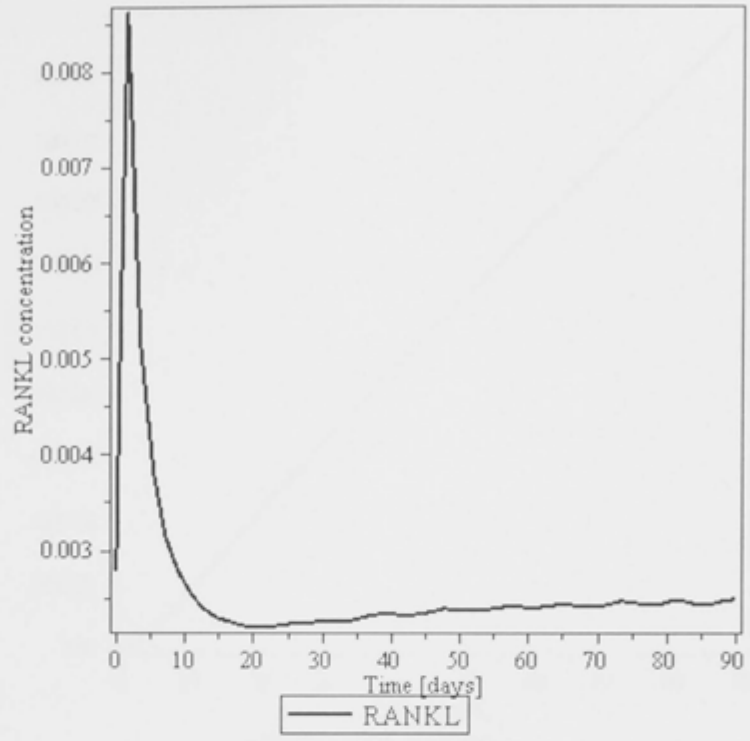

Figure 6.3: RANKL concentration dynamics during three-month application

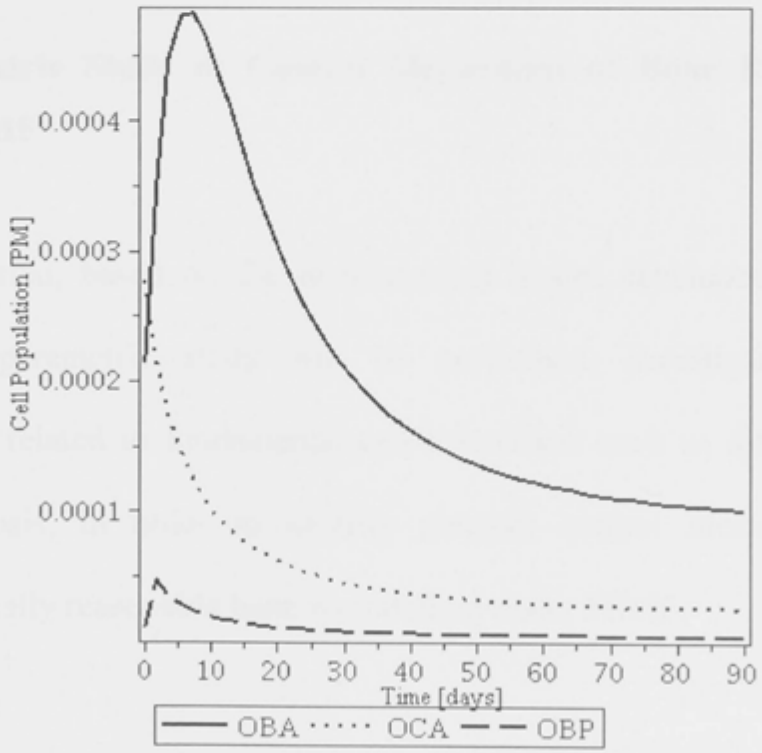

Figure 6.4: OBA, OCA and OBP cell population dynamics during three-month PEMF application

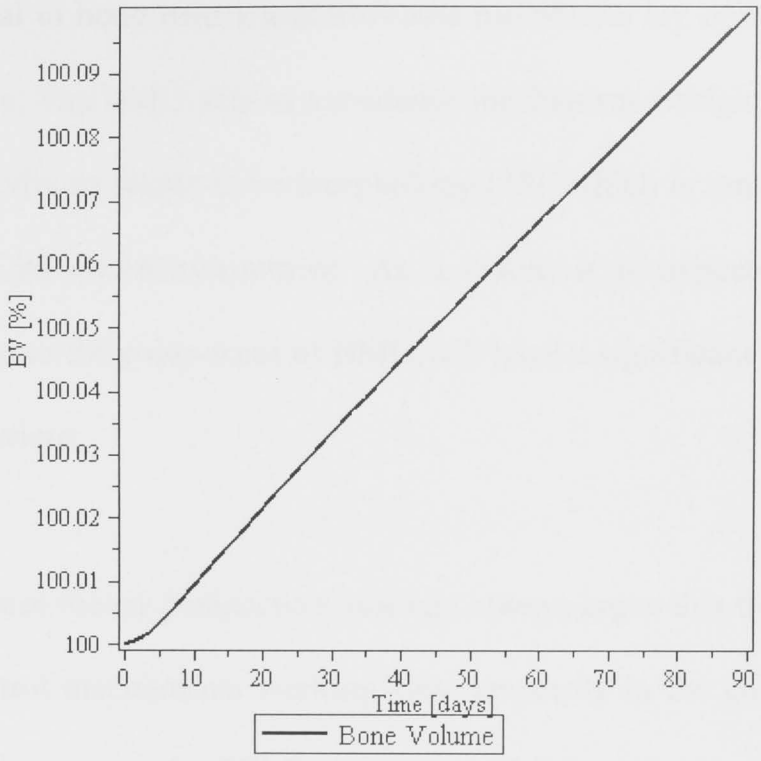

Figure 6.5: Bone volume percentage dynamics during three-month PEMF application

6.3 Parametric Study of Control Mechanism of Bone Remodelling under PEMF

In this section, based on the mathematical model developed above, an extensive parametric study will be performed, investigating model parameters related to fundamental cell behaviours such as differentiation and apoptosis, in order to identify putative control mechanisms for physiologically reasonable bone remodelling under PEMF.

The functional outputs of the bone remodelling system, such as bone loss or gain, or homeostasis, are executed by BMUs whereby osteoclasts absorb

bone mineral in bone matrix and activated osteoblasts lay down the newly formed bone. The BMU acts as a mediator mechanism, bridging individual cellular activity to whole bone morphology [25], which is sensitive to any changes in its microenvironment. As a result, it is expected that any modification to the component of BMU will have a significant effect on its output behaviour.

From a control theory perspective, one can always argue that there must be several control mechanisms working simultaneously in the complex bone remodelling system under PEMF, governing BMU's response to changes in its microenvironment by modifying differentiation or apoptosis rates of bone cells. This paper will apply perturbations to the bone remodelling system under PEMF (which is in a steady state) by down- and up-regulating its parameters in random combination groups of five differentiation and apoptosis rate parameters: DF_{obu}, DF_{ocp}, DF_{obp}, A_{oba} and A_{oca}. In this case, each parameter in each group (groups of one, two, three, four and finally all five parameters at one time) could be up- or down-regulated. Using the simple combination theory, the total number of permutation can be calculated, which is $242 = \sum_{i=1}^{5} C_5^i \cdot 2^i$. Then, in order to investigate the system behaviour for a wide range of changes, the exponentially changed factor (1.5^{α}) is now applied to each of the five

differentiation and apoptosis rate parameters, whereby the exponent ex ranges from -10 to 10 in step increases of 0.5. The assessment of each of the parameter combinations to the system behaviour is chosen as the responses of bone volume, which are sampled on the 90^{th} day to stand for the maximum change. Using Matlab (see the Matlab code in Appendix D.2), all 242 graphs can be plotted. Then, summarising all the plots of bone volume *versus* variation of exponent ex, it is found that there are three subsets of curves, which are plotted in Figure 6.6.

Figure 6.6a and Figure 6.6b demonstrate an exponential increase and decrease of bone volume respectively, for increasing the model parameter exponentially (exponent ex from -10 to 10). This type of behaviour is considered as physiologically unrealistic from a biological perspective and obtained for quite a large range of model parameter combinations. Conversely, Figure 6.6c represents the other extreme, whereby only minor changes of bone volume occur during the entire range of parameter variation. These three types of response curves are excluded from further analysis because they do not provide an effective control mechanism for bone volume.

In [20] the 'idealised' regulatory response by functionally active BMUs is discussed. As mentioned previously, the bone remodelling system starts

from a steady state in which it can be identified that $\Delta BV = 0$, and concentrations of various hormones and growth factors cause initial values of differentiation and apoptosis rates in BMUs. In order to respond to minor changes in concentrations, it is expected that BMUs should be rather insensitive to these fluctuations. Therefore, from Figure 5.2, point A can be recognised as the threshold concentration, which means any change of model parameter underneath A causes no change in bone volume. In addition, a region around the usual operation status of BMUs should be found with relatively small gradients of changes in bone volume in response to changes in differentiation rates (regions C–D and D–E in Figure 5.2), with larger gradients for larger changes in differentiation rates (region E-F in Figure 5.2). It is expected that this response in bone volume change will remain limited if the differentiation rates increase significantly (region further after point F in Figure 5.2) because the unlimited rise in bone volume is not physiologically realistic. Conversely, it is expected that the rate of bone volume change would also decrease in a limited manner if the differentiation rates decrease significantly. In fact, physiologically, it is reasonable for the bone volume change to be zero for extremely small differentiation rates. Additionally, it can be observed from Figure 5.2 that point F marks the maximum change in bone volume (ΔB max). Since point A is the maximum concentration that does not lead to further modifications

of bone volume, there must be a transition region from point C to A, which is characterised by point B, the lowest value of bone volume.

Having found a potential 'ideal response curve', a search for the response curves that may meet these requirements can now begin. Encouragingly, a small number of curves have been identified that possess similarity to the idealised response curve. Table 6.2 summarises all the parameter combinations that produce idealised response curves. In Figure 6.7, the physiologically-realistic response curve is plotted, which corresponds to the parameter permutation involving three parameters (A_{OBA}, A_{OCA}, A_{OST} =-/+/+) and is similar to the idealised response curve shown in Figure 5.2.

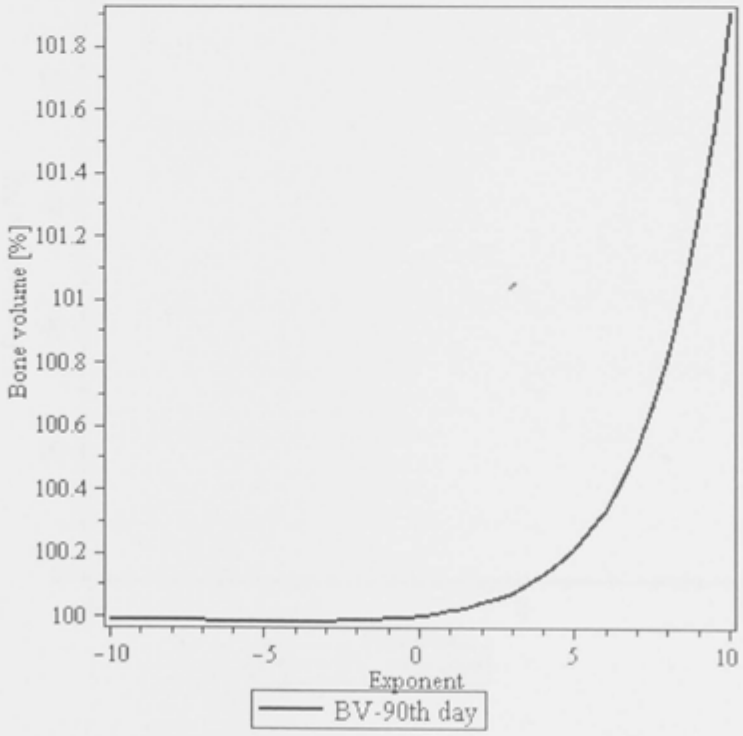

(a)

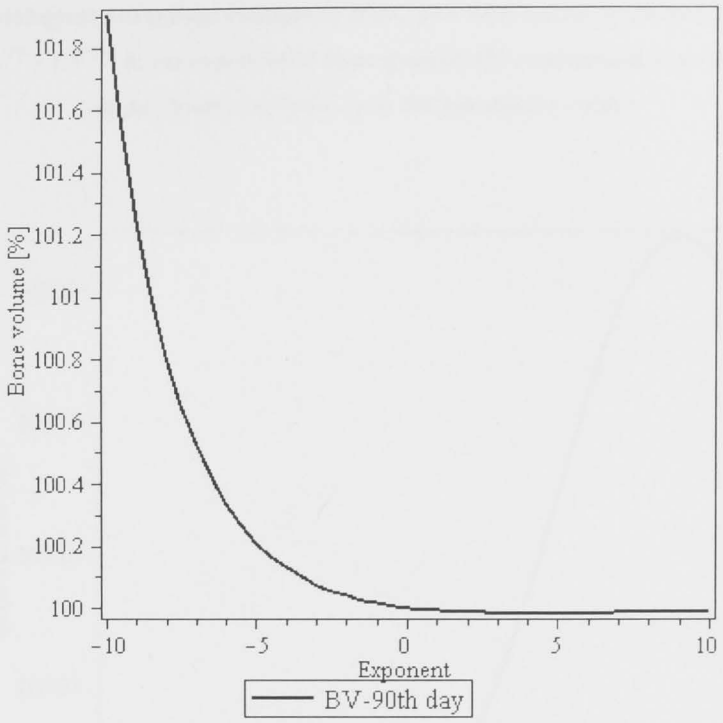
101.8
101.6
101.4
101.2
101
100.8
100.6
100.4
100.2
100
Bone volume [%]
-10
-5
0
5
10
Exponent
BV-90th day

(b)

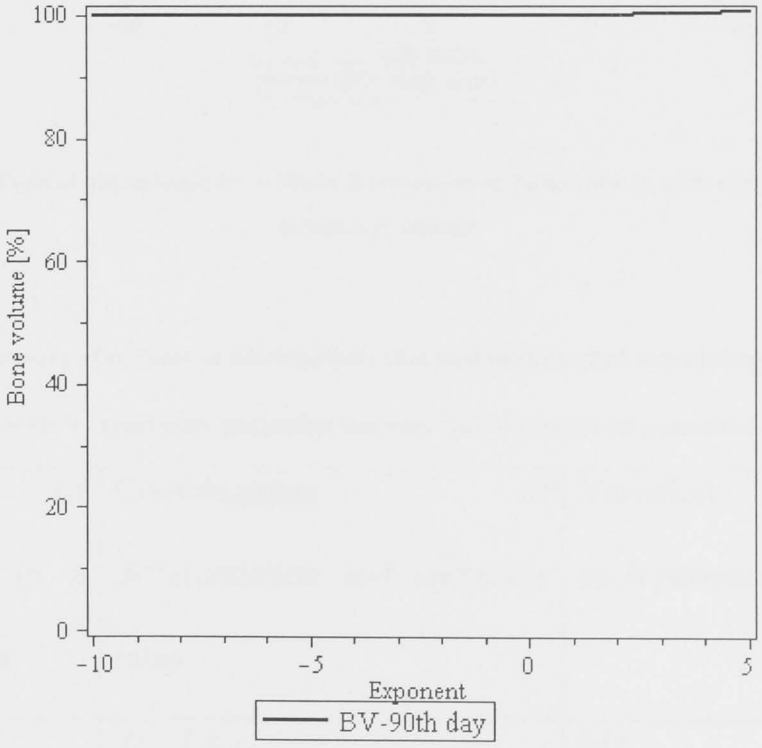
100
80
60
40
20
0
Bone volume [%]
-10
-5
0
5
Exponent
BV-90th day

(c)

Figure 6.6: Physiological unrealistic changes of BMC and BFE *versus* combined changes of model parameter $[1.5^{-10} - 1.5^{+10}]$ p: (a) exponential bone growth, (b) exponential bone decrease and (c) slight changes of bone. (p is the parameter value)

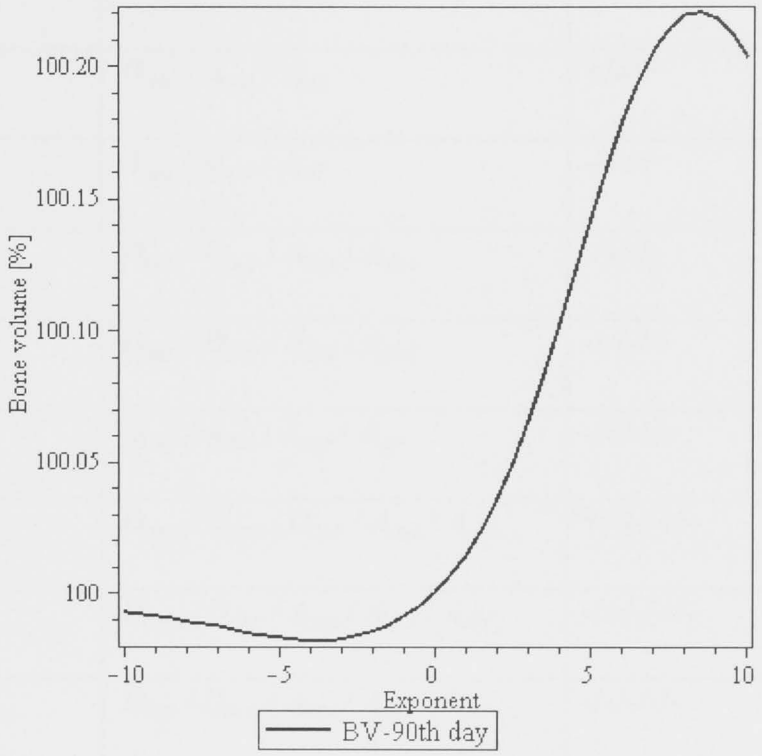

Figure 6.7: Typical physiologically realistic fluctuations of bone volume with combinations of parameter change

Table 6.2: Summary of parameter combinations that lead to controlled remodelling process. The variation with '+' represents parameter increase and '-' represents parameter decrease

Number of parameters in a combination	Combinations of differentiation and apoptosis rates	Variation of each parameter
2	D_{OBP} / A_{OBA}	+/+
2	D_{OCP} / A_{OST}	+/-

2	A_{OBA} / A_{OCA}	-/+
3	D_{OBP} / A_{OBA} / A_{OCA}	-/+/-
3	D_{OBP} / A_{OBA} / A_{OCA}	-/-/+
3	D_{OBP} / A_{OBA} / A_{OST}	+/-/+
3	A_{OBA} / A_{OCA} / A_{OST}	-/+/+
4	D_{OBP} / D_{OCP} / A_{OBA} / A_{OCA}	-/-/-/-
4	D_{OBP} / D_{OCP} / A_{OBA} / A_{OCA}	-/-/-/+
4	D_{OBP} / A_{OBA} / A_{OCA} / A_{OST}	-/+/+/-
5	D_{OBU} / D_{OBP} / D_{OCP} / A_{OBA} / A_{OST}	+/-/-/+/-
5	D_{OBU} / D_{OBP} / A_{OBA} / A_{OCA} / A_{OST}	-/+/-/+/-
5	D_{OBP} / D_{OCP} / A_{OBA} / A_{OCA} / A_{OST}	-/-/-/-/-
5	D_{OBP} / D_{OCP} / A_{OBA} / A_{OCA} / A_{OST}	+/-/-/+/-

6.4 Summary

In this chapter, a mathematical model of bone remodelling under PEMF at the cellular level was proposed based on experimental results and the author's previous work. This model incorporates the latest experimental findings through extensive literature review and summarises that PEMF applies its physiological effects via the RANK/RANKL/OPG pathway. Specifically, PEMF promotes the secretion of OPG and inhibits the

production of RANKL, which suppresses the overall population of the osteoclasts that absorb bone minerals. Based on this model, the numerical investigation demonstrates the concentration dynamics of growth factors OPG and cytokines RANKL, and the population dynamics of OBA, OBP and OCA. More importantly, a parametric study of bone remodelling under PEMF was conducted in order to understand the control mechanism of bone remodelling at the cellular level under PEMF.

This work will further the understanding of bone remodelling under PEMF and the indentified control mechanisms are able to help develop combined pharmacological and PEMF therapies to cure bone loss diseases such as osteoporosis.

Chapter 7: Conclusions and Future Work

7.1 Conclusions

In this thesis, a mathematical framework of bone remodelling under mechanical stimulus and PEMF at the cellular level was developed by means of the computational system biology approach.

This framework is comprised of three major models. The model of bone remodelling biological system at the cellular level that is able to simulate the anabolic effect of PTH when applied intermittently as a therapy to treat osteoporosis in clinical practice. Based on the first model, the factor of mechanical stimulus is taken into account in bone remodelling system at the cellular level. This model is then validated by comparison with experimental results, followed by the parametric study of the control mechanism of bone remodelling under mechanical stimulus at the cellular level. The last model is bone remodelling under PEMF at the cellular level, based on which the control mechanism is also investigated and a small number of possible control mechanisms are identified.

In Chapter 3, a model of bone remodelling at the cellular level is developed for the first time that is able to simulate the anabolic effect of PTH when

applied intermittently. This model integrates the latest progresses in the bone biology of remodelling and current advances in mathematics into the model, such as applying the law of mass action to describe the reactions of receptors and corresponding ligands, including PTH (P) with its receptor, RANKL with OPG, RANKL with RANK and IGF with its receptor. It also uses balance equations to govern the evolution of the number of principal cells in each compartment such as osteoblasts and osteoclasts. This model is developed as the platform of mathematical modelling of bone remodelling at the cellular level, based on which the factors such as mechanical stimulus and PEMF are taken into account and corresponding models are developed in Chapters 4, 5 and 6.

In Chapter 4, the model of bone remodelling under mechanical stimulus was developed at the cellular level. A number of new features have been proposed for the first time in this field, such as: osteocyte being the physical mediator of mechanotransduction in bone remodelling under mechanical stimulus; three new rate equations describing changes of OST, NO and PGE_2 being incorporated in the model; the effect of loading frequency on bone mechanosensitivity being investigated; the influence of the number of loading cycles during a loading day and the recovery of bone mechanosensitivity between two loading bouts as well as during the whole loading period being investigated; and the Hill equation being extended to

two ligands binding to the same cell. The good agreement between the simulations and the experimental results is very encouraging, and indicates the correct understanding of the mechanical bone remodelling at the cellular level.

In Chapter 5, based on the work in Chapter 4, the parametric study of mechanical bone remodelling model was conducted in order to understand the control mechanism of mechanical bone remodelling at the cellular level. Consequently, an extensive parametric study investigating model parameter space related to cell differentiation and apoptosis, which describes the fundamental cell lineage behaviours, was performed to investigate such a scenario. After analysing all of the 728 permutations of the six model parameters, a small number of parameter combinations that are able to cause physiologically realistic responses were successfully identified.

The originality of this work is that it is the first time that a parametric study of the control mechanism of bone remodelling under mechanical stimulus has been performed in the field of bone remodelling. This work will further the understanding of mechanical bone remodelling and the identified control mechanisms are able to help develop combined pharmacological and mechanical therapies to treat bone loss diseases.

In Chapter 6, a mathematical model of bone remodelling under PEMF at the cellular level was proposed based on experimental results and the author's previous work. This model incorporates the latest experimental findings through extensive literature review and summarises that PEMF applies its physiological effects via the RANK/RANKL/OPG pathway. Specifically, PEMF promotes the secretion of OPG and inhibits the production of RANKL, which suppresses the overall population of osteoclasts that absorb bone minerals. Based on this model, the numerical investigation demonstrates the concentration dynamics of growth factors OPG and cytokines RANKL, and the population dynamics of OBA, OBP and OCA. More importantly, parametric study of bone remodelling under PEMF was performed in order to understand the control mechanism of bone remodelling at the cellular level under PEMF.

The quantitative analysis performed using this mathematical framework will improve the understanding of bone remodelling, which is of great importance to human beings, especially the elder population in our society. Based on the identified possible control mechanisms of bone remodelling, some 'virtual therapies' could be designed and tested by *in vitro* and *in vivo* experiments. The experimentally proved therapies could become potential real therapies to treat bone loss diseases such as osteoporosis.

7.2 Future Work

Future work could focus on the following assumptions and limitations on which the proposed framework is based:

- The bone remodelling initiated by mechanical stimuli starts by programmed death in osteocytes [134]. It is still not known what factors cause osteocyte death. In the model, the osteocyte death at the beginning of bone remodelling is not taken into account.
- The amounts of uncommitted OBU and OCP are assumed very large, for which reason the numbers of OBU and OCP do not appear in the model.
- In the numerical simulations, the RANK concentration is fixed and this assumption could be relaxed in a future study.
- The hypothesis that PTH endogenous production is considered as constant and no further regulated in the framework .
- The framework is based on the so-called 'convergence hypothesis' that all the activities of resorptive or anti-resorptive agents converge at the level of RANKL and OPG through which the final effects are achieved. More factors could be introduced into the bone remodelling system in order to account for their effects that are supported by experimental observations.

- The change in bone shape, namely the macroscopic bone surface remodelling, is not included here, which explains why there is no spatial distribution in the current model.
- Coupling between mechanical and electro-magnetic bone remodelling because of piezoelectricity of bone is assumed minimal in the thesis, further experimental and theoretical research could be performed to verify this assumption.
- Further experimental verification of the bone-remodelling model under PEMF could be conducted in the future.

Appendix A

Model's Parameters [6]

Symbol	Unit	Valve	Description
C^S	pM	5×10^{-3}	Value of C to get half differentiation flux
D_A	Day^{-1}	0.7	Rate of osteoclast apoptosis caused by TGF-β
d_B	Day^{-1}	0.7	Differentiation rate of responding osteoblasts
D_C	pM Day^{-1}	2.1×10^{-3}	Differentiation rate of osteoclast precursor
D_R	pM Day^{-1}	7×10^{-4}	Differentiation rate osteoblast progenitors
f_0	No dimension	0.05	Fixed proportion
I_L	pM Day^{-1}	$0-10^6$	Rate of administration of RANKL
I_O	pM Day^{-1}	$0-10^6$	Rate of administration of OPG
I_P	pM Day^{-1}	$0-10^6$	Rate of administration of PTH
K	pM	10	Fixed concentration of RANK
k_1	pM^{-1} Day^{-1}	10^{-2}	Rate of OPG-RANKL binding
k_2	Day^{-1}	10	Rate of OPG-RANKL unbinding
k_3	pM^{-1} Day^{-1}	5.8×10^{-4}	Rate of RANK-RANKL binding

k_4	Day^{-1}	1.7×10^{-2}	Rate of RANK-RANKL unbinding
k_5	$pM^{-1}\ Day^{-1}$	0.02	Rate of PTH binding with its receptor
k_6	Day^{-1}	3	Rate of PTH unbinding
k_B	Day^{-1}	0.189	Rate of elimination of AOB
K_L^P	pmol/pmol cells	3×10^6	Maximum number of RANKL attached on each cell surface
k_O	Day^{-1}	0.35	Rate of elimination of OPG
K_O^P	pmol day^{-1}/pmol cells	2×10^5	Minimal rate of production of OPG per cell
k_P	day^{-1}	86	Rate of elimination of PTH
r_L	pM day^{-1}	10^3	Rate of RANKL production and elimination
S_P	pM day^{-1}	250	Rate of synthesis of systemic PTH
R^S	pM	5×10^{-2}	Value of R to get half differentiation flux
m_1	% $cell^{-1}\ d^{-1}$	122	Average rate of bone resorbed per day per AOC
m_2	% $cell^{-1}\ d^{-1}$	195	Average rate of bone formed per day per AOB

Appendix B

Parameter values and descriptions (most parameter values are from [6, 20] except otherwise indicated)

Symbol	Unit	Value	Description
D_{OBU}	pM/day	7×10^{-4}	Differentiation rate of uncommitted OB progenitors
D_{OBP}	pM/day	5.348	Differentiation rate of preosteoblasts
D_{OCP}	pM/day	2.1×10^{-3}	Differentiation rate of preosteoclasts
A_{OBA}	pM/day	1.890×10^{-1}	Rate of elimination of OBA
A_{OCA}	pM/day	7.000×10^{-1}	Rate of elimination of OCA
A_{OST}	pM/day	3.1×10^{-2}	Rate of elimination of OST [66, 67]
$K_{D1,T\beta}$	pM	4.545×10^{-3}	Activation coefficient related to TGF-β binding on OBU
$K_{D2,T\beta}$	pM	1.416×10^{-3}	Repression coefficient related to TGF-β binding on OBP
$K_{D3,T\beta}$	pM	4.545×10^{-3}	Activation coefficient of TGF-β binding on OCA
$K_{D4,PTH}$	pM	1.500×10^{2}	Activation coefficient for $RANKL_{eff}$ on OBP related to PTH binding
$K_{D5,PTH}$	pM	2.226×10^{-1}	Repression coefficient for OPG production related to PTH binding on OBA
$K_{D6,RL}$	pM	1.500×10^{2}	Activation coefficient related to RANKL binding on OCP
$K_{D7,NO}$	pM	1.573×10	Activation coefficient for OPG production on OBA related to NO [66, 67]
$K_{D8,NO}$	pM	2.189×10	Repression coefficient for RANKL production on OBP related to NO [66, 67]
$K_{D9,P2}$	pM	3.674	Activation coefficient for OBU differentiation related to PGE_2 [66, 67]
RK	pM	1×10	Unchanged concentration of RANK
R_{RL}	-	3×10^{6}	Maximum RANKL on OBP
β_{PTH}	pM/cell	2.5×10^{2}	Synthesis rate of systemic PTH
β_{RL}	pM/cell	1.684×10^{4}	Production rate of RANKL per OBP
β_{OPG}	pM/cell	1.464×10^{8}	Production rate of OPG per OBA
$\tilde{D}_{PTH}$	pM/day	8.6×10	Rate of degradation of PTH
$\tilde{D}_{RL}$	pM/cell	1.013×10	Rate of degradation of RANKL

$\tilde{D}_{OPG}$	pM/cell	3.5×10^{-1}	Rate of degradation of OPG
$\tilde{D}_{T\beta}$	pM/cell	1×10^{0}	Rate of degradation of TGF-β
$\tilde{D}_{NO}$	pM/cell	1×10^{3}	Rate of degradation of NO [66, 67]
$\tilde{D}_{P2}$	pM/cell	1×10^{2}	Rate of degradation of T PGE_2 [66, 67]
$k_{T\beta}$	-	0.5	Relative influence of TGF-β binding in OBU differentiation
k_{P2}	-	0.5	Relative influence of PGE_2 in OBU differentiation
k_{PTH}	-	0.7	Relative influence of PTH binding in production of OPG in OBA
k_{NO}	-	0.3	Relative influence of NO in production of OPG in OBA
$K_{A1,RL}$	pM^{-1}	1×10^{-3}	Association binding constant RANKL-OPG
$K_{A2,RL}$	pM^{-1}	3.412×10^{-2}	Association binding constant RANKL-RANK
OPG_{max}	pM	2×10^{8}	Maximum possible OPG concentration
α	%	1	TGF-β content stored in bone matrix
K_{res}	day^{-1}	1	Relative rate of bone resorption
K_{for}	day^{-1}	1.571	Relative rate of bone formation
K_{to}	day^{-1}	1.552×10	Relative rate of bone turnover [66, 67]
T_{OBA}	pM/day	0.15	Rate of trapped OBA in bone matrix [66, 67]
K_{NO}	pM/day	2×10^{4}	Secretion rate of NO by osteocytes [66, 67]
K_{P2}	pM/day	1×10^{2}	Secretion rate of PGE_2 by osteocytes [66, 67]
T_{acc}	day	24	time constant describing the rate at which accommodation takes place [128]
τ	h	6	a time constant [127]

Appendix C

Parameter values and descriptions [17, 26]

Symbol	Unit	Value	Description
D_{OBU}	pM/day	7×10^{-4}	Differentiation rate of uncommitted OB progenitors
D_{OBP}	pM/day	5.348	Differentiation rate of preosteoblasts
D_{OCP}	pM/day	2.1×10^{-3}	Differentiation rate of preosteoclasts
A_{OBA}	pM/day	1.890×10^{-1}	Rate of elimination of OBA
A_{OCA}	pM/day	7.000×10^{-1}	Rate of elimination of OCA
A_{OST}	pM/day	3.1×10^{-2}	Rate of elimination of OST
$K_{D1,T\beta}$	pM	4.545×10^{-3}	Activation coefficient related to TGF-β binding on OBU
$K_{D2,T\beta}$	pM	1.416×10^{-3}	Repression coefficient related to TGF-β binding on OBP
$K_{D3,T\beta}$	pM	4.545×10^{-3}	Activation coefficient of TGF-β binding on OCA
$K_{D4,PTH}$	pM	1.500×10^{2}	Activation coefficient for $RANKL_{eff}$ on OBP related to PTH binding
$K_{D5,PTH}$	pM	2.226×10^{-1}	Repression coefficient for OPG production related to PTH binding on OBA
$K_{D6,RL}$	pM	1.500×10^{2}	Activation coefficient related to RANKL binding on OCP
$K_{D7,NO}$	pM	1.573×10	Activation coefficient for OPG production on OBA related to NO
$K_{D8,NO}$	pM	2.189×10	Repression coefficient for RANKL production on OBP related to NO
$K_{D9,P2}$	pM	3.674	Activation coefficient for OBU differentiation related to PGE_2
RK	pM	1×10	Unchanged concentration of RANK
R_{RL}	-	3×10^{6}	Maximum RANKL on OBP
β_{PTH}	pM/cell	2.5×10^{2}	Synthesis rate of systemic PTH
β_{RL}	pM/cell	1.684×10^{4}	Production rate of RANKL per OBP
β_{OPG}	pM/cell	1.464×10^{8}	Production rate of OPG per OBA
$\tilde{D}_{PTH}$	pM/day	8.6×10	Rate of degradation of PTH
$\tilde{D}_{RL}$	pM/cell	1.013×10	Rate of degradation of RANKL
$\tilde{D}_{OPG}$	pM/cell	3.5×10^{-1}	Rate of degradation of OPG
$\tilde{D}_{T\beta}$	pM/cell	1×10^{0}	Rate of degradation of TGF-β

$\tilde{D}_{NO}$	pM/cell	1×10^{3}	Rate of degradation of NO
$\tilde{D}_{P2}$	pM/cell	1×10^{2}	Rate of degradation of T PGE_2
$k_{T\beta}$	-	0.5	Relative influence of TGF-β binding in OBU differentiation
k_{P2}	-	0.5	Relative influence of PGE_2 in OBU differentiation
k_{PTH}	-	0.7	Relative influence of PTH binding in production of OPG in OBA
k_{NO}	-	0.3	Relative influence of NO in production of OPG in OBA
$K_{A1,RL}$	pM^{-1}	1×10^{-3}	Association binding constant RANKL-OPG
$K_{A2,RL}$	pM^{-1}	3.412×10^{-2}	Association binding constant RANKL-RANK
OPG_{max}	pM	2×10^{8}	Maximum possible OPG concentration
α	%	1	TGF-β content stored in bone matrix
k_{res}	day^{-1}	1	Relative rate of bone resorption
k_{for}	day^{-1}	1.571	Relative rate of bone formation
K_{to}	day^{-1}	1.552×10	Relative rate of bone turnover
T_{OBA}	pM/day	0.15	Rate of trapped OBA in bone matrix
K_{NO}	pM/day	2×10^{4}	Secretion rate of NO by osteocytes
K_{P2}	pM/day	1×10^{2}	Secretion rate of PGE_2 by osteocytes

Appendix D

D.1 Matlab Code of Parametric Study of Control Mechanism of Bone Remodeling under Mechanical Stimulus

```
DG[rl] := 1.013e1;

DG[p2] := 3.;

DG[no] := 0.7e2;

DG[opg] := 3.5e-1;

DG[Tbeta] := 1;

DG[pth] := 8.6e1;

Tr[oba] := .15;

K[D1, Tbeta] := 4.545e-3;

K[D2, Tbeta] := 1.416e-3;

K[D3, Tbeta] := 4.545e-3;

K[D4, pth] := 1.5e2;

K[D5, pth] := 2.226e-1;

K[D6, rl] := 1.306e1;

K[D7, no] := 1.573e1;

K[D8, no] := 2.189e1;

K[D9, p2] := 3.674;

S[Tbeta] := 0;

P[pth, d] := 0;
```

```
P[rl, d] := 0;

P[opg, d] := 0;

RK := 1;

R[rl] := 3e6;

beta[pth] := 2.5e2;

beta[rl] := 1.684e4;

beta[opg] := 1.464e8;

Opg[maxi] := 2e8;

K[A1, rl] := 1e-3;

K[A2, rl] := 3.412e-2;

alpha := 1;

B[res] := 1;

B[form] := 24.876;

tau := 6;

PR[no] := 0.35e5;

PR[p2] := 0.25e3;

T[rest] := 3;

N := 360;

f := 2;

AP := 3.2;

kk[Tbeta] := .3;

kk[p2] := .7;
```

```
kk[pth] := .7;

kk[no] := .3;

FEC := 12.52;

T[acc] := 24;

total := 1;

with(combinat);

paraindex := [1, 2, 3, 4, 5, 6];

for i to 6 do

        paracomb[i] := choose(paraindex, i);

                for j to factorial(6)/(factorial(6-i)*factorial(i)) do

                        for k from 0 to 2^i-1 do

                                paravalue := [0.7e-3, 5.348, 0.21e-2, .189, .7,

                                0.31e-1];

                                        for l to i do

                                                c[0, k] := k;

                                                c[l, k] := iquo(c[l-1, k], 2);

                                                b[l, k] := irem(c[l-1, k], 2);

                                                if b[l, k] = 0 then b[l, k] := -1 endif;

                                                indexnum := paracomb[i][j][l];

                                                paravalue[indexnum] :=paravalue[in

                                                dexnum]*1.5^(b[l, k]*pq);

                                        end do:
```

```
        DF[obu] := paravalue[1];
        DF[obp] := paravalue[2];
        DF[ocp] := paravalue[3];
        A[oba] := paravalue[4];
        A[oca] := paravalue[5];
        A[ost] := paravalue[6];
        print(total, "DF[obu]=", DF[obu], "DF[obp]=",
DF[obp], "DF[ocp]=", DF[ocp], "A[oba]=", A
[oba], "A[oca]=", A[oca], "A[ost]=", A[ost]);
TGF[beta] :=(alpha*B[res]*OCA(t)+S[Tbeta])/DG[Tbet
a];
PI[Tbeta, act, obu] :=
TGF[beta]/(K[D1,Tbeta]+TGF[beta]);
PI[Tbeta, rep, obp] := 1/(1+TGF[beta]/K[D2, Tbeta]);
        PI[Tbeta, act, oca] := TGF[beta]/(K[D3,
        Tbeta]+TGF[beta]);
        PTH := (beta[pth]+P[pth, d])/DG[pth];
        PI[pth, act, obp] := PTH/(K[D4, pth]+PTH);
        PI[pth, rep, oba] := 1/(1+PTH/K[D5, pth]);
        PI[no, act, oba] := NO(t)/(K[D7, no]+NO(t));
        PI[no, rep, obp] := 1/(1+NO(t)/K[D8, no]);
        PI[p2, act, obu] := P2(t)/(K[D9, p2]+P2(t));
```

R[PFSS] := 2*Pi*AP*f;

OPG := (beta[opg]*OBA(t)*(kk[pth]*PI[pth,rep, oba]+kk[no]*PI[no, act, oba])+P[opg, d])/(beta[opg]*OBA(t)*(kk[pth]*PI[pth, rep, oba]+kk[no]*PI[no,act,oba])/Opg[maxi]+DG[opg]);

RL :=R[rl]*OBP(t)*PI[pth,act,obp]*(beta[rl]*OB P(t)*PI[no, rep, obp]+P[rl, d])/((1+K[A1, rl]*OPG+K[A2,rl]*RK)*(beta[rl]*OBP(t)*PI[no, rep,obp]+DG[rl]*R[rl]*OBP(t)*PI[pth, act, obp]));

PI[rl, act, ocp] := RL/(K[D6, rl]+RL);

eq1 :=diff(OBP(t),t)=DF[obu]*(kk[Tbeta]*PI[Tb eta, act, obu]+kk[p2]*PI[p2, act, obu])-DF[obp]*OBP(t)*PI[Tbeta, rep, obp];

eq2 :=diff(OBA(t),t)=DF[obp]*OBP(t)*PI[Tbeta, rep, obp]-A[oba]*OBA(t);

eq3 := diff(OST(t), t) = Tr[oba]*OBA(t)-A[ost]*OST(t);

eq4 := diff(OCA(t), t) = DF[ocp]*PI[rl,act,ocp]-A[oca]*OCA(t)*PI[Tbeta, act, oca];

```
eq5 := diff(NO(t), t) =
PR[no]*R[PFSS]*OST(t)*(1-exp(-
T[rest]/tau))*ln(1+N)*ln(f+.5)*exp(-t/T[acc])-
DG[no]*NO(t);
eq6 := diff(P2(t), t) =
PR[p2]*R[PFSS]*OST(t)*(1-exp(-
T[rest]/tau))*ln(1+N)*ln(f+.5)*exp(-t/T[acc])-
DG[p2]*P2(t);
eq7 := diff(BMC(t), t) = B[form]*(OBA(t)-
0.2126991130e-3)-B[res]*(OCA(t)-
0.2769166993e-3);
eq8 := diff(BFE(t), t) = diff(BMC(t),
t)+FEC*sqrt(OBA(t)+OCA(t));
ics1 := OBA(0) = 0.2126991130e-3, OST(0) =
0.1029189256e-2, OBP(0) = 0.8986869185e-5,
OCA(0) =0.2769166993e-3,
NO(0) = 0, P2(0) = 0, BMC(0) = 100,BFE(0) =
100;
ans1 := dsolve({eq1, eq2, eq3, eq4, eq5, eq6, eq7,
eq8, ics1}, {BFE(t), BMC(t), NO(t), OBA(t),
OBP(t), OCA(t), OST(t), P2(t)}, type = numeric,
maxfun = 0, parameters = [pq]);
```

```
                plotcoord1 := [seq([0, 0], i = 1 .. 41)];
                plotcoord2 := [seq([0, 0], i = 1 .. 41)];
                ii := 1;
                    for qq from -10 by .5 to 10 do
                        ans1(parameters = [qq]);
                        plotcoord1[ii]  :=[qq,rhs(ans1(100)[3
                        ])];
                        plotcoord2[ii]  :=[qq,rhs(ans1(100)[2
                        ])];
                        ii := ii+1;
                    end do:
            results[total]   :=plot([plotcoord1,plotcoord2],color   =
            black, linestyle = [1, 3], legend = ["BMC-100th day",
            "BFE-100th day"], labels = ["Exponent", " [%]"], axes =
            boxed,      labeldirections      =      [HORIZONTAL,
            VERTICAL]);
                total := total+1;
            end do:
        end do:
end do:
total := 1;
with(combinat);
```

```
paraindex := [1, 2, 3, 4, 5, 6];
for i to 6 do
    paracomb[i] := choose(paraindex, i);
        for j to factorial(6)/(factorial(6-i)*factorial(i)) do
            for k from 0 to 2^i-1 do
                paravalue := [0.7e-3, 5.348, 0.21e-2, .189, .7,
                0.31e-1];
                    for l to i do
                        c[0, k] := k;
                        c[l, k] := iquo(c[l-1, k], 2);
                        b[l, k] := irem(c[l-1, k], 2);
                        if b[l, k] = 0 then b[l, k] := -1 endif;
                        indexnum := paracomb[i][j][l];
                        paravalue[indexnum] :=paravalue[in
                        dexnum]*1.5^(b[l, k]*pq);
                    end do:
                DF[obu] := paravalue[1];
                DF[obp] := paravalue[2];
                DF[ocp] := paravalue[3];
                A[oba] := paravalue[4];
                A[oca] := paravalue[5];
                A[ost] := paravalue[6];
```

```
print(total, "DF[obu]=", DF[obu], "DF[obp]=",
DF[obp], "DF[ocp]=", DF[ocp], "A[oba]=", A
[oba], "A[oca]=", A[oca], "A[ost]=", A[ost]);
TGF[beta] :=(alpha*B[res]*OCA(t)+S[Tbeta])/DG[Tbet
a];
PI[Tbeta, act, obu] :=
TGF[beta]/(K[D1,Tbeta]+TGF[beta]);
PI[Tbeta, rep, obp] := 1/(1+TGF[beta]/K[D2, Tbeta]);
        PI[Tbeta, act, oca] := TGF[beta]/(K[D3,
        Tbeta]+TGF[beta]);
        PTH := (beta[pth]+P[pth, d])/DG[pth];
        PI[pth, act, obp] := PTH/(K[D4, pth]+PTH);
        PI[pth, rep, oba] := 1/(1+PTH/K[D5, pth]);
        PI[no, act, oba] := NO(t)/(K[D7, no]+NO(t));
        PI[no, rep, obp] := 1/(1+NO(t)/K[D8, no]);
        PI[p2, act, obu] := P2(t)/(K[D9, p2]+P2(t));
        R[PFSS] := 2*Pi*AP*f;
        OPG := (beta[opg]*OBA(t)*(kk[pth]*PI[pth,rep,
        oba]+kk[no]*PI[no, act, oba])+P[opg,
        d])/(beta[opg]*OBA(t)*(kk[pth]*PI[pth, rep,
        oba]+kk[no]*PI[no,act,oba])/Opg[maxi]+DG[opg
        ]);
```

RL :=R[rl]*OBP(t)*PI[pth,act,obp]*(beta[rl]*OB
P(t)*PI[no, rep, obp]+P[rl, d])/((1+K[A1,
rl]*OPG+K[A2,rl]*RK)*(beta[rl]*OBP(t)*PI[no,
rep,obp]+DG[rl]*R[rl]*OBP(t)*PI[pth, act,
obp]));

PI[rl, act, ocp] := RL/(K[D6, rl]+RL);

eq1 :=diff(OBP(t),t)=DF[obu]*(kk[Tbeta]*PI[Tb
eta, act, obu]+kk[p2]*PI[p2, act, obu])-
DF[obp]*OBP(t)*PI[Tbeta, rep, obp];

eq2 :=diff(OBA(t),t)=DF[obp]*OBP(t)*PI[Tbeta,
rep, obp]-A[oba]*OBA(t);

eq3 := diff(OST(t), t) = Tr[oba]*OBA(t)-
A[ost]*OST(t);

eq4 := diff(OCA(t), t) = DF[ocp]*PI[rl,act,ocp]-
A[oca]*OCA(t)*PI[Tbeta, act, oca];

eq5 := diff(NO(t), t) =
PR[no]*R[PFSS]*OST(t)*(1-exp(-
T[rest]/tau))*ln(1+N)*ln(f+.5)*exp(-t/T[acc])-
DG[no]*NO(t);

eq6 := diff(P2(t), t) =
PR[p2]*R[PFSS]*OST(t)*(1-exp(-

```
T[rest]/tau))*ln(1+N)*ln(f+.5)*exp(-t/T[acc])-
DG[p2]*P2(t);
eq7 := diff(BMC(t), t) = B[form]*(OBA(t)-
0.2126991130e-3)-B[res]*(OCA(t)-
0.2769166993e-3);
eq8 := diff(BFE(t), t) = diff(BMC(t),
t)+FEC*sqrt(OBA(t)+OCA(t));
ics1 := OBA(0) = 0.2126991130e-3, OST(0) =
0.1029189256e-2, OBP(0) = 0.8986869185e-5,
OCA(0) =0.2769166993e-3,
NO(0) = 0, P2(0) = 0, BMC(0) = 100,BFE(0) =
100;
ans1 := dsolve({eq1, eq2, eq3, eq4, eq5, eq6, eq7,
eq8, ics1}, {BFE(t), BMC(t), NO(t), OBA(t),
OBP(t), OCA(t), OST(t), P2(t)}, type = numeric,
maxfun = 0, parameters = [pq]);
plotcoord1 := [seq([0, 0], i = 1 .. 41)];
plotcoord2 := [seq([0, 0], i = 1 .. 41)];
ii := 1;
        for qq from -10 by .5 to 10 do
                ans1(parameters = [qq]);
```

```
                    plotcoord1[ii] :=[qq,rhs(ans1(100)[3
                    ])];
                    plotcoord2[ii] :=[qq,rhs(ans1(100)[2
                    ])];
                    ii := ii+1;
                end do:
            results[total] :=plot([plotcoord1,plotcoord2],color =
            black, linestyle = [1, 3], legend = ["BMC-100th day",
            "BFE-100th day"], labels = ["Exponent", " [%]"], axes =
            boxed, labeldirections = [HORIZONTAL,
            VERTICAL]);
                total := total+1;
            end do:
        end do:
end do:
with(combinat);
paraindex := [1, 2, 3, 4, 5, 6];
for i to 6 do
    paracomb[i] := choose(paraindex, i);
        for j to factorial(6)/(factorial(6-i)*factorial(i)) do
            for k from 0 to 2^i-1 do
```

```
paravalue := [0.7e-3, 5.348, 0.21e-2, .189, .7,
0.31e-1];
        for l to i do
            c[0, k] := k;
            c[l, k] := iquo(c[l-1, k], 2);
            b[l, k] := irem(c[l-1, k], 2);
            if b[l, k] = 0 then b[l, k] := -1 endif;
            indexnum := paracomb[i][j][l];
            paravalue[indexnum] :=paravalue[in
            dexnum]*1.5^(b[l, k]*pq);
        end do:
    DF[obu] := paravalue[1];
    DF[obp] := paravalue[2];
    DF[ocp] := paravalue[3];
    A[oba] := paravalue[4];
    A[oca] := paravalue[5];
    A[ost] := paravalue[6];
    print(total, "DF[obu]=", DF[obu], "DF[obp]=",
DF[obp], "DF[ocp]=", DF[ocp], "A[oba]=", A
[oba], "A[oca]=", A[oca], "A[ost]=", A[ost]);
TGF[beta] :=(alpha*B[res]*OCA(t)+S[Tbeta])/DG[Tbet
a];
```

```
PI[Tbeta, act, obu] :=
TGF[beta]/(K[D1,Tbeta]+TGF[beta]);
PI[Tbeta, rep, obp] := 1/(1+TGF[beta]/K[D2, Tbeta]);
        PI[Tbeta, act, oca] := TGF[beta]/(K[D3,
        Tbeta]+TGF[beta]);
        PTH := (beta[pth]+P[pth, d])/DG[pth];
        PI[pth, act, obp] := PTH/(K[D4, pth]+PTH);
        PI[pth, rep, oba] := 1/(1+PTH/K[D5, pth]);
        PI[no, act, oba] := NO(t)/(K[D7, no]+NO(t));
        PI[no, rep, obp] := 1/(1+NO(t)/K[D8, no]);
        PI[p2, act, obu] := P2(t)/(K[D9, p2]+P2(t));
        R[PFSS] := 2*Pi*AP*f;
        OPG := (beta[opg]*OBA(t)*(kk[pth]*PI[pth,rep,
        oba]+kk[no]*PI[no, act, oba])+P[opg,
        d])/(beta[opg]*OBA(t)*(kk[pth]*PI[pth, rep,
        oba]+kk[no]*PI[no,act,oba])/Opg[maxi]+DG[opg
        ]);
        RL :=R[rl]*OBP(t)*PI[pth,act,obp]*(beta[rl]*OB
        P(t)*PI[no, rep, obp]+P[rl, d])/((1+K[A1,
        rl]*OPG+K[A2,rl]*RK)*(beta[rl]*OBP(t)*PI[no,
        rep,obp]+DG[rl]*R[rl]*OBP(t)*PI[pth, act,
        obp]));
```

```
PI[rl, act, ocp] := RL/(K[D6, rl]+RL);
eq1 :=diff(OBP(t),t)=DF[obu]*(kk[Tbeta]*PI[Tb
eta, act, obu]+kk[p2]*PI[p2, act, obu])-
DF[obp]*OBP(t)*PI[Tbeta, rep, obp];
eq2 :=diff(OBA(t),t)=DF[obp]*OBP(t)*PI[Tbeta,
rep, obp]-A[oba]*OBA(t);
eq3 := diff(OST(t), t) = Tr[oba]*OBA(t)-
A[ost]*OST(t);
eq4 := diff(OCA(t), t) = DF[ocp]*PI[rl,act,ocp]-
A[oca]*OCA(t)*PI[Tbeta, act, oca];
eq5 := diff(NO(t), t) =
PR[no]*R[PFSS]*OST(t)*(1-exp(-
T[rest]/tau))*ln(1+N)*ln(f+.5)*exp(-t/T[acc])-
DG[no]*NO(t);
eq6 := diff(P2(t), t) =
PR[p2]*R[PFSS]*OST(t)*(1-exp(-
T[rest]/tau))*ln(1+N)*ln(f+.5)*exp(-t/T[acc])-
DG[p2]*P2(t);
eq7 := diff(BMC(t), t) = B[form]*(OBA(t)-
0.2126991130e-3)-B[res]*(OCA(t)-
0.2769166993e-3);
```

```
eq8 := diff(BFE(t), t) = diff(BMC(t),
t)+FEC*sqrt(OBA(t)+OCA(t));
ics1 := OBA(0) = 0.2126991130e-3, OST(0) =
0.1029189256e-2, OBP(0) = 0.8986869185e-5,
OCA(0) =0.2769166993e-3,
NO(0) = 0, P2(0) = 0, BMC(0) = 100,BFE(0) =
100;
ans1 := dsolve({eq1, eq2, eq3, eq4, eq5, eq6, eq7,
eq8, ics1}, {BFE(t), BMC(t), NO(t), OBA(t),
OBP(t), OCA(t), OST(t), P2(t)}, type = numeric,
maxfun = 0, parameters = [pq]);
plotcoord1 := [seq([0, 0], i = 1 .. 41)];
plotcoord2 := [seq([0, 0], i = 1 .. 41)];
ii := 1;
        for qq from -10 by .5 to 10 do
                ans1(parameters = [qq]);
                plotcoord1[ii] :=[qq,rhs(ans1(100)[3
                ])];
                plotcoord2[ii] :=[qq,rhs(ans1(100)[2
                ])];
                ii := ii+1;
        end do:
```

```
                results[total]  :=plot([plotcoord1,plotcoord2],color =
                black, linestyle = [1, 3], legend = ["BMC-100th day",
                "BFE-100th day"], labels = ["Exponent", " [%]"], axes =
                boxed,  labeldirections  =  [HORIZONTAL,
                VERTICAL]);
                        total := total+1;
                end do:
        end do:
end do:
```

D.2 Matlab Code of Parametric Study of Control Mechanism of Bone Remodeling under PEMF

```
DG[rl] := 1.013*10;
DG[opg] := 3.5*10^(-1);
DG[Tbeta] := 1;
DG[pth] := 8.6*10;
Tr[oba] := .15;
K[D1, Tbeta] := 4.545*10^(-3);
K[D2, Tbeta] := 1.416*10^(-3);
K[D3, Tbeta] := 4.545*10^(-3);
K[D4, pth] := 1.5*10^2;
```

```
K[D5, pth] := 2.226*10^(-1);

K[D6, rl] := 1.306*10;

S[Tbeta] := 0;

P[pth, d] := 0;

P[rl, d] := 0;

P[opg, d] := 0;

RK := 1;

R[rl] := 3*10^6;

beta[pth] := 2.5*10^2;

beta[rl] := 1.684*10^4;

beta[opg] := 1.464*10^8;

Opg[maxi] := 2*10^8;

K[A1, rl] := 10^(-3);

K[A2, rl] := 3.412*10^(-2);

alpha := 1;

B[res] := 1;

B[form] := 1.571;

F[opg] := 2;

F[rl] := .5;

total := 1;

with(combinat);

paraindex := [1, 2, 3, 4, 5];
```

```
for i to 5 do
    paracomb[i] := choose(paraindex, i);
    for j to factorial(5)/(factorial(5-i)*factorial(i)) do
        for k from 0 to 2^i-1 do
            paravalue := [0.7e-3, 5.348, 0.21e-2, .189, .7];
            for l to i do
                c[0, k] := k;
                c[l, k] := iquo(c[l-1, k], 2);
                b[l, k] := irem(c[l-1, k], 2);
                if b[l, k] = 0 then b[l, k] := -1 end if;
                indexnum := paracomb[i][j][l];
                paravalue[indexnum] :=paravalue[indexnum]*1.5
                ^(b[l, k]*pq);
            end do:
            DF[obu] := paravalue[1];
            DF[obp] := paravalue[2];
            DF[ocp] := paravalue[3];
            A[oba] := paravalue[4];
            A[oca] := paravalue[5];
           print(total, "DF[obu]=", DF[obu], "DF[obp]=", DF[obp],
       "DF[ocp]=", DF[ocp], "A[oba]=", A[oba], "A[oca]=", A[oca]);
       TGF[beta] := (alpha*B[res]*OCA(t)+S[Tbeta])/DG[Tbeta];
```

PI[Tbeta, act, obu] := TGF[beta]/(K[D1, Tbeta]+TGF[beta]);

PI[Tbeta, rep, obp] := 1/(1+TGF[beta]/K[D2, Tbeta]);

PI[Tbeta, act, oca] := TGF[beta]/(K[D3, Tbeta]+TGF[beta]);

PTH := (beta[pth]+P[pth, d])/DG[pth];

PI[pth, act, obp] := PTH/(K[D4, pth]+PTH);

PI[pth, rep, oba] := 1/(1+PTH/K[D5, pth]);

OPG :=(beta[opg]*OBA(t)*PI[pth,rep,oba]+P[opg,d])/(beta[o
pg]*OBA(t)*PI[pth, rep, oba]/Opg[maxi]+DG[opg]);

RL[eff] := R[rl]*OBP(t)*PI[pth, act, obp];

RL := R[rl]*OBP(t)*PI[pth, act, obp]*(beta[rl]*OBP(t)+P[rl,
d])/((1+K[A1,rl]*OPG+K[A2,rl]*RK)*(beta[rl]*OBP(t)+DG[
rl]*OBP(t)*PI[pth, act, obp]));

PI[rl, act, ocp] := RL/(K[D6, rl]+RL);

eq1 := diff(OBP(t), t) = DF[obu]*PI[Tbeta, act, obu]-
DF[obp]*OBP(t)*PI[Tbeta, rep, obp];

eq2 := diff(OBA(t), t) = DF[obp]*OBP(t)*PI[Tbeta, rep, obp]-
A[oba]*OBA(t);

eq3 := diff(OCA(t), t) = DF[ocp]*PI[rl, act, ocp]-
A[oca]*OCA(t)*PI[Tbeta, act, oca];

eq4 := diff(BV(t), t) = B[form]*(OBA(t)-0.2126991130e-3)-
B[res]*(OCA(t)-0.2769166993e-3);

```
        ics := OBP(0) = 0.8986869185e-5, OBA(0) = 0.2126991130e-
        3, OCA(0) = 0.2769166993e-3, BV(0) = 100; ans :=
        dsolve({eq1, eq2, eq3, eq4, ics},{BV(t),OBA(t), OBP(t),
        OCA(t)}, type = numeric, maxfun = 0, parameters = [pq]);

        plotcoord1 := [seq([0, 0], i = 1 .. 41)];
        ii := 1;
            for qq from -10 by .5 to 10 do
                ans(parameters = [qq]);
                plotcoord1[ii] := [qq, rhs(ans(90)[2])];
                ii := ii+1;
            end do:
        results[total] := plot([plotcoord1], color = black, linestyle = 1,
        thickness = 2, legend = ["BV-90th day"], labels = ["Exponent",
        " Bone volume [%]"], axes = boxed, labeldirections =
        [HORIZONTAL, VERTICAL]);
            total := total+1;
        end do:
    end do:
end do:
with(combinat);
paraindex := [1, 2, 3, 4, 5];
```

```
for i to 5 do
    paracomb[i] := choose(paraindex, i);
    for j to factorial(5)/(factorial(5-i)*factorial(i)) do
        for k from 0 to 2^i-1 do
            paravalue := [0.7e-3, 5.348, 0.21e-2, .189, .7];
            for l to i do
                c[0, k] := k;
                c[l, k] := iquo(c[l-1, k], 2);
                b[l, k] := irem(c[l-1, k], 2);
                if b[l, k] = 0 then b[l, k] := -1 end if;
                indexnum := paracomb[i][j][l];
                paravalue[indexnum] :=paravalue[indexnum]*1.5
                ^(b[l, k]*pq);
            end do:
            DF[obu] := paravalue[1];
            DF[obp] := paravalue[2];
            DF[ocp] := paravalue[3];
            A[oba] := paravalue[4];
            A[oca] := paravalue[5];
           print(total, "DF[obu]=", DF[obu], "DF[obp]=", DF[obp],
    "DF[ocp]=", DF[ocp], "A[oba]=", A[oba], "A[oca]=", A[oca]);
    TGF[beta] := (alpha*B[res]*OCA(t)+S[Tbeta])/DG[Tbeta];
```

```
PI[Tbeta, act, obu] := TGF[beta]/(K[D1, Tbeta]+TGF[beta]);

PI[Tbeta, rep, obp] := 1/(1+TGF[beta]/K[D2, Tbeta]);

PI[Tbeta, act, oca] := TGF[beta]/(K[D3, Tbeta]+TGF[beta]);

PTH := (beta[pth]+P[pth, d])/DG[pth];

PI[pth, act, obp] := PTH/(K[D4, pth]+PTH);

PI[pth, rep, oba] := 1/(1+PTH/K[D5, pth]);

OPG :=(beta[opg]*OBA(t)*PI[pth,rep,oba]+P[opg,d])/(beta[o
pg]*OBA(t)*PI[pth, rep, oba]/Opg[maxi]+DG[opg]);

RL[eff] := R[rl]*OBP(t)*PI[pth, act, obp];

RL := R[rl]*OBP(t)*PI[pth, act, obp]*(beta[rl]*OBP(t)+P[rl,
d])/((1+K[A1,rl]*OPG+K[A2,rl]*RK)*(beta[rl]*OBP(t)+DG[
rl]*OBP(t)*PI[pth, act, obp]));

PI[rl, act, ocp] := RL/(K[D6, rl]+RL);

eq1 := diff(OBP(t), t) = DF[obu]*PI[Tbeta, act, obu]-
DF[obp]*OBP(t)*PI[Tbeta, rep, obp];

eq2 := diff(OBA(t), t) = DF[obp]*OBP(t)*PI[Tbeta, rep, obp]-
A[oba]*OBA(t);

eq3 := diff(OCA(t), t) = DF[ocp]*PI[rl, act, ocp]-
A[oca]*OCA(t)*PI[Tbeta, act, oca];

eq4 := diff(BV(t), t) = B[form]*(OBA(t)-0.2126991130e-3)-
B[res]*(OCA(t)-0.2769166993e-3);
```

```
            ics := OBP(0) = 0.8986869185e-5, OBA(0) = 0.2126991130e-
            3, OCA(0) = 0.2769166993e-3, BV(0) = 100; ans :=
            dsolve({eq1, eq2, eq3, eq4, ics},{BV(t),OBA(t), OBP(t),
            OCA(t)}, type = numeric, maxfun = 0, parameters = [pq]);

            plotcoord1 := [seq([0, 0], i = 1 .. 41)];
            ii := 1;
                for qq from -10 by .5 to 10 do
                    ans(parameters = [qq]);
                    plotcoord1[ii] := [qq, rhs(ans(90)[2])];
                    ii := ii+1;
                end do:
            results[total] := plot([plotcoord1], color = black, linestyle = 1,
            thickness = 2, legend = ["BV-90th day"], labels = ["Exponent",
            " Bone volume [%]"], axes = boxed, labeldirections =
            [HORIZONTAL, VERTICAL]);
                total := total+1;
            end do:
        end do:
    end do:
    with(combinat);
    paraindex := [1, 2, 3, 4, 5];
```

```
for i to 5 do
    paracomb[i] := choose(paraindex, i);
    for j to factorial(5)/(factorial(5-i)*factorial(i)) do
        for k from 0 to 2^i-1 do
            paravalue := [0.7e-3, 5.348, 0.21e-2, .189, .7];
            for l to i do
                c[0, k] := k;
                c[l, k] := iquo(c[l-1, k], 2);
                b[l, k] := irem(c[l-1, k], 2);
                if b[l, k] = 0 then b[l, k] := -1 end if;
                indexnum := paracomb[i][j][l];
                paravalue[indexnum] :=paravalue[indexnum]*1.5
                ^(b[l, k]*pq);
            end do:
            DF[obu] := paravalue[1];
            DF[obp] := paravalue[2];
            DF[ocp] := paravalue[3];
            A[oba] := paravalue[4];
            A[oca] := paravalue[5];
           print(total, "DF[obu]=", DF[obu], "DF[obp]=", DF[obp],
       "DF[ocp]=", DF[ocp], "A[oba]=", A[oba], "A[oca]=", A[oca]);
       TGF[beta] := (alpha*B[res]*OCA(t)+S[Tbeta])/DG[Tbeta];
```

PI[Tbeta, act, obu] := TGF[beta]/(K[D1, Tbeta]+TGF[beta]);

PI[Tbeta, rep, obp] := 1/(1+TGF[beta]/K[D2, Tbeta]);

PI[Tbeta, act, oca] := TGF[beta]/(K[D3, Tbeta]+TGF[beta]);

PTH := (beta[pth]+P[pth, d])/DG[pth];

PI[pth, act, obp] := PTH/(K[D4, pth]+PTH);

PI[pth, rep, oba] := 1/(1+PTH/K[D5, pth]);

OPG :=(beta[opg]*OBA(t)*PI[pth,rep,oba]+P[opg,d])/(beta[o

pg]*OBA(t)*PI[pth, rep, oba]/Opg[maxi]+DG[opg]);

RL[eff] := R[rl]*OBP(t)*PI[pth, act, obp];

RL := R[rl]*OBP(t)*PI[pth, act, obp]*(beta[rl]*OBP(t)+P[rl,

d])/((1+K[A1,rl]*OPG+K[A2,rl]*RK)*(beta[rl]*OBP(t)+DG[

rl]*OBP(t)*PI[pth, act, obp]));

PI[rl, act, ocp] := RL/(K[D6, rl]+RL);

eq1 := diff(OBP(t), t) = DF[obu]*PI[Tbeta, act, obu]-

DF[obp]*OBP(t)*PI[Tbeta, rep, obp];

eq2 := diff(OBA(t), t) = DF[obp]*OBP(t)*PI[Tbeta, rep, obp]-

A[oba]*OBA(t);

eq3 := diff(OCA(t), t) = DF[ocp]*PI[rl, act, ocp]-

A[oca]*OCA(t)*PI[Tbeta, act, oca];

eq4 := diff(BV(t), t) = B[form]*(OBA(t)-0.2126991130e-3)-

B[res]*(OCA(t)-0.2769166993e-3);

```
        ics := OBP(0) = 0.8986869185e-5, OBA(0) = 0.2126991130e-
        3, OCA(0) = 0.2769166993e-3, BV(0) = 100; ans :=
        dsolve({eq1, eq2, eq3, eq4, ics},{BV(t),OBA(t), OBP(t),
        OCA(t)}, type = numeric, maxfun = 0, parameters = [pq]);


        plotcoord1 := [seq([0, 0], i = 1 .. 41)];
        ii := 1;
            for qq from -10 by .5 to 10 do
                ans(parameters = [qq]);
                plotcoord1[ii] := [qq, rhs(ans(90)[2])];
                ii := ii+1;
            end do:
        results[total] := plot([plotcoord1], color = black, linestyle = 1,
        thickness = 2, legend = ["BV-90th day"], labels = ["Exponent",
        " Bone volume [%]"], axes = boxed, labeldirections =
        [HORIZONTAL, VERTICAL]);
            total := total+1;
        end do:
    end do:
end do:
```

Bibliography

[1] G. A. Rodan and T. J. Martin, "Role of osteoblasts in hormonal control of bone resorption - A hypothesis," *Calcified Tissue International,* vol. 33, pp. 349-351, 1981.

[2] D. B. Burr, A. G. Robling, and C. H. Turner, "Effects of biomechanical stress on bones in animals," *Bone,* vol. 30, pp. 781-6, May 2002.

[3] A. M. Parfitt, "Targeted and nontargeted bone remodeling: relationship to basic multicellular unit origination and progression," *Bone,* vol. 30, pp. 5-7, 2002.

[4] A. J. Black, J. Topping, B. Durham, R. G. Farquharson, and W. D. Fraser, "A Detailed Assessment of Alterations in Bone Turnover, Calcium Homeostasis, and Bone Density in Normal Pregnancy," *Journal of Bone and Mineral Research,* vol. 15, pp. 557-563, 2000.

[5] M. Kroll, "Parathyroid hormone temporal effects on bone formation and resorption," *Bulletin of Mathematical Biology,* vol. 62, pp. 163-188, 2000.

[6] V. Lemaire, F. L. Tobin, L. D. Greller, C. R. Cho, and L. J. Suva, "Modeling the interactions between osteoblast and osteoclast activities in bone remodeling," *Journal of Theoretical Biology,* vol. 229, pp. 293-309, Aug 7 2004.

[7] A. C. Karaplis and D. Goltzman, "PTH and PTHrP Effects on the Skeleton," *Reviews in Endocrine & Metabolic Disorders,* vol. 1, pp. 331-341, 2000.

[8] H. Dobnig and R. T. Turner, "The Effects of Programmed Administration of Human Parathyroid Hormone Fragment (1-34) on Bone Histomorphometry and Serum Chemistry in Rats," *Endocrinology,* vol. 138, pp. 4607-4612, November 1, 1997 1997.

[9] M. R. Rubin and J. P. Bilezikian, "New anabolic therapies in osteoporosis," *Endocrinology & Metabolism Clinics of North America,* vol. 32, pp. 285-307, 2003.

[10] Rachel M. Locklin, S. Khosla, R. T. Turner, and B. L. Riggs, "Mediators of the biphasic responses of bone to intermittent and continuously administered parathyroid hormone," *Journal of Cellular Biochemistry,* vol. 89, pp. 180-190, 2003.

[11] C. Berg, K. Neumeyer, and P. Kirkpatrick, "Teriparatide," *Nat Rev Drug Discov,* vol. 2, pp. 257-8, Apr 2003.

[12] Gossling, R. H, Bernstein, A. R, Abbott, and J, *Treatment of ununited tibial fractures : a comparison of surgery and pulsed*

electromagnetic fields (PEMF) vol. 15. Thorofare, NJ, ETATS-UNIS: Slack, 1992.

[13] Robert J. Fitzsimmons, S. L. Gordon, J. Kronberg, T. Ganey, and A. A. Pilla, "A pulsing electric field (PEF) increases human chondrocyte proliferation through a transduction pathway involving nitric oxide signaling," *Journal of Orthopaedic Research,* vol. 26, pp. 854-859, 2008.

[14] E. Y. S. Chao, N. Inoue, T. K. K. Koo, and Y. H. Kim, "Biomechanical Considerations of Fracture Treatment and Bone Quality Maintenance in Elderly Patients and Patients with Osteoporosis," *Clinical Orthopaedics and Related Research,* vol. 425, 2004.

[15] P. Pivonka, J. Zimak, D. W. Smith, B. S. Gardiner, C. R. Dunstan, N. A. Sims, T. John Martin, and G. R. Mundy, "Theoretical investigation of the role of the RANK-RANKL-OPG system in bone remodeling," *Journal of Theoretical Biology,* vol. 262, pp. 306-316, 2010.

[16] C. Rattanakul, Y. Lenbury, N. Krishnamara, and D. J. Wolwnd, "Modeling of bone formation and resorption mediated by parathyroid hormone: response to estrogen/PTH therapy," *Biosystems,* vol. 70, pp. 55-72, Jun 2003.

[17] S. V. Komarova, R. J. Smith, S. J. Dixon, S. M. Sims, and L. M. Wahl, "Mathematical model predicts a critical role for osteoclast autocrine regulation in the control of bone remodeling," *Bone,* vol. 33, pp. 206-215, Aug 2003.

[18] S. V. Komarova, "Mathematical model of paracrine interactions between osteoclasts and osteoblasts predicts anabolic action of parathyroid hormone on bone," *Endocrinology,* vol. 146, pp. 3589-3595, Aug 2005.

[19] L. K. Potter, L. D. Greller, C. R. Cho, M. E. Nuttall, G. B. Stroup, L. J. Suva, and F. L. Tobin, "Response to continuous and pulsatile PTH dosing: A mathematical model for parathyroid hormone receptor kinetics," *Bone,* vol. 37, pp. 159-169, Aug 2005.

[20] P. Pivonka, J. Zimak, D. W. Smith, B. S. Gardiner, C. R. Dunstan, N. A. Sims, T. John Martin, and G. R. Mundy, "Model structure and control of bone remodeling: A theoretical study," *Bone,* vol. 43, pp. 249-263, 2008.

[21] D. J. Hadjidakis and I. I. Androulakis, "Bone Remodeling," *Annals of the New York Academy of Sciences,* vol. 1092, pp. 385-396, December 1, 2006 2006.

[22] H. M. Frost, *bone remodelling dynamics* vol. 59. Illinois: Springfield, 1963.

[23] A. G. Robling, A. B. Castillo, and C. H. Turner, "Biomechanical and molecular regulation of bone remodeling," *Annual Reviews,* vol. 8, pp. 455-498, 2006.

[24] A. M. Parfitt, "Osteonal and hemi-osteonal remodeling: The spatial and temporal framework for signal traffic in adult human bone," *Journal of Cellular Biochemistry,* vol. 55, pp. 273-286, 1994.

[25] H. M. Frost, "Intermediary organization of the skeleton," *Boca Raton, Fl: CRC Press,* 1986.

[26] H. M. Frost, "Dynamics of bone remodelling," *Bone Biodynamics,* 1964.

[27] T. Suda, N. Takahashi, N. Udagawa, E. Jimi, M. T. Gillespie, and T. J. Martin, "Modulation of Osteoclast Differentiation and Function by the New Members of the Tumor Necrosis Factor Receptor and Ligand Families," *Endocr Rev,* vol. 20, pp. 345-357, June 1, 1999 1999.

[28] S. Khosla, "Minireview: The OPG/RANKL/RANK System," *Endocrinology,* vol. 142, pp. 5050-5055, December 1, 2001 2001.

[29] W. J. Boyle, W. S. Simonet, and D. L. Lacey, "Osteoclast differentiation and activation," *Nature,* vol. 423, pp. 337-342, 2003.

[30] D. B. Burr, "Targeted and nontargeted remodeling," *Bone,* vol. 30, pp. 2-4, 2002.

[31] S.-K. Lee and J. A. Lorenzo, "Parathyroid Hormone Stimulates TRANCE and Inhibits Osteoprotegerin Messenger Ribonucleic Acid Expression in Murine Bone Marrow Cultures: Correlation with Osteoclast-Like Cell Formation," *Endocrinology,* vol. 140, pp. 3552-3561, August 1, 1999 1999.

[32] Q. Fu, R. L. Jilka, S. C. Manolagas, and C. A. O'Brien, "Parathyroid Hormone Stimulates Receptor Activator of NFkappa B Ligand and Inhibits Osteoprotegerin Expression via Protein Kinase A Activation of cAMP-response Element-binding Protein," *J. Biol. Chem.,* vol. 277, pp. 48868-48875, December 6, 2002 2002.

[33] L. C. Hofbauer, S. Khosla, C. R. Dunstan, D. L. Lacey, W. J. Boyle, and B. L. Riggs, "The Roles of Osteoprotegerin and Osteoprotegerin Ligand in the Paracrine Regulation of Bone Resorption," *Journal of Bone and Mineral Research,* vol. 15, pp. 2-12, 2000.

[34] Yanan Wang, Qing-hua Qin, and S. Kalyanasundaram, "A theoretical model for simulating effect of Parathyroid Hormone on bone metabolism at cellular level," *Journal of Molecular & Cellular Biomechanics,* vol. 6, pp. 101-112, 2009.

[35] J. E. Zerwekh, L. A. Ruml, F. Gottschalk, and C. Y. C. Pak, "The Effects of Twelve Weeks of Bed Rest on Bone Histology, Biochemical Markers of Bone Turnover, and Calcium Homeostasis

in Eleven Normal Subjects," *Journal of Bone and Mineral Research,* vol. 13, pp. 1594-1601, 1998.

[36] V. Schneider, V. Oganov, A. LeBlanc, A. Rakmonov, L. Taggart, A. Bakulin, C. Huntoon, A. Grigoriev, and L. Varonin, "Bone and body mass changes during space flight," *Acta Astronautica,* vol. 36, pp. 463-466, 1995.

[37] S. J. Warden, "Breaking the rules for bone adaptation to mechanical loading," *J Appl Physiol,* vol. 100, pp. 1441-1442, May 1, 2006 2006.

[38] A. G. Robling, F. M. Hinant, D. B. Burr, and C. H. Turner, "Improved Bone Structure and Strength After Long-Term Mechanical Loading Is Greatest if Loading Is Separated Into Short Bouts," *J. Bone. Miner. Res.,* vol. 17, pp. 1545-1554, 2002.

[39] C. MacKay, C. Lorincz, and R. Zernicke, "Mechanisms of bone remodeling during weight-bearing exercise," *Applied Physiology, Nutrition, and Metabolism,* vol. 31, pp. 655-660, 2006.

[40] P. Nijweide, E. Burger, and J. Klein-Nulend, *The osteocyte.* San Diego CA USA: Academic Press, 2002.

[41] M. L. Knothe Tate, R. Steck, M. R. Forwood, and P. Niederer, "In vivo demonstration of load-induced fluid flow in the rat tibia and its potential implications for processes associated with functional adaptation," *The Journal of Experimental Biology,* vol. 203, pp. 2737-2745, September 15, 2000 2000.

[42] S. Weinbaum, S. C. Cowin, and Y. Zeng, "A model for the excitation of osteocytes by mechanical loading-induced bone fluid shear stresses," *Journal of Biomechanics,* vol. 27, pp. 339-60, Mar 1994.

[43] J. Klein-Nulend, R. G. Bacabac, and M. G. Mullender, "Mechanobiology of bone tissue," *Pathologie-biologie,* vol. 53, pp. 576-580, 2005.

[44] A. D. Bakker, K. Soejima, J. Klein-Nulend, and E. H. Burger, "The production of nitric oxide and prostaglandin E2 by primary bone cells is shear stress dependent," *Journal of Biomechanics,* vol. 34, pp. 671-677, 2001.

[45] R. G. Bacabac, T. H. Smit, M. G. Mullender, S. J. Dijcks, J. J. V. Loon, and J. Klein-Nulend, "Nitric oxide production by bone cells is fluid shear stress rate dependent," *Biochemical and biophysical research communications,* vol. 315, pp. 823-829, 2004.

[46] M. Mullender, A. El Haj, Y. Yang, M. van Duin, E. Burger, and J. Klein-Nulend, "Mechanotransduction of bone cellsin vitro: Mechanobiology of bone tissue," *Medical and Biological Engineering and Computing,* vol. 42, pp. 14-21, 2004.

[47] N. E. Ajubi, J. Klein-Nulend, P. J. Nijweide, T. Vrijheid-Lammers, M. J. Alblas, and E. H. Burger, "Pulsating Fluid Flow Increases Prostaglandin Production by Cultured Chicken Osteocytes-A

Cytoskeleton-Dependent Process," *Biochemical and Biophysical Research Communications,* vol. 225, pp. 62-68, 1996.

[48] N. E. Ajubi, J. Klein-Nulend, M. J. Alblas, E. H. Burger, and P. J. Nijweide, "Signal transduction pathways involved in fluid flow-induced PGE2 production by cultured osteocytes," *Am J Physiol Endocrinol Metab,* vol. 276, pp. E171-178, January 1, 1999 1999.

[49] E. H. Burger and J. Klein-Nulend, "Mechanotransduction in bone—role of the lacuno-canalicular network," *FASEB J.,* vol. 13, pp. 101-112, May 1, 1999 1999.

[50] T. J. Chambers, S. Fox, C. J. Jagger, J. M. Lean, and J. W. M. Chow, "The role of prostaglandins and nitric oxide in the response of bone to mechanical forces," *Osteoarthritis and Cartilage,* vol. 7, pp. 422-423, 1999.

[51] A. Bakker, J. Klein-Nulend, and E. Burger, "Mechanotransduction in bone cells proceeds via activation of COX-2, but not COX-1," *Biochemical and biophysical research communications,* vol. 305, pp. 677-683, 2003.

[52] M. Joldersma, J. Klein-Nulend, A. M. Oleksik, I. C. Heyligers, and E. H. Burger, "Estrogen enhances mechanical stress-induced prostaglandin production by bone cells from elderly women," *Am J Physiol Endocrinol Metab,* vol. 280, pp. E436-442, March 1, 2001 2001.

[53] J. Klein-Nulend, J. G. H. Sterck, J. G. H. Sterck, C. M. Semeins, P. Lips, M. Joldersma, J. A. Baart, and E. H. Burger, "Donor Age and Mechanosensitivity of Human Bone Cells," *Osteoporosis International,* vol. 13, pp. 137-146, 2002.

[54] F.-S. Wang, C.-J. Wang, Y.-J. Chen, Y.-T. Huang, H.-C. Huang, P.-R. Chang, Y.-C. Sun, and K. D. Yang, "Nitric Oxide Donor Increases Osteoprotegerin Production and Osteoclastogenesis Inhibitory Activity in Bone Marrow Stromal Cells from Ovariectomized Rats," *Endocrinology,* vol. 145, pp. 2148-2156, May 1, 2004 2004.

[55] E. H. Burger, J. Klein-Nulend, and T. H. Smit, "Strain-derived canalicular fluid flow regulates osteoclast activity in a remodelling osteon-proposal," *Journal of biomechanics,* vol. 36, pp. 1453-1459, 10/01 2003.

[56] S. H. R. Rob J. van'T Hof, "Nitric oxide and bone," *Immunology,* vol. 103, pp. 255-261, 2001.

[57] X. Fan, E. Roy, L. Zhu, T. C. Murphy, C. Ackert-Bicknell, C. M. Hart, C. Rosen, M. S. Nanes, and J. Rubin, "Nitric Oxide Regulates Receptor Activator of Nuclear Factor-{kappa}B Ligand and Osteoprotegerin Expression in Bone Marrow Stromal Cells," *Endocrinology,* vol. 145, pp. 751-759, February 1, 2004 2004.

[58] M. Machwate, S. Harada, C. T. Leu, G. Seedor, M. Labelle, M. Gallant, S. Hutchins, N. Lachance, N. Sawyer, D. Slipetz, K. M. Metters, S. B. Rodan, R. Young, and G. A. Rodan, "Prostaglandin Receptor EP4 Mediates the Bone Anabolic Effects of PGE2," vol. 60, pp. 36-41, July 1, 2001 2001.

[59] S. Keila, A. Kelner, and M. Weinreb, "Systemic prostaglandin E2 increases cancellous bone formation and mass in aging rats and stimulates their bone marrow osteogenic capacity in vivo and in vitro," *J Endocrinol,* vol. 168, pp. 131-139, January 1, 2001 2001.

[60] L. G. Raisz, "Physiology and Pathophysiology of Bone Remodeling," *Clin. Chem.,* vol. 45, pp. 1353-1358, August 1, 1999 1999.

[61] M. G. Mullender, R. Huiskes, and H. Weinans, "A physiological approach to the simulation of bone remodeling as a self organization control process," *Journal of Biomechanics,* vol. 27, pp. 1389-1394, 1994.

[62] R. Ruimerman, P. Hilbers, B. van Rietbergen, and R. Huiskes, "A theoretical framework for strain-related trabecular bone maintenance and adaptation," *J. Biomech.,* vol. 38, pp. 931-941, Apr 2005.

[63] R. Ruimerman, R. Huiskes, G. H. Van Lenthe, and J. D. Janssen, "A Computer-simulation Model Relating Bone-cell Metabolism to Mechanical Adaptation of Trabecular Architecture," *Computer Methods in Biomechanics and Biomedical Engineering,* vol. 4, pp. 433 - 448, 2001.

[64] H. Weinans, R. Huiskes, and H. J. Grootenboer, "The behavior of adaptive bone-remodeling simulation models," *Journal of biomechanics,* vol. 25, pp. 1425-41, Dec 1992.

[65] J. Li, H. Li, L. Shi, A. S. L. Fok, C. Ucer, H. Devlin, K. Horner, and N. Silikas, "A mathematical model for simulating the bone remodeling process under mechanical stimulus," *Dental Materials,* vol. 23, pp. 1073-1078, 2007.

[66] S. Maldonado, R. Findeisen, and F. Allgower, "Describing force-induced bone growth and adaptation by a mathematical model," *Journal of Musculoskeletal and Neuronal Interactions,* vol. 8, pp. 15-7, Jan-Mar 2008.

[67] S. Maldonado, S. Borchers, R. Findeisen, and F. Allgower, "Mathematical modeling and analysis of force induced bone growth," *Conf Proc IEEE Eng Med Biol Soc,* vol. 1, pp. 3154-7, 2006.

[68] E. Tanaka, S. Yamamoto, Y. Aoki, T. Okada, and H. Yamada, "Formulation of a mathematical model for mechanical bone remodeling process," *Jsme International Journal Series C-*

Mechanical Systems Machine Elements and Manufacturing, vol. 43, pp. 830-836, Dec 2000.

[69] C. Brighton and P. Magnusson, "Electrically induced osteogenesis. Its clinical use in treating nonunion," in *Bioelectric repair and growth*, E. e. a. Fukuda, Ed. Nisimura: Niigata, 1985, pp. 3-19.

[70] E. Fukuda and I. Yasuda, "On the piezoelectric effect of bone," *Journal of the Physical Socity of Japan,* vol. 12, pp. 1158-1162, 1957.

[71] D. A. Grande, F. P. Magee, A. M. Weinstein, and B. R. McLeod, "The effect of low-energy combined AC and DC magnetic fields on articular cartilage metabolism," *Ann N Y Acad Sci,* vol. 635, pp. 404-7, 1991.

[72] C. A. L. Bassett and R. J. Pawluk, "Effects of Electric Currents on Bone In Vivo," *Nature,* vol. 204, pp. 652-654, 1964.

[73] C. Bassett, "Pulsing electromagnetic fields: A new method to modify cell behavior in calcified and noncalcified tissues," *Calcified Tissue International,* vol. 34, pp. 1-8, 1982.

[74] K. Kubota, N. Yoshimura, M. Yokota, R. J. Fitzsimmons, and M. E. Wikesjo, "Overview of effects of electrical stimulation on osteogenesis and alveolar bone," *J Periodontol,* vol. 66, pp. 2-6, Jan 1995.

[75] G. I. Mammi, R. Rocchi, R. Cadossi, L. Massari, and G. C. Traina, "The electrical stimulation of tibial osteotomies. Double-blind study," *Clin Orthop Relat Res,* pp. 246-53, Mar 1993.

[76] D. C. Fredericks, J. V. Nepola, J. T. Baker, J. Abbott, and B. Simon, "Effects of Pulsed Electromagnetic Fields on Bone Healing in a Rabbit Tibial Osteotomy Model," *Journal of Orthopaedic Trauma,* vol. 14, pp. 93-100, 2000.

[77] W. H. Chang, L. T. Chen, J. S. Sun, and F. H. Lin, "Effect of pulse-burst electromagnetic field stimulation on osteoblast cell activities," *Bioelectromagnetics,* vol. 25, pp. 457-65, Sep 2004.

[78] Trock, H. D, Bollet, J. A, Markoll, and R, *The effect of pulsed electromagnetic fields in the treatment of osteoarthritis of the knee and cervical spine. Report of randomized, double blind, placebo controlled trials* vol. 21. Toronto, ON, CANADA: Journal of Rheumatology Publishing, 1994.

[79] K. Chang and W. H.-S. Chang, "Pulsed electromagnetic fields prevent osteoporosis in an ovariectomized female rat model: A prostaglandin E2 associated process," *Bioelectromagnetics,* vol. 24, pp. 189-198, 2003.

[80] R. J. Linovitz, M. Pathria, M. Bernhardt, D. Green, M. D. Law, R. A. McGuire, P. X. Montesano, G. Rechtine, R. M. Salib, J. T. Ryaby, J. S. Faden, R. Ponder, L. R. Muenz, F. P. Magee, and S. A. Garfin,

"Combined Magnetic Fields Accelerate and Increase Spine Fusion: A Double-Blind, Randomized, Placebo Controlled Study," *Spine,* vol. 27, 2002.

[81] H. M. Frost, *Intermediary organization of the skeleton*: Boca Raton, Fla. : CRC Press, 1986.

[82] D. M. Anderson, E. Maraskovsky, W. L. Billingsley, W. C. Dougall, M. E. Tometsko, E. R. Roux, M. C. Teepe, R. F. DuBose, D. Cosman, and L. Galibert, "A homologue of the TNF receptor and its ligand enhance T-cell growth and dendritic-cell function," *Nature,* vol. 390, pp. 175-179, 1997.

[83] C. H. Lohmann, Z. Schwartz, Y. Liu, Z. Li, B. J. Simon, V. L. Sylvia, D. D. Dean, L. F. Bonewald, H. J. Donahue, and B. D. Boyan, "Pulsed electromagnetic fields affect phenotype and connexin 43 protein expression in MLO-Y4 osteocyte-like cells and ROS 17/2.8 osteoblast-like cells," *Journal of Orthopaedic Research,* vol. 21, pp. 326-334, 2003.

[84] K. Chang, W. H.-S. Chang, M.-L. Wu, and C. Shih, "Effects of different intensities of extremely low frequency pulsed electromagnetic fields on formation of osteoclast-like cells," *Bioelectromagnetics,* vol. 24, pp. 431-439, 2003.

[85] K. J. McLeod and C. T. Rubin, "The effect of low-frequency electrical fields on osteogenesis," *Journal of Bone and Joint Surgery,* vol. 74, pp. 920-929, 1992.

[86] M. A. Vander Molen, H. J. Donahue, C. T. Rubin, and K. J. McLeod, "Osteoblastic networks with deficient coupling: differential effects of magnetic and electric field exposure," *Bone,* vol. 27, pp. 227-231, 2000.

[87] Tabrah, F, Hoffmeier, M, Gilbert, J. R. F, Batkin, S, Bassett, and L. C. A, *Bone density changes in osteoporosis-prone women exposed to pulsed electromagnetic fields (PEMFs)* vol. 5. Duham, NC, ETATS-UNIS: American Society for Bone and Mineral Research, 1990.

[88] Y. Wang and Q.-H. Qin, "Parametric study of control mechanism of cortical bone remodeling under mechanical stimulus," *Acta Mechanica Sinica,* vol. 26, pp. 37-44, 2010.

[89] N. A. Defranoux, C. L. Stokes, D. L. Young, and A. J. Kahn, "In silico modeling and simulation of bone biology: a proposal," *J Bone Miner Res,* vol. 20, pp. 1079-84, Jul 2005.

[90] C. H. Kim, E. Takai, H. Zhou, D. von Stechow, R. Muller, D. W. Dempster, and X. E. Guo, "Trabecular bone response to mechanical and parathyroid hormone stimulation: the role of mechanical microenvironment," *J Bone Miner Res,* vol. 18, pp. 2116-25, Dec 2003.

[91] R. M. Neer, C. D. Arnaud, J. R. Zanchetta, R. Prince, G. A. Gaich, J.-Y. Reginster, A. B. Hodsman, E. F. Eriksen, S. Ish-Shalom, H. K. Genant, O. Wang, B. H. Mitlak, D. Mellstrom, E. S. Oefjord, E. Marcinowska-Suchowierska, J. Salmi, H. Mulder, J. Halse, and A. Z. Sawicki, "Effect of Parathyroid Hormone (1-34) on Fractures and Bone Mineral Density in Postmenopausal Women with Osteoporosis," *N Engl J Med,* vol. 344, pp. 1434-1441, May 10, 2001 2001.

[92] J. F. Whitfield, P. Morley, and G. E. Willick, "Bone growth stimulators. New tools for treating bone loss and mending fractures," *Vitam Horm,* vol. 65, pp. 1-80, 2002.

[93] J. Wang, J. Zhou, C. M. Cheng, J. J. Kopchick, and C. A. Bondy, "Evidence supporting dual, IGF-I-independent and IGF-I-dependent, roles for GH in promoting longitudinal bone growth," *J Endocrinol,* vol. 180, pp. 247-255, February 1, 2004 2004.

[94] L. R. Donahue and C. J. Rosen, "IGFs and bone: the osteoporosis connection revisited," *Proc Soc Exp Biol Med,* vol. 219, pp. 1–7, 1998.

[95] D. Goltzman, "Interactions of PTH and PTHrP with the PTH/PTHrP Receptor and with Downstream Signaling Pathways: Exceptions That Provide the Rules," *Journal of Bone and Mineral Research,* vol. 14, pp. 173-177, 1999.

[96] S. L. Teitelbaum, "Bone Resorption by Osteoclasts," *Science,* vol. 289, pp. 1504-1508, September 1, 2000 2000.

[97] J. E. Aubin and E. Bonnelye, "Osteoprotegerin and its Ligand: A New Paradigm for Regulation of Osteoclastogenesis and Bone Resorption," *Osteoporosis International,* vol. 11, pp. 905-913, 2000.

[98] D. L. Halladay, R. R. Miles, K. Thirunavukkarasu, S. Chandrasekhar, T. J. Martin, and J. E. Onyia, "Identification of signal transduction pathways and promoter sequences that mediate parathyroid hormone 1-38 inhibition of osteoprotegerin gene expression," *Journal of Cellular Biochemistry,* vol. 84, pp. 1-11, 2002.

[99] Y. Isogai, T. Akatsu, T. Ishizuya, A. Yamaguchi, M. Hori, N. Takahashi, and T. Suda, "Parathyroid hormone regulates osteoblast differentiation positively or negatively depending on the differentiation stages," *J Bone Miner Res,* vol. 11, pp. 1384-93, Oct 1996.

[100] M. Zaidi, "Skeletal remodeling in health and disease," *Nature Medicine,* vol. 13, pp. 791-801, Jul 2007.

[101] M. M. Tondravi, S. R. McKercher, K. Anderson, J. M. Erdmann, M. Quiroz, R. Maki, and S. L. Teitelbaum, "Osteopetrosis in mice lacking haematopoietic transcription factor PU.1," *Nature,* vol. 386, pp. 81-84, 1997.

[102] H. Yoshida, S.-I. Hayashi, T. Kunisada, M. Ogawa, S. Nishikawa, H. Okamura, T. Sudo, L. D. Shultz, and S.-I. Nishikawa, "The murine mutation osteopetrosis is in the coding region of the macrophage colony stimulating factor gene," *Nature,* vol. 345, pp. 442-444, 1990.

[103] G. Franzoso, L. Carlson, L. Xing, L. Poljak, E. W. Shores, K. D. Brown, A. Leonardi, T. Tran, B. F. Boyce, and U. Siebenlist, "Requirement for NF-kappa B in osteoclast and B-cell development," *Genes Dev.,* vol. 11, pp. 3482-3496, December 15, 1997 1997.

[104] K. Matsuo, D. L. Galson, C. Zhao, L. Peng, C. Laplace, K. Z. Q. Wang, M. A. Bachler, H. Amano, H. Aburatani, H. Ishikawa, and E. F. Wagner, "Nuclear Factor of Activated T-cells (NFAT) Rescues Osteoclastogenesis in Precursors Lacking c-Fos," *J. Biol. Chem.,* vol. 279, pp. 26475-26480, June 18, 2004 2004.

[105] H. Hsu, D. L. Lacey, C. R. Dunstan, I. Solovyev, A. Colombero, E. Timms, H.-L. Tan, G. Elliott, M. J. Kelley, I. Sarosi, L. Wang, X.-Z. Xia, R. Elliott, L. Chiu, T. Black, S. Scully, C. Capparelli, S. Morony, G. Shimamoto, M. B. Bass, and W. J. Boyle, "Tumor necrosis factor receptor family member RANK mediates osteoclast differentiation and activation induced by osteoprotegerin ligand," *Proceedings of the National Academy of Sciences,* vol. 96, pp. 3540-3545, March 30, 1999 1999.

[106] J. E. Aubin, "Bone stem cells," *Journal of Cellular Biochemistry,* vol. 72, pp. 73-82, 1998.

[107] R. L. Jilka, R. S. Weinstein, T. Bellido, A. M. Parfitt, and S. C. Manolagas, "Osteoblast Programmed Cell Death (Apoptosis): Modulation by Growth Factors and Cytokines," *Journal of Bone and Mineral Research,* vol. 13, pp. 793-802, 1998.

[108] G. D. Roodman, "Cell biology of the osteoclast," *Experimental Hematology,* vol. 27, pp. 1229-1241, 1999.

[109] L. F. Bonewald and S. L. Dallas, "Role of active and latent transforming growth factor ? in bone formation," *Journal of Cellular Biochemistry,* vol. 55, pp. 350-357, 1994.

[110] L. F. Bonewald and S. L. Dallas, "Role of active and latent transforming growth factor Beta in bone formation," *Journal of Cellular Biochemistry,* vol. 55, pp. 350-357, 1994.

[111] T. Alliston, L. Choy, P. Ducy, G. Karsenty, and R. Derynck, "TGF-beta-induced repression of CBFA1 by Smad3 decreases cbfa1 and osteocalcin expression and inhibits osteoblast differentiation," *The EMBO Journal,* vol. 20, pp. 2254-72, May 1 2001.

[112] E. M. Greenfield, Y. Bi, and A. Miyauchi, "Regulation of osteoclast activity," *Life Sciences,* vol. 65, pp. 1087-1102, 1999.

[113] D. J. Knauer, H. S. Wiley, and D. D. Cunningham, "Relationship between epidermal growth factor receptor occupancy and mitogenic response. Quantitative analysis using a steady state model system," *J. Biol. Chem.,* vol. 259, pp. 5623-5631, May 10, 1984 1984.

[114] D. A. Lauffenburger and J. J. Linderman, "Receptors. Models for binding, trafficking, and signalling," *Oxford University Press US,* p. 376, 1996.

[115] D. W. Dempster, F. Cosman, M. Parisien, V. Shen, and R. Lindsay, "Anabolic actions of parathyroid hormone on bone," *Endocr Rev,* vol. 14, pp. 690-709, Dec 1993.

[116] X. W. Meng, X. G. Liang, R. Birchman, D. D. Wu, D. W. Dempster, R. Lindsay, and V. Shen, "Temporal expression of the anabolic action of PTH in cancellous bone of ovariectomized rats," *J Bone Miner Res,* vol. 11, pp. 421-9, Apr 1996.

[117] A. M. Parfitt, "The cellular basis of bone turnover and bone loss: a rebuttal of the osteocytic resorption--bone flow theory," *Clinical Orthopaedics and Related Research,* pp. 236-47, 1977.

[118] S. Doty, "Morphological evidence of gap junctions between bone cells," *Calcified Tissue International,* vol. 33, pp. 509-512, 1981.

[119] F. Shapiro, "Variable Conformation of GAP Junctions Linking Bone Cells: A Transmission Electron Microscopic Study of Linear, Stacked Linear, Curvilinear, Oval, and Annular Junctions," *Calcified Tissue International,* vol. 61, pp. 285-293, 1997.

[120] A. V. Hill, "The possible effects of the aggregation of the molecules of hemoglobin on its dissociation curves," *J. Physiol. (Lond.),* vol. 40, 1910.

[121] U. Alon, *An Introduction to Systems Biology: Design Principles of Biological Circuits*. New York, USA: CRC Press, 2007.

[122] L. K. Saxon, A. G. Robling, I. Alam, and C. H. Turner, "Mechanosensitivity of the rat skeleton decreases after a long period of loading, but is improved with time off," *Bone,* vol. 36, pp. 454-464, 2005.

[123] G. Bergmann, F. Graichen, and A. Rohlmann, "hip joint force measurements," *Available from <http://www.medizin.fu-berlin.de/missing.html>,* 2003.

[124] C. H. Turner, M. R. Forwood, and M. W. Otter, "Mechanotransduction in bone: do bone cells act as sensors of fluid flow?," *FASEB J.,* vol. 8, pp. 875-878, August 1, 1994 1994.

[125] S. J. Warden and C. H. Turner, "Mechanotransduction in the cortical bone is most efficient at loading frequencies of 5-10 Hz," *Bone,* vol. 34, pp. 261-270, 02/01 2004.

[126] C. Rubin, G. Xu, and S. Judex, "The anabolic activity of bone tissue, suppressed by disuse, is normalized by brief exposure to extremely

low-magnitude mechanical stimuli," *FASEB J.,* vol. 15, pp. 2225-2229, October 1, 2001 2001.

[127] A. G. Robling, D. B. Burr, and C. H. Turner, "Recovery periods restore mechanosensitivity to dynamically loaded bone," *J Exp Biol,* vol. 204, pp. 3389-3399, October 1, 2001 2001.

[128] J. L. Schriefer, S. J. Warden, L. K. Saxon, A. G. Robling, and C. H. Turner, "Cellular accommodation and the response of bone to mechanical loading," *Journal of Biomechanics,* vol. 38, pp. 1838-1845, 2005.

[129] J. Klein-Nulend, A. van der Plas, C. M. Semeins, N. E. Ajubi, J. A. Frangos, P. J. Nijweide, and E. H. Burger, "Sensitivity of osteocytes to biomechanical stress in vitro," *FASEB J.,* vol. 9, pp. 441-445, March 1, 1995 1995.

[130] C. M. Riggs, L. E. Lanyon, and A. Boyde, "Functional associations between collagen fibre orientation and locomotor strain direction in cortical bone of the equine radius," *Anatomy and Embryology,* vol. 187, pp. 231-238, 1993.

[131] A. Ascenzi and E. Bonucci, "The tensile properties of single osteons," *The Anatomical record,* vol. 158, pp. 375-86, Aug 1967.

[132] A. Ascenzi and E. Bonucci, "The compressive properties of single osteons," *The Anatomical record,* vol. 161, pp. 377-91, Jul 1968.

[133] D. B. Burr, T. Hirano, C. H. Turner, C. Hotchkiss, R. Brommage, and J. M. Hock, "Intermittently administered human parathyroid hormone(1-34) treatment increases intracortical bone turnover and porosity without reducing bone strength in the humerus of ovariectomized cynomolgus monkeys," vol. 16, pp. 157-65, Jan 2001.

[134] B. S. Noble, N. Peet, H. Y. Stevens, A. Brabbs, J. R. Mosley, G. C. Reilly, J. Reeve, T. M. Skerry, and L. E. Lanyon, "Mechanical loading: biphasic osteocyte survival and targeting of osteoclasts for bone destruction in rat cortical bone," *Am. J. Physiol. Cell. Physiol.,* vol. 284, pp. C934-943, April 1, 2003 2003.

[135] K. Chang, W. H.-S. Chang, S. Huang, S. Huang, and C. Shih, "Pulsed electromagnetic fields stimulation affects osteoclast formation by modulation of osteoprotegerin, RANK ligand and macrophage colony-stimulating facto," *Journal of Orthopaedic Research,* vol. 23, pp. 1308-1314, 2005.

[136] Z. Schwartz, M. Fisher, C. Lohmann, B. Simon, and B. Boyan, "Osteoprotegerin (OPG) Production by Cells in the Osteoblast Lineage is Regulated by Pulsed Electromagnetic Fields in Cultures Grown on Calcium Phosphate Substrates," *Annals of Biomedical Engineering,* vol. 37, pp. 437-444, 2009.

[137] T. Bodamyali, B. Bhatt, F. J. Hughes, V. R. Winrow, J. M. Kanczler, B. Simon, J. Abbott, D. R. Blake, and C. R. Stevens, "Pulsed

Electromagnetic Fields Simultaneously Induce Osteogenesis and Upregulate Transcription of Bone Morphogenetic Proteins 2 and 4 in Rat Osteoblastsin Vitro," *Biochemical and Biophysical Research Communications,* vol. 250, pp. 458-461, 1998.

[138] H. H. Guerkov, C. H. Lohmann, Y. Liu, D. D. Dean, B. J. Simon, J. D. Heckman, Z. Schwartz, and B. D. Boyan, "Pulsed Electromagnetic Fields Increase Growth Factor Release by Nonunion Cells," *Clinical Orthopaedics and Related Research,* vol. 384, 2001.

[139] C. H. Lohmann, Z. Schwartz, Y. Liu, H. Guerkov, D. D. Dean, B. Simon, and B. D. Boyan, "Pulsed electromagnetic field stimulation of MG63 osteoblast-like cells affects differentiation and local factor production," *Journal of Orthopaedic Research,* vol. 18, pp. 637-646, 2000.

[140] A. Yajima, M. Ochi, and Y. Hirose, "Effects of pulsing electromagnetic fields on gene expression of bone morphogenetic proteins in human osteoblastic cell line in vitro," *Journal of bone and Mineral Research,* vol. 11, p. 381, 1996.

[141] M. Nagai and M. Ota, "Pulsating Electromagnetic Field Stimulates mRNA Expression of Bone Morphogenetic Protein-2 and -4," *Journal of Dental Research,* vol. 73, pp. 1601-1605, 1994.

[142] L. Massari, G. Caruso, V. Sollazzo, and S. Setti, "Pulsed electromagnetic fields and low intensity pulsed ultrasound in bone tissue," *Clinical Cases in Mineral and Bone Metabolism,* vol. 6, pp. 149-154, 2009.

[143] X. Zhang, J. Zhang, X. Qu, and J. Wen, "Effects of Different Extremely Low-Frequency Electromagnetic Fields on Osteoblasts," *Electromagnetic Biology and Medicine,* vol. 26, pp. 167 - 177, 2007.

[144] C. A. Bassett, S. N. Mitchell, and S. R. Gaston, "Treatment of ununited tibial diaphyseal fractures with pulsing electromagnetic fields," *Journal of Bone and Joint Surgery,* vol. 63, pp. 511-523, 1981.

[145] G. G. Hannay, D. I. Leavesley, and M. J. Pearcy, "Timing of pulsed electromagnetic field stimulation does not affect the promotion of bone cell development," *Bioelectromagnetics,* vol. 26, 2005.

[146] J. K.-J. Li, J. C.-A. Lin, H. C. Liu, and W. H.-S. Chang, "Cytokine Release from Osteoblasts in Response to Different Intensities of Pulsed Electromagnetic Field Stimulation," *Electromagnetic Biology and Medicine,* vol. 26, pp. 153 - 165, 2007.